Application of Multiobjective Optimization in Chemical Engineering Design and Operation

By

Salim Fettaka

A thesis submitted to the Faculty of Graduate and Post-Doctoral Studies in partial fulfillment of the requirements for the degree of

Masters of Applied Science

Department of Chemical and Biological Engineering
Faculty of Engineering
University of Ottawa

July 2012

Acknowledgments

"If I have seen further than others, it is by standing upon the shoulders of giants."

Isaac Newton

First, I would like to express my sincere gratitude to my supervisors Dr. Jules Thibault and Dr. Yash Gupta for giving me the opportunity to work on this research project and invaluable guidance and ideas.

Financial support provided by the Ontario Government and the Natural Sciences and Engineering Research Council of Canada (NSERC) for this project is gratefully acknowledged.

Last but not least, I would like to thank my family and friends for their encouragement and support, they have given me. This thesis would not have been possible if it were not for the support of everyone.

Statement of contributions of collaborators

I hereby declare that I am the sole author of this thesis and that no part of this work has been submitted or accepted for any other degree.

Dr. Jules Thibault and Dr. Yash Gupta supervised this thesis. Both supervisors provided continual guidance throughout this work and made editorial comments and corrections to the written work presented. The responsibilities of the author, Salim Fettaka, in order to fulfill the requirements of this thesis were as follows:

1. To conduct research in the area of multiobjective optimization in order to study commonly utilized multiobjective optimization techniques, and to determine how they could be improved.
2. To develop a new technique for approximating the Pareto domain.
3. To apply the new technique to the optimization of complex chemical engineering problems.
4. To produce three papers for publication based on research performed.
5. To produce a written thesis in partial fulfillment of the requirements for obtaining a Masters in Applied Science.

Signature:

Abstract

The purpose of this research project is the design and optimization of complex chemical engineering problems, by employing evolutionary algorithms (EAs). EAs are optimization techniques which mimic the principles of genetics and natural selection. Given their population-based approach, EAs are well suited for solving multiobjective optimization problems (MOOPs) to determine Pareto-optimal solutions. The Pareto front refers to the set of non-dominated solutions which highlight trade-offs among the different objectives.

A broad range of applications have been studied, all of which are drawn from the chemical engineering field. The design of an industrial packed bed styrene reactor is initially studied with the goal of maximizing the productivity, yield and selectivity of styrene. The dual population evolutionary algorithm (DPEA) was used to circumscribe the Pareto domain of two and three objective optimization case studies for three different configurations of the reactor: adiabatic, steam-injected and isothermal. The Pareto domains were then ranked using the net flow method (NFM), a ranking algorithm that incorporates the knowledge and preferences of an expert into the optimization routine.

Next, a multiobjective optimization of the heat transfer area and pumping power of a shell-and-tube heat exchanger is considered to provide the designer with multiple Pareto-optimal solutions which capture the trade-off between the two objectives. The optimization was performed using the fast and elitist non-dominated sorting genetic algorithm (NSGA-II) on two case studies from the open literature. The algorithm was also used to determine the impact of using discrete standard values of the tube length, diameter and thickness rather than using continuous values to obtain the optimal heat transfer area and pumping power.

In addition, a new hybrid algorithm called the FP-NSGA-II, is developed in this thesis by combining a front prediction algorithm with the fast and elitist non-dominated sorting genetic algorithm-II (NSGA-II). Due to the significant computational time of evaluating objective functions in real life engineering problems, the aim of this hybrid approach is to better approximate the Pareto front of difficult constrained and unconstrained problems while keeping the computational cost similar to NSGA-II. The new algorithm is tested on benchmark problems from the literature and on a heat exchanger network problem.

Résumé

Le but de ce projet de recherche est la modélisation et l'optimisation de problèmes complexes de génie chimique, en employant des algorithmes évolutionnaires (AEs). Les AEs sont des techniques d'optimisation qui imitent les principes de la génétique et la sélection naturelle. Compte tenu de leur approche basée sur la population, les AEs sont bien adaptés pour résoudre les problèmes d'optimisation multi-objectifs afin de déterminer les solutions optimales donnant le domaine de Pareto. Le domaine de Pareto réfère à l'ensemble des solutions non-dominées qui mettent en évidence les compromis entre les différents objectifs.

Une large gamme d'applications reliées au domaine du génie chimique a été utilisée. La conception d'un réacteur industriel de styrène est d'abord étudiée afin de maximiser la productivité, le rendement et la sélectivité de styrène. L'algorithme évolutionnaire de deux populations (DPEA) a été utilisé pour circonscrire le domaine de Pareto pour des problèmes ayant deux et trois objectifs d'optimisation et trois différentes configurations du réacteur: adiabatique, vapeur injectée et isotherme. Les domaines de Pareto ont ensuite été classés en utilisant la méthode des flux nets (NFM), qui intègre les connaissances et les préférences d'un expert.

Ensuite, une optimisation multi-objectifs de la surface de transfert de chaleur et de la puissance associée aux pompes d'un échangeur thermique tubulaire est présentée. Les solutions optimales donnant le domaine de Pareto permettent de visualiser les compromis entre les deux critères objectifs qui doivent tous les deux être minimisés. L'optimisation a été réalisée en utilisant l'algorithme génétique basé sur la non-domination et l'élitisme des solutions (NSGA-II) pour deux études de cas tirées de la littérature. L'algorithme a également été utilisé pour déterminer l'impact de l'utilisation de valeurs standards discrètes pour la longueur, le diamètre et l'épaisseur des tuyaux plutôt que d'utiliser des valeurs continues sur le domaine de Pareto.

Finalement, un nouvel algorithme hybride appelé le FP-NSGA-II, est développé en combinant un simple algorithme de prédiction avec NSGA-II. Le nouvel algorithme a été testé sur les problèmes de référence de la littérature et sur un problème de réseau d'échangeurs de chaleur. Les résultats indiquent que cette approche hybride permet de mieux approximer le domaine de Pareto pour des problèmes complexes tout en gardant un temps de calcul similaire à l'algorithme NSGA-II.

Contents

List of figures

List of tables

Chapter 1: Introduction

1.1 Introduction

Many chemical engineering processes involve the simultaneous optimization of multiple objective variables. These objectives are often conflicting or competing with each other. Consequently the optimization is more difficult as improving one objective will worsen another. This type of problem is known as a multiobjective optimization problem (MOOP). Unlike single objective optimization where there is one best solution, multiobjective optimization generates a set of optimal solutions.

Since the topic of the thesis is relatively foreign to most chemical engineers, a simple illustrative example is to introduce the basic concepts and definitions of multiobjective optimization. This simple illustrative example considers the transport of a given volumetric flow rate of a fluid through a pipeline. The aim of this MOOP is to minimize two *objective functions* or *objective criteria*: the mass of the pipeline per linear meter and the pumping power. The minimization of the mass of the pipeline is desired since it leads to a reduction in its capital cost whereas the minimization of the pumping power is important since it leads to lower operating costs. The two *objective variables*, mass of the pipeline and pumping power, can be computed as a function of two *decision variable*s: the pipeline outer diameter (D_o) and the discharge pressure (P_{dis}). To maintain a constant flow rate for all cases, the feed pressure will obviously need to be adjusted which will in turn impact on the pumping power. Figure 1.1 shows the *decision variable space* and the. Every *point* or *pair of decision variables* in the decision variable space provides a solution in the objective variable space. Decision variables can be *design variables* and *operating variables*.

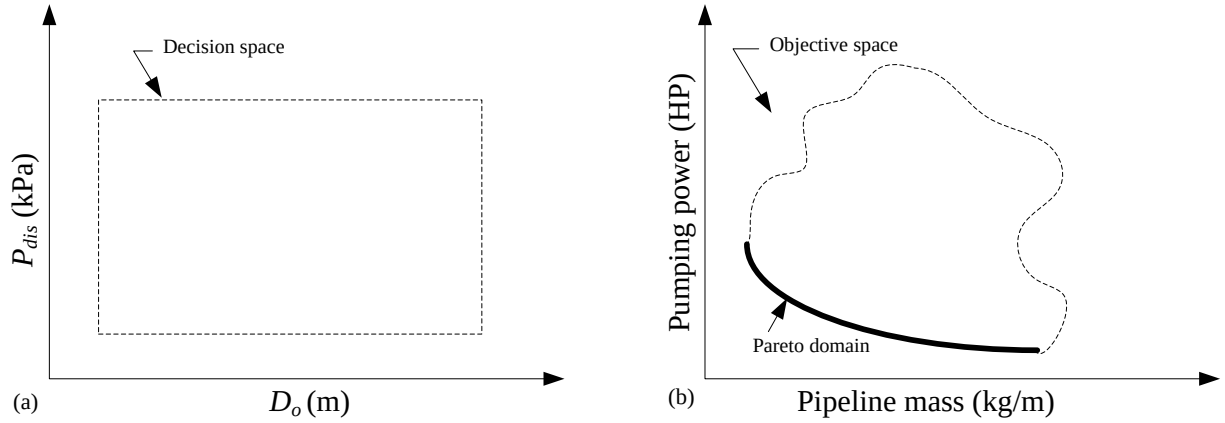

Figure 1.1 - Decision variable space (a) and objective variable space (b) of a simple pipeline example.

Given that the two objective variables, the mass of material to construct the pipeline and the pumping power to accommodate the required flow of fluid, are conflicting with each other and they cannot be decreased at the same time to maintain *optimal design* conditions, there exists a trade-off between them. Table 1.1 presents three feasible solutions taken from the objective variable space in view of illustrating the *concept of dominance* on which are based the majority of multiobjective optimization algorithms. Performing a pairwise comparison between solutions 1 and 2, it can be observed that solution 1 has a smaller pipeline mass whereas it has a higher pumping power than solution 2. Hence none of these two solutions can be said to be better than the other with respect to both objectives. They are referred to as *non-dominated* solutions. For the pairwise comparison between solutions 2 and 3, it can be observed that solution 3 is worse than solution 2 in terms of both objective variables and hence solution 3 is said to be *dominated* or, in other words, solution 2 *dominates* solution 3. Similarly, a pairwise comparison between solutions 1 and 3 indicates that these two solutions are non-dominated with respect to each other. In the analysis of these three solutions, it can be concluded that the *domination score* (i.e. the number of times a solution is dominated following a complete pairwise comparison) of solutions 1 and 2 is 0 whereas it is 1 for solution 3. In summary, a solution is said to be non-dominated if it is not worse than another solution in all its *objectives* and it is better with respect to at least one objective (Deb, 2001). The Pareto domain refers to the set of non-dominated solutions which is indicated with a solid line on Figure 1.1(b).

Table 1.1 - Three solutions of the illustrative pipeline example.

Solution	Pipeline mass (kg/m)	Pumping power (HP)
1	260.	900
2	270	400
3	280	700

Several optimization methods exist to find the Pareto domain. Among them, multiobjective evolutionary algorithms (MOEAs) have attracted significant research interest in recent years to solve complex problems in chemical engineering. This is due to their population based approach that generates multiple Pareto-optimal solutions in a single run, as opposed to a series of separate runs as in the case of the traditional techniques. In addition, MOEAs handle better complex and discontinuous Pareto domains which usually cause difficulties with traditional techniques (Deb, 2001; Haupt and Haupt, 2004).

MOEAs are population-based search techniques that mimic the principles of genetics and natural selection. The procedure is relatively simple. An initial population is generated by randomly selecting vectors of decision variables. In the example considered above, each vector of decision variables consists of random values of the pipeline diameter and the discharge pressure. For each vector of decision variables, the values of the objective variables are then calculated. Usually, the initial and subsequent populations must be sufficiently large to properly define or circumscribe the Pareto domain. By analogy to naturally-evolving systems, the vector of decision variables is often referred to as *chromosomes*. The objective values for each chromosome are computed using the *objective functions*. To *select* which solutions to keep as a parent for the next generation, a *fitness* value is assigned to each one. Fitness can be directly based on the objectives values, or can be defined to include population diversity in order to avoid getting trapped in local optima and search the decision variable space thoroughly.

Crossover and *mutation* are two genetic operators used to alter the composition of the chromosomes and to evolve the population towards better solutions. Crossover involves the exchange of information between two parents to create children, much like natural reproduction process. On the other hand, mutation randomly changes the decision variables of a chromosome that resembles the natural mutation of the genetic code. This allows the introduction of new individuals into the population.

The subject of this thesis is mainly focused on two goals. The first aspect is the application of multiobjective evolutionary algorithms (MOEAs) in chemical engineering

problems. The second aspect is the development of a novel algorithm to better approximate the Pareto front of difficult problems without compromising the computational time.

Within this thesis, applications were examined from the fields of chemical reaction engineering and heat transfer. One application is the optimization of an industrial styrene packed bed reactor using the dual population evolutionary algorithm (DPEA) investigated by Halsall-Whitney et al. (2003), and ranking of the Pareto domain using the net flow method (NFM) previously used by Thibault (2008). Two other applications are the design of a shell-and-tube heat exchanger and a heat exchanger network using the fast and elitist non-dominated sorting genetic algorithm (NSGA-II) proposed by Deb et al. (2002). Such optimization allows the decision-maker or expert to consider a wide range of Pareto optimal solutions, and select the best one based on his preference and experience, a difficult task when systems are complex.

This thesis also presents a novel hybrid algorithm called the FP-NSGA-II, by combining a gradient projection algorithm with the fast and elitist non-dominated sorting genetic algorithm-II (NSGA-II) (Fettaka et al., 2012). The performance of this new algorithm was evaluated using a large number of literature benchmark problems and applied to the design of a heat exchanger network. The competitive advantage of the proposed algorithm is the ability to better approximate the Pareto front of difficult constrained and unconstrained problems while keeping the computational cost similar to NSGA-II, currently one of the most popular MOEA. The results indicate that FP-NSGA-II improves the performance of NSGA-II, currently for a variety of benchmark test problems exhibiting different characteristics (Fettaka et al., 2012).

1.2 Research objectives

The main objectives of this thesis are:

1. To conduct a multiobjective optimization of the productivity, selectivity and yield of an industrial styrene reactor using dual population evolutionary algorithm (DPEA) to circumscribe the Pareto domain and the net flow method (NFM) as a ranking algorithm.
2. To conduct a multiobjective optimization study for the minimization of both the heat transfer area and pumping power of a shell-and-tube heat exchanger using the fast and elitist non-dominated sorting genetic algorithm (NSGA-II).
3. To develop a novel method called FP-NSGA-II to better approximate the Pareto front of difficult constrained and unconstrained problems without compromising

the computational time, and its application to a three-objective heat exchanger network problem.

1.3 Thesis structure

This thesis consists of 5 chapters. The first chapter includes a general introduction and a list of research objectives undertaken during the course of this research. Chapters 2 through 4 contain papers that have been submitted or published in scientific journals. Due to the paper-based structure, the repetition of some common concepts was inevitable in these chapters. The papers are printed in their originally published or submitted state except for changes in format. Chapter 5 contains a general discussion which is related to Chapters 2 through 4 and offers several conclusions and recommendations for future work.

1.4 References

Deb, K. (2001). *Multi-objective optimization using evolutionary algorithms*. New York: Wiley.

Deb K., Argawal S., Pratap A., Meyarivan T. (2002). A fast and elitist multi-objective genetic algorithm: NSGA-II. *IEEE Transactions on Evolutionary Computation* (6). pp 182-197.

Fettaka S., Thibault J., Gupta Y. (2012). A New Algorithm Using Front Prediction and Non-Dominated Sorting for Solving Two and Three-Objective Optimization Problems. *Computers and Operations Research* (Submitted).

Halsall-Whitney, H., Taylor, D., and Thibault, J. (2003). Multicriteria optimization of gluconic acid production using net flow. *Bioprocess and Biosystems Engineering* 25 (5), pp. 299-307.

Haupt R.L., and Haupt S.E. (2004). *Practical Genetic Algorithms* New York: Wiley.

Thibault, J. (2008). Net flow and rough sets: Two methods for ranking the pareto domain. In G. Rangaiah (Ed.), *Multi-Objective Optimization: Techniques and Applications in Chemical Engineering*. World Scientific Publishing.

Chapter 2: Multiobjective optimization of an industrial styrene reactor using the dual population evolutionary algorithm (DPEA)

Salim Fettaka, Yash Gupta and Jules Thibault
Department of Chemical and Biological Engineering
University of Ottawa

Abstract

In the past few years, multiobjective evolutionary algorithms (MOEAs) have gained a lot of interest as a reliable option to optimize problems with conflicting objectives in science and engineering. These algorithms generate an optimal set of trade-off solutions referred to as the Pareto domain. In this investigation, a MOEA was used to optimize simultaneously conflicting design variables of an industrial styrene reactor. The dual population evolutionary algorithm (DPEA) was implemented to optimize the productivity, yield and selectivity of styrene. To evaluate the robustness and versatility of the algorithm, two and three objective optimization case studies were conducted for three different configurations of the reactor: adiabatic, steam-injected and isothermal.

Results indicated that DPEA is a robust optimization strategy to generate a well-defined Pareto domain with a wide range of solutions. In addition, the Pareto-optimal solutions of the steam-injected configuration were superior to the adiabatic reactor and to a portion of the isothermal configuration. The optimal operating conditions corresponding to the Pareto domains were also slightly better in terms of profit when compared with previously published studies. The Pareto domains were then ranked using the net flow method (NFM), a ranking algorithm that incorporates the knowledge and preferences of an expert into the optimization routine.

Keywords: Multiobjective optimization, styrene reactor, genetic algorithm.

Publication Status: International Journal of Chemical Reaction Engineering10 (A9), 2012. DOI: 10.1515/1542-6580.2828

2.1 Introduction

Styrene is the simplest aromatic monomer used for the production of various plastic polymers in the petrochemical industry, which include polystyrene, acrylonitrile-butadiene-styrene copolymer (ABS), styrene-acrylonitrile resins (SAN), as well as styrene-butadiene latex, styrene-butadiene rubber (SBR), and various other unsaturated polyester resins (Li et al., 1982; Chen et al., 2006; Denis et al., 1992).

The production of styrene is accomplished through two manufacturing routes namely the dehydrogenation and coproduction with propylene oxide, both of which use ethyl benzene as the starting material. Over 90% of the commercial styrene is produced through the first route of the catalytic dehydrogenation of ethyl benzene. This route offers several advantages since it is simpler and more versatile as the production can be scaled depending on the demand, in contrast to the propylene oxide route where the profitability depends on the market demand of both co-products: propylene oxide and styrene, which makes it less flexible when the price of one of the co-products changes (Chen et al., 2006).

The many commercial applications of styrene ensure a very high demand for the production of styrene. Historically, styrene has ranked fourth among the most produced monomers in the United States behind ethylene, vinyl chloride and propylene (Chen et al., 2006). The total styrene world demand in 2006 was estimated at 26×10^6 t, with high growth in South America, Eastern Europe, and the Middle East markets. Large plants can reach a production capacity of more than 500 000 tons per year (Chen et al., 2006).

Despite the history of the industrial manufacturing of styrene, opportunities remain for further improvement of the productivity, selectivity and yield of the process that can reduce costs and generate additional revenue.

Published research papers seeking the optimization of the styrene manufacturing process can be classified into one of two basic categories. The first category, known as single objective optimization or the aggregating method, consists of finding the global minimum or maximum of an aggregating function composed of the weighted sum of the individual objectives. The second category, known as multiobjective optimization or non-aggregating method, involves the simultaneous optimization of multiple objectives that are often conflicting. Unlike single objective optimization where there exists a unique optimal solution, multiobjective optimization generates a set of Pareto-optimal solutions. The Pareto domain refers to the set of non-dominated

solutions which present trade-offs among the different objectives. A solution is said to be non-dominated if it is not worse than another solution in all its objectives and it is better with respect to at least one objective (Deb, 2001).

A number of earlier studies on the optimization of the styrene process were in fact single objective optimizations. In 1969, Sheel and Crowe employed a profit objective optimization to evaluate adiabatic and steam-injected reactor configurations where a fraction of the steam was added further along the reactor bed. They selected steam temperature, steam flow rate and reactor length as the decision variables. Later Clough and Ramirez (1976) proposed another profit function with different decision variables: the steam to ethyl benzene ratio, ethyl benzene pre-heater exit temperature, and steam temperature. In both studies, better results were obtained using the steam-injected reactor, which led Clough and Ramirez (1976) to construct a pilot plant to validate their results.

In another study, Sheppard et al. (1986) used an objective profit function to compare the effect of the selectivity and activity of the catalyst for both adiabatic and steam-injected reactors. The profit function had two decision variables: steam to ethyl benzene ratio and steam inlet temperature. It was shown that the selectivity of the catalyst rather than its activity had greater impact on the profitability of the process.

Although single objective optimization has been often used in the literature, this method suffers from several disadvantages such as the lack of information about the trade-offs amongst various competing objectives and the difficulty to assign the relative weighting to each individual objective in a single profit function (Deb, 2001; Haupt and Haupt, 2004).

In recent years, significant progress has been made in multiobjective optimization and its applications in chemical engineering. Multiobjective optimization advantages include the generation of multiple Pareto-optimal solutions that give the decision maker or expert a global perspective about trade-offs between conflicting objectives, the ability to optimize functions without requiring information about function derivatives and therefore application in non-convex, non-concave and discontinuous problems (Deb, 2001; Haupt and Haupt, 2004).

Yee et al. (2003) were the first to use multiobjective optimization to determine the optimal design and operating conditions for both adiabatic and steam-injected industrial styrene reactors. They selected a non-dominated sorted genetic algorithm (NSGA) with productivity,

selectivity, and yield as the objectives and four decision variables namely the temperature of ethyl benzene, steam to ethyl benzene ratio, pressure and initial molar flow rate of ethyl benzene.

In 2005, Babu et al. carried out a similar multiobjective optimization of an adiabatic industrial styrene reactor with the multiobjective differential evolution (MODE) to obtain the optimal operating conditions of the adiabatic styrene packed bed reactor. Using the same objectives and decision variables as those of Yee et al. (2003), they reported an improvement in circumscribing the Pareto domain.

In addition, a multiobjective optimization study on the styrene production process was performed by Tarafdar et al. (2005) with the elitist non-dominated sorting genetic algorithm (NSGA-II). The objectives were to maximize the styrene flow rate and selectivity, and to minimize the total heat duty. Three reactor configurations were considered: single bed, steam-injected, and double bed with interheating. Their results indicated that the heat duty of a double bed reactor with interheating was comparable to that of the steam-injected reactor but lower than the single bed reactor (Tarafdar et al., 2005).

Abdollahi et al. (2007) carried a multiobjective optimization of three radial flow reactors in series through an oxidative reheat process using the Levenberg-Marquardt algorithm. The objective variables were the yield and selectivity of styrene. The design variables consisted of the steam flow rate into the second and third reactors and the fraction of oxygen injected to the secondary injection port of the second reactor. When compared to industrial plant data, their results indicated an improvement in the styrene selectivity and yield.

More recently Gujarathi and Babu (2010) reported another multiobjective optimization study of the adiabatic and steam-injected styrene reactors using MODE, with the temperature of steam going into the reactor as an additional decision variable. Their results indicated that some improvement was required in the MODE algorithm because it was unable to generate a Pareto domain with a diverse set of non-dominated solutions in the case of the optimization of styrene yield and productivity. For the adiabatic reactor, 14 non-dominated solutions were generated, and for the steam-injected configuration only 4 solutions were generated (Gujarathi and Babu, 2010). They reported that MODE is able to generate better optimal solutions than previously published results (Yee et al., 2003; Babu et al., 2005) although they did not mention the values of the steam temperature that led to their optimal solutions.

When solving multiobjective problems, optimization algorithms face two challenges. First, the obtained non-dominated solutions should be as close as possible to the true Pareto domain, and second, the non-dominated solutions should have diversity and variation to adequately cover the objective space (Zitzler et al., 1999; Deb, 2001). In this study, the dual population evolutionary algorithm (DPEA) is applied to optimize the productivity, yield and selectivity of an industrial styrene reactor. DPEA has been successfully used in the past for numerous engineering problems (Halsall-Whitney et al., 2003; Viennet et al., 1996; Thibault, 2008). This algorithm is presented in the following section. To evaluate the robustness and versatility of the algorithm, two- and three-objective optimization case studies are considered with three different styrene reactor configurations: adiabatic, steam-injected and isothermal.

Although significant effort has been devoted to the multiobjective optimization of the styrene process and the generation of the Pareto domain during the last decade, much less attention has so far been paid to ranking the Pareto domain based on the preferences of a decision maker or an expert. Previous multiobjective optimization studies used a simple profit function to rank the Pareto-optimal solutions.

Many studies exist in the literature on incorporating the conscious as well as intuitive preferences of an expert to rank the Pareto domain (Brans et al., 1984; Derot et al., 1997; Doumpos et al., 2002; Halsall-Whitney, 2004; Scarelli et al., 2002; Thibault, 2008; Triantaphyllou, 2000). Among the many ranking methods used to transform the preferences of an expert to a set of rules for ranking the Pareto domain, the net flow method (NFM) is considered in this investigation.

This paper briefly describes the models used for simulating the styrene manufacturing process and the methods for generating the Pareto domain using the DPEA and for ranking the Pareto domain using the NFM. Results of the optimization study are discussed and the best optimal operating conditions are compared with previously published literature values for the catalytic dehydrogenation of ethyl benzene in both adiabatic and steam-injected reactors (Yee et al., 2003; Babu et al., 2005).

2.2 Description of the process and methods

2.2.1 Process overview

A process flow diagram of the manufacturing of styrene by the catalytic dehydrogenation of ethyl benzene to produce styrene is shown in Figure 2.1 (Li and Hubbel, 1982; Chen et al., 2006; Denis and Castor, 1992) and has been described in Yee et al. (2003). After mixing fresh ethyl benzene with recycled ethyl benzene and steam, the mixture is preheated with the reactor effluent in heat exchangers. The temperature of the mixture is then raised above 857 K by mixing with superheated steam before entering the fixed bed catalytic reactor (Li et al., 1982; Denis et al., 1992). In addition to providing the required heat of reaction, superheated steam prevents coke formation and reduces the partial pressure of styrene and hydrogen, thereby favouring the forward reaction to produce styrene. The steam to ethyl benzene molar ratio in the feed is an important factor in the design and operation of the reactor, and is typically in the range of 7 to 20 (Yee et al., 2003). The reactor effluent is cooled in a series of heat exchangers, preheating the ethyl benzene-steam feed mixture, and then sent to the separation section to separate the valuable styrene product from the by-products present in the reactor effluent stream.

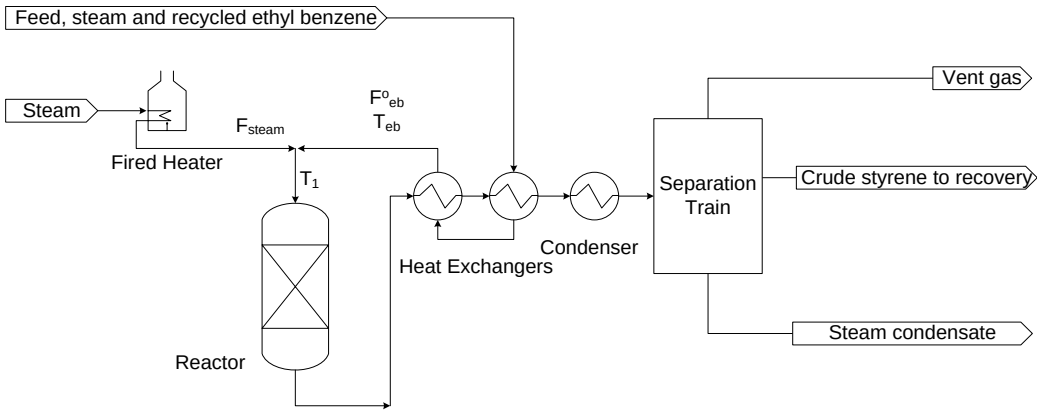

Figure 2.1 - Schematic diagram of the manufacture of styrene by the catalytic dehydrogenation of ethyl benzene.

2.2.2 Reactor modeling and simulation

Knowledge of the styrene reaction kinetics is essential for not only modeling the styrene packed bed reactor, but also for understanding and comparing the results of the multiobjective optimization with industrial data. There are numerous published studies on the kinetics and

modeling of the catalytic dehydrogenation of ethyl benzene to produce styrene. Studies on kinetics of the catalytic dehydrogenation of styrene were pioneered by Wenner et al. (1948) who produced rate data from experiments for two types of catalysts. However, it was not until 1969 that the first reactor modeling, simulation and optimization of the styrene reactor using a pseudo homogenous model have been reported by Sheel and Crowe (1969). They obtained the reaction kinetics and heat of reaction for an industrial adiabatic styrene reactor with Shell 105 catalyst, a promoted iron-oxide-potassium catalyst (62% Fe_2O_3, 36% K_2CO_3, and 2% Cr_2O_3). Later, Sheppard et al. (1986) determined several reaction kinetics models based on manufacturers' data for the Shell 105 and 015 catalysts.

Based on the industrial data reported by Sheel and Crowe (1969), Elnashaie et al. (1993) developed a heterogeneous model to take into consideration diffusion into the catalyst pellet. Abdalla et al. (1994) developed kinetics data for a pseudo-homogeneous and heterogeneous model of three promoted iron oxide catalysts. The kinetics of the catalytic dehydrogenation of ethyl benzene to styrene was also studied in a composite palladium membrane reactor by Hermann et al. (1997) who published a mathematical simulation. More recently, Lee and Froment (2008) reported kinetics using a heterogeneous model for a potassium-promoter iron catalyst.

Among the kinetic models, the pseudo homogeneous model developed by Sheel and Crowe (1969) has been widely used in the literature for multiobjective optimization of the styrene industrial reactor (Yee et al., 2003; Babu et al., 2005; Tarafdar et al., 2005; Gujarathi and Babu, 2010). This is due to the fact that the pseudo-homogeneous and heterogeneous models give close results to the homogeneous model and requires significantly less development and computing time (Yee et al., 2003; Babu et al., 2005). Since the kinetic expressions for the pseudo-homogeneous model were obtained experimentally from an industrial reactor, it is important to emphasize that they are valid for the design and operating conditions of that reactor.

The six main reactions occurring in the styrene reactor are:

$$C_6H_5CH_2CH_3 \Leftrightarrow C_6H_5CHCH_2 + H_2 \quad (2.1)$$

$$C_6H_5CH_2CH_3 \rightarrow C_6H_6 + C_2H_4 \quad (2.2)$$

$$C_6H_5CH_2CH_3 + H_2 \rightarrow C_6H_5CH_3 + CH_4 \quad (2.3)$$

$$2H_2O + C_2H_4 \rightarrow 2CO + 4H_2 \quad (2.4)$$

$$H_2O + CH_4 \rightarrow CO + 3H_2 \quad (2.5)$$

$$H_2O + CO \rightarrow CO_2 + H_2 \quad (2.6)$$

The reaction of the dehydrogenation of ethyl benzene (Eq. (2.1)) is an endothermic reversible reaction catalyzed by an iron oxide-potassium oxide catalyst. Low pressure and high temperature shift the thermodynamic equilibrium towards the styrene product as it produces two moles of product for every mole of reactant. Although the equilibrium conversion of ethyl benzene can reach 80% (Yee et al., 2003), the time and temperature required to achieve such a high conversion would result in the thermal cracking of the catalyst. In addition, the styrene yield is further lowered by competing side reactions (Eqs. (2.2) and (2.3)) where benzene and toluene are produced. The rate of by-products formation increases with temperature and, as a result, there is a compromise that must be struck in choosing the operating temperature to maximize the styrene conversion. Furthermore, the reactor effluent must have a high styrene yield compared to the by-products to make the separation downstream easier and lower in costs. This places strong requirements on the catalyst to achieve high styrene selectivity and yield at low temperatures.

To model the industrial styrene reactor using the pseudo homogeneous model (Sheel and Crowe, 1969), it was assumed that the styrene packed bed behaves as an ideal plug flow reactor and the kinetic rate expressions account for the mass transfer within the catalyst pellets. Appendix A lists the rate equations used to simulate the industrial reactor. The design and operating conditions were the industrial ones given by Sheel and Crowe (1969), and corrected by Crowe (1992). Additional data was obtained from Elnashaie and Elshishini (1994). As mentioned earlier, these rate expressions are valid only for the particle size and design and operating conditions that prevailed in the industrial reactor.

Simulations were performed on a personal computer with Intel Core 2 Duo CPU T5450 of 1.66 and 1.33 GHz and 2.00 GB of RAM. In order to solve the system of eight differential equations, the subroutine ODE 45 in MATLAB was invoked to carry out the IV-order Runge-Kutta method, as it was done in previous multiobjective optimization studies.

A comparison between the simulation using the reported data for the industrial packed bed reactor (Sheel and Crowe, 1969) and previous simulations reported in the literature (Yee et al., 2003; Babu et al., 2005) is presented in Table 2.1. All simulation results are very close to each other and to the industrial data. Simulation values obtained in the present study were

slightly closer to the industrial data. Yee et al. (2003) used the kinetics and property data from Elnashaie and Elshishini (1994) although some errors were found in the frequency factor for the first reaction and constants for molar heat capacities of the components. Instead, Babu et al. (2005) relied on the values of constants for molar heat capacity and frequency factors from Smith and Van Ness (1975) for organic species and Elnashaie and Elshishini (1994) for inorganic species. In this simulation, the frequency factors and activation energy values for the six reactions were obtained from the original source (Sheel and Crowe, 1969; Elnashaie and Elshishini, 1994) and the molar heat capacity constants for all species were taken from Smith et al. (2005).

Table 2.1 - Comparison of the simulation values with the industrial data (Sheel and Crowe, 1969; Yee et al., 2003; Babu et al., 2005).

Quantity at reactor exit	Industrial data	Yee et al. (2003)	Babu et al. (2005)	Present study
Exit pressure (bar)	2.32	2.33	2.33	2.32
Exit temperature (K)	850.00	849.75	850.08	849.94
Ethyl benzene conversion (%)	47.25	46.74	46.78	46.84
Ethyl benzene flow rate (kmol/h)	19.45	19.63	19.61	19.60
Styrene flow rate (kmol/h)	15.57	15.40	15.37	15.42
Benzene flow rate (kmol/h)	1.50	1.44	1.46	1.45
Toluene flow rate (kmol/h)	2.03	2.05	2.07	2.05

2.2.3 Multiobjective optimization

The objectives used in this multiobjective optimization of styrene are the maximization of styrene productivity (F_{st}), selectivity (S_{st}) and yield (Y_{st}). These objectives, some of which are conflicting, were used in previous optimization studies (Yee et al., 2003; Babu et al., 2005; Gujarathi and Babu, 2010). High values of the productivity and yield are desired since they are strongly correlated with the profitability of the plant. In addition, a high selectivity is also desired to reduce the size of the separation units downstream of the reactor and, as a result, reduce both the capital and operating costs. These three objectives functions are defined by Equations (2.7)-(2.9):

$$Max\ f_1 = F_{st} \tag{2.7}$$

$$Max\ f_2 = S_{st} = \frac{F_{st} - F_{st}^{o}}{F_{eb}^{o} - F_{eb}} \tag{2.8}$$

$$Max\ f_3 = Y_{st} = \frac{F_{st} - F_{st}^o}{F_{eb}^o} \tag{2.9}$$

This study considered four decision variables to find the optimal operating conditions of the adiabatic and isothermal reactor configurations. These decision variables are listed, along with their range and units, in Table 2.2. In order to be consistent with previous optimization studies, the ranges of the decision variables are the same as the one reported by Yee et al. (2003) and Babu et al. (2005). The ethyl benzene feed temperature (T_{eb}) range is set between 550 and 800 K. This is due to the fact that a T_{eb} value below 550 K would result in a low temperature of ethyl benzene and steam mixture at the entrance of the reactor (T_1) for reaction to occur. However, at values of T_{eb} above 800 K, there is an increase in by-product formation from competing side reactions that significantly decrease styrene yield (Clough et al., 1976).

The inlet pressure (P) was varied from 1 to 2.63 bars. This is in accordance with industrial practice (Yee et al., 2003). The steam over reactant ratio (*SOR*) ranged between 7 and 20. At *SOR* values below 7, coke deposits would form on the catalyst surface and decrease ethyl benzene conversion. However, if *SOR* is increased to above 20, the process might not be profitable as additional costs are associated with excess steam and its separation further downstream. The initial ethyl benzene flow rate F_{eb}^o is set between -25% and +10% of the nominal value of 36.87 kmol/h, as it is most often easier to scale down than to scale up production capacity in industry (Yee et al., 2003).

Table 2.2 - Ranges of decision variables for the multiobjective optimization of the adiabatic and isothermal reactors.

Variables	**Identifier**	**Range**	
		Adiabatic and isothermal	Steam injected
Ethyl benzene feed temperature	T_{eb} (K)	550-800	550-800
Inlet pressure	P (bar)	1-2.63	1-2.63
Steam to ethyl benzene molar ratio	*SOR*	7-20	7-20
Initial ethyl benzene flow rate	F^o_{eb} (kmol/h)	27.56-40.56	27.56-40.56
Fraction of steam used at the reactor inlet	δ	-	0.1-1
Relative location of the injection port	λ	-	0.1-1

The isothermal reactor configuration, although practically infeasible for this endothermic reaction as the temperature along the packed bed would have to be maintained constant, is included as a limiting case to determine the maximum styrene yield of all three configurations.

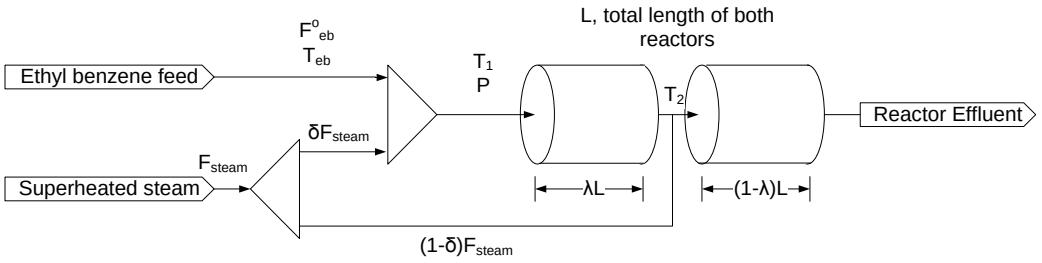

Figure 2.2 - Schematic diagram of a styrene reactor with steam-injection along the reactor length.

For the case of the steam-injected configuration illustrated in Figure 2.2, a fraction (δ) of the steam is mixed with ethyl benzene at the reactor entrance while the remaining steam is injected at a fraction (λ) of the total reactor length. This is different from the adiabatic configuration, where steam is mixed with ethyl benzene stream only at the reactor entrance to supply the endothermic heat of reaction. It should be mentioned that the adiabatic reactor is a special case of the steam-injected reactor where δ is equal to 1.

The selected decision variables for the steam-injected reactor shown in Table 2.2 consist of the previous four decision variables plus two additional variables: δ and λ. The bounds were the same as in previous optimization studies (Yee et al., 2003; Babu et al., 2005; Gujarathi and Babu, 2010).

It is common practice in industry to add a fraction of steam to the ethyl benzene feed to prevent its decomposition before the reactor. In this study, 50.4 kmol/h of steam are added to the ethyl benzene feed to be consistent with previous multiobjective studies (Yee et al., 2003; Babu et al., 2005; Gujarathi and Babu, 2010).

A schematic block flow diagram of the decision variables and objectives used for the multiobjective optimization of styrene for the steam-injected process is shown in Figure 2.3.

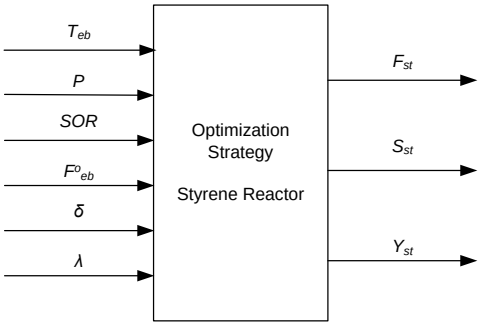

Figure 2.3 - Objectives used during the development of the Pareto domain and optimization of the styrene reactor.

In addition to the above constraints on the decision variables, additional constraints are placed on the total steam flow rate (F_{steam}), the temperature at the entrance of the reactor (T_1), and the temperature at the injection port (T_2). These constraints are based on the size and temperature limitations of the reactor (Yee et al., 2003).

$$F_{steam} < 454\ kmol/h \tag{2.10}$$

$$850 < T_1 < 925\ K \tag{2.11}$$

$$850 < T_2 < 925\ K \tag{2.12}$$

The upper bound on F_{steam} is set to 454 kmol/h to prevent high steam throughput in the condenser which may exceed its design specifications (Sheel and Crowe, 1969). The lower bound of 850 K on T_1 and T_2 is to ensure sufficiently high reaction rates and the upper bound of 925 K is to prevent the deactivation of catalyst in the fixed bed reactor (Clough et al., 1976). It should be mentioned that Eq. (2.12) does not apply for adiabatic reactor and isothermal reactors.

2.2.4 Dual population evolutionary algorithm

The Pareto domain is the set of all feasible solutions that are non-dominated by other solutions in that set. A solution X_1 is said to dominate another solution X_2 if the values of all objectives for X_1 are not worse than those of X_2, and the value of at least one objective for X_1 is better than the corresponding X_2.

Different algorithms exist in the literature to circumscribe the Pareto domain from an initial population of solutions. The algorithm used in this paper is the dual population evolutionary algorithm (DPEA). This algorithm incorporates the concepts of domination to generate the Pareto domain. The general approach used is described as follows (Halsall-Whitney et al., 2003; Viennet et al., 1996; Thibault, 2008):

1. In the first step of the evolutionary genetic algorithm, an initial set of N points is randomly generated. Each of these points consists of the values of the decisions variables (inputs) within their acceptable ranges. In this study, 2500 such points were generated to adequately determine the Pareto domain from their acceptable ranges shown in Table 2.2. At each of these points, the values of the objective functions (outputs) are calculated and each point is initially assigned a domination level of 0.

2. In the next step, the objective functions of all the points are compared to the others (one point versus another at a time) to determine the dominance level of each point. If a point is dominated by another, its domination level is increased by 1. Once the comparison is completed, the points are sorted according to their domination level in an ascending order.
3. The non-dominated points of the population (with domination level of zero) and a portion of the dominated points with the lowest domination levels are retained in the new population (next iteration). Let *N* be the total number of points in the original population (*e.g.*, 2500) and N_0 the number of non-dominated points, then the number of points retained in the new population is given by:

$$N_{keep} = N_0 + INT\left(F_S\left(N - N_0\right)\right) \qquad (2.13)$$

Where F_S is the survival fraction of the least dominated points and ranges from 0 to 1, and *INT(X)* returns the integer value of *X*. In this study, the survival fraction was set to 0.3.

4. This subset of N_{keep} points is then used to find replacements for the discarded points. Each replacement point is found by an interpolation between two randomly selected points, one point from the non-dominated points and one point from the retained fraction of the dominated points, using the following equation.

$$U_v^{I+1} = \phi_v U_{v,i}^I + \left(1 - \phi_v\right) U_{v,j}^I \qquad (2.14)$$

where $U_{v,j}^I$ denotes the v^{th} decision variable of point *j* and at I^{th} iteration. ϕ_v is a randomly selected number between 0 and 1 and is different for every decision variable and generation (iteration). The name dual population evolutionary algorithm (DPEA) stems from the fact that one point is drawn from each of the two populations comprised of the non-dominated points and retained dominated points.

5. The outputs are then calculated for each of the replacement points (that have been added to the N_{keep} points). The dominance level of the *N* points in the new generation (iteration) is set back to zero.

Steps (2) through (5) are repeated until *N* non-dominated points are obtained.

As discussed in the previous section, the optimization problem involves constraints on some operating variables (Eqs. 10-12). In this study, a solution is discarded if it was outside the constraint boundaries to prevent it from mating in the next generation.

2.2.5 Net flow method

Once the Pareto domain has been circumscribed, several methods can be used to rank the Pareto-optimal solutions based on decision-maker preferences. Some of these techniques are compromise programming (Yu, 1973, Zeleny, 1973), marginal rate of substitution approach (Miettinen, 1999), pseudo-weight vector approach (Deb, 2001), net flow method (NFM) and rough set method (RSM) (Thibault, 2008). In this investigation, the net flow method (NFM), considered to be a very robust method, was used to rank the Pareto domain (Brans et al., 1984; Derot et al., 1997; Doumpos et al., 2002; Halsall-Whitney, 2004; Scarelli et al., 2002; Triantaphyllou, 2000). The NFM algorithm, a hybrid of PROMETHEE II and ELECTRE III proposed by Kiss et al. (2002), is described in details in Thibault (2008). In NFM, the knowledge of the decision maker or expert is included in the optimization process via four ranking parameters namely: relative weight (W_m), indifference threshold (Q_m), preference threshold (P_m), and veto threshold (V_m).

1. The first parameter is the relative weight W_m that is assigned to each of the M objective function or criterion such that:

$$\sum_{m=1}^{M} W_m = 1 \qquad (2.15)$$

2. The second parameter is the indifference threshold Q_m. It refers to the range of variation within each objective function for which the decision-maker does not favour one solution over another.
3. The third parameter is the preference threshold P_m. It represents the difference between two values of a given objective for which the decision maker favours one solution over the other.
4. The fourth parameter is the veto threshold V_m, which serves to ban a solution relative to another solution if the difference between the values of an objective exceeds this threshold even for only one objective function or criterion.

The values of the three thresholds are set by the decision-maker to rank the Pareto domain (Roy, 1978) such that: $0 \le Q_m \le P_m \le V_m$. The procedure to rank the Pareto domain is summarised below:

1. In the first step, the differences between an objective function is calculated for all pairs of solutions by using the following equation. This calculation is performed for all other objective functions. In Equation (2.16), *i* and *j* refer to solutions *i* and *j*.

$$\Delta_m[i, j] = F_m(i) - F_m(j) \begin{cases} i \in [1, N] \\ j \in [1, N] \\ m \in [1, M] \end{cases} \qquad (2.16)$$

   where *N* is the total number of solutions in the Pareto domain. The above expression for $\Delta_m[i, j]$ is for cases where the objective function is being minimized. For maximization cases, the right hand side of the equation is multiplied by -1.

2. The second step is to compute the individual concordance index $c_m[i, j]$ for each objective *m* using the indifference and preference thresholds. The equation is given by Roy (1978):

$$c_m[i, j] = \begin{cases} 1 & if \ \Delta_m[i, j] \le Q_m \\ \dfrac{P_m - \Delta_m[i, j]}{P_m - Q_m} & if \ Q_m < \Delta_m[i, j] \le P_m \\ 0 & if \ \Delta_m[i, j] > P_m \end{cases} \qquad (2.17)$$

   The individual concordance index determines whether solution *i* is significantly better than solution *j* with respect to a given objective *m*. If the difference $\Delta_m[i, j]$ is less than the indifference threshold Q_m, the corresponding individual concordance index $c_m[i, j]$ is set to one. If $\Delta_m[i, j]$ is between the indifference and preference thresholds, it varies linearly from 1 to 0. If the $\Delta_m[i, j]$ value is larger than the preference threshold, the individual concordance index is set to 0.

3. The third step consists of calculating the global concordance index $C[i, j]$ when comparing solution *i* to solution *j*. It corresponds to the weighted sum of individual concordance indices:

$$C[i, j] = \sum_{m=1}^{M} W_m c_m[i, j] \qquad \begin{cases} i \in [1, N] \\ j \in [1, N] \end{cases} \qquad (2.18)$$

4. The fourth step is to determine the discordance index $D_m[i, j]$ using the preference and veto thresholds:

$$D_m[i, j] = \begin{cases} 0 & if\ \ \Delta_m[i, j] \le P_m \\ \dfrac{\Delta_m[i, j] - P_m}{V_m - P_m} & if\ \ P_m < \Delta_m[i, j] \le V_m \\ 1 & if\ \ \Delta_m[i, j] > V_m \end{cases} \qquad (2.19)$$

The discordance index determines whether solution *i* is significantly worse than solution *j* for a given objective *m* (Roy, 1978). If the difference is smaller than the preference threshold, the discordance index $D_m[i, j]$ is set to zero. If the difference $\Delta_m[i, j]$ is between the preference and veto thresholds, $D_m[i, j]$ varies linearly from 0 to 1. Otherwise, if the difference is larger than the veto threshold the discordance index is set to 1.

5. The fifth step is to compute the outranking matrix $\sigma[i, j]$ using the global concordance $C[i, j]$ and discordance $D_m[i, j]$ according to the following equation:

$$\sigma[i, j] = C[i, j]\left(\prod_{m=1}^{M} \left(1 - \left(D_m[i, j]\right)\right)^3 \right) \qquad \begin{cases} i \in [1, N] \\ j \in [1, N] \end{cases} \qquad (2.20)$$

The value of $\sigma[i, j]$ determines whether solution *i* outranks solution *j* in terms of the *M* objective functions. A value of $\sigma[i, j]$ near 0 signifies that solution *j* outranks solution *i*, whereas a value near 1 means that solution *i* outranks solution *j* or is close in value to solution *j*. When there are no discordant objectives, the outranking matrix is the same as the global concordance matrix. Although it should be mentioned that one discordant objective is sufficient for an element of the outranking matrix to be equal to zero. This is referred to as the outranking relation, which depends on the three thresholds mentioned earlier (Roy, 1978).

6. The last step is to assign a score to the solutions of the Pareto domain using the individual outranking elements. The score is calculated using Equation (2.21):

$$\sigma_i = \sum_{j=1}^{N} \sigma[i, j] - \sum_{j=1}^{N} \sigma[j, i] \qquad (2.21)$$

where the first term determines the relationship between the element *i* and the rest of the solutions in the Pareto domain, whereas the second term determines the relationship between

the rest of solutions and solution *i*. The solutions are then ranked from the highest to the lowest value. The solution with the highest value corresponds to the solution that best satisfies the preferences of the decision maker.

2.3 Results and discussion

In this paper, the dual population evolutionary algorithm (DPEA) is used to circumscribe the Pareto domain in view of optimizing the productivity F_{st}, the yield Y_{st} and the selectivity S_{st} of an industrial-scale styrene reactor. Two- and three-objective optimization case studies were carried out for the three different configurations of the reactor, namely adiabatic, steam-injected and isothermal. These test case studies were selected to compare the ability and the robustness of DPEA to generate a well-defined Pareto domain and the range of solutions in the Pareto domain.

The design parameters and operating conditions of the industrial styrene packed bed reactor are given in Table A.4. The inlet temperature T_1 of the ethyl benzene and steam mixture is set to 922.59 K, identical to the industrial value used by Sheel and Crowe (1969). During the optimization, variables T_{eb} and *SOR* are decision variables (inputs) and the temperature of superheated steam is fixed at 1025 K at a pressure of 600 kPa (Clough et al., 1976). The inlet temperature T_1 is obtained by performing an energy balance following the random selection of T_{eb}, *SOR*, and δ.

2.3.1 Case 1: Maximization of F_{st} and S_{st}

In the first case study, two conflicting objectives, the selectivity S_{st} and productivity F_{st}, were maximized simultaneously. The Pareto domains obtained for the adiabatic, the steam-injected, and the isothermal reactor configurations using the evolutionary algorithm DPEA are shown in Figure 2.4. The industrial operating point is also shown on the graph. It is interesting to observe that based on the reactor model the industrial solution is a dominated solution with respect to all three Pareto domains.

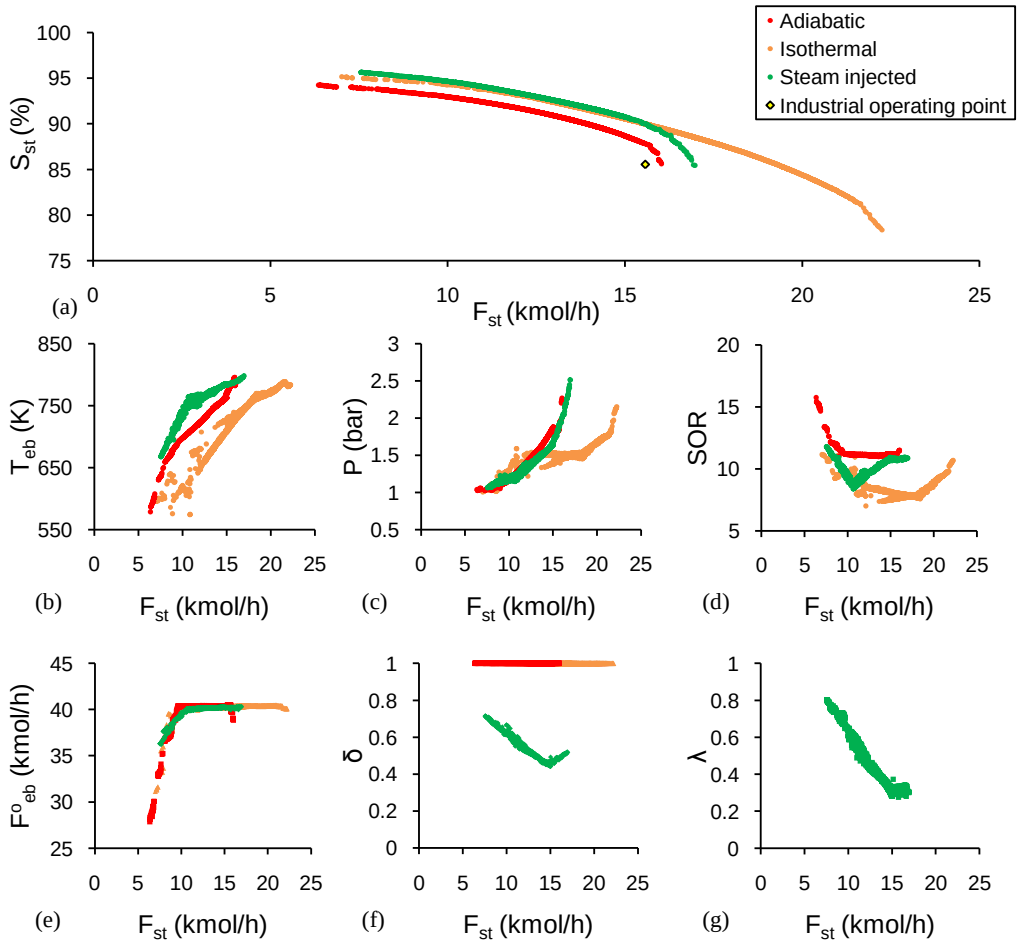

Figure 2.4 - (a) Pareto domains generated using DPEA for case study 1; (b-g) Plots of the decision variables as a function the production rate.

The highest values of the productivity were observed for the isothermal reactor configuration followed by the steam-injected configuration and lastly the adiabatic configuration. With respect to selectivity, the steam-injected configuration had the highest value followed by the isothermal and the adiabatic reactors. Although, the isothermal reactor solutions can reach much higher styrene productivity (up to 22.25 kmol/h), the steam-injected configuration dominated the isothermal configuration until a productivity of 15.63 kmol/h. This originally came as a surprise, as one might think that the isothermal configuration would have the highest productivity and selectivity and thus would dominate the steam-injected solutions.

To gain a greater insight, the solutions in the Pareto domains of the steam-injected and isothermal reactors with equal productivity F_{st} were compared. The decision and objective

variables for two non-dominated solutions for the steam-injected and isothermal configurations with the same styrene productivity of 15.01 kmol/h are listed in Table 2.3. The corresponding profiles of temperature, pressure, and the molar flow rates of styrene, benzene and toluene along the length of the reactor are plotted in Figure 2.5.

Table 2.3 - Comparison of steam-injected and isothermal solutions with equal styrene productivity in case study 1.

Parameter	Steam-injected	Isothermal
T_{eb}(K)	785.38	711.37
P (bar)	1.63	1.50
SOR	10.92	8.12
F^{o}_{eb} (kmol/h)	40.31	40.39
δ	0.44	1
λ	0.28	-
F_{st} (kmol/h)	15.01	15.01
S_{st} (%)	90.74	90.54
Y_{st} (%)	35.57	35.50
F_{bz} (kmol/h)	0.95	0.97
F_{tol} (kmol/h)	1.50	1.52

Figure 2.5a shows the temperature profile along the length of the reactor for the isothermal and steam-injected configurations with the same styrene productivity of 15.01 kmol/h and decision variables listed in Table 2.3. For the steam-injected configuration, a fraction of the superheated steam is added at the entrance of the reactor to increase the initial temperature. The temperature decreases until the injection port at which point the remaining fraction of the superheated steam is added to increase the temperature. It is interesting to note that a higher temperature at the point of injection than at the entrance of the reactor is preferred to reach optimal conditions. The average temperature along the bed is higher for the isothermal configuration than for the steam-injected reactor. It is also observed that higher pressure prevails for the steam-injected configuration to increase the styrene flow rate compared to the isothermal configuration. The steam-injected configuration achieved higher styrene selectivity by having a lower molar flow rate of benzene and toluene at the end of the reactor. This is due to the inherent kinetics of the chemical reactions involved. Given that the frequency factor A as well as the activation energy E_a for reactions (2) and (3) are higher than reaction (1) as shown in Table A.1, the benzene and toluene side reactions have a higher dependency on temperature. In the case of the steam-injected configuration, the rate constant of the benzene and toluene producing reaction will decrease more rapidly than that of styrene with the temperature decrease before and after the injection port, resulting in higher styrene selectivity. One might determine the optimal number of

reactor beds to improve the productivity while keeping a higher selectivity than the isothermal configuration.

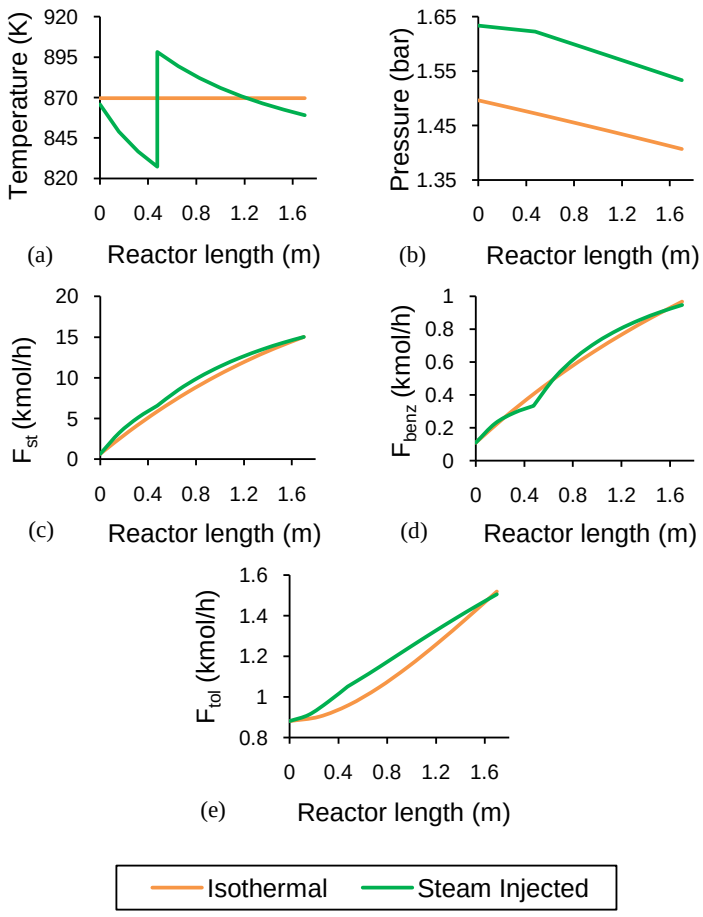

Figure 2.5 - Profiles of the (a) temperature; (b) pressure; (c) styrene (d) benzene and (e) toluene molar flow rates along the reactor for case study 1 under the operating conditions listed in Table 2.3.

The Pareto domain obtained for the adiabatic and steam-injected configurations are similar to those obtained by Babu et al. (2005) and Yee et al. (2003). Because the number of points in the Pareto domain is much higher in this study, the Pareto domain is better circumscribed and the range of the two objective functions are larger than previously obtained with $F_{st} \in$[6.39,16.03] and [7.01,16.97] kmol/h for adiabatic and the steam-injected

configurations, respectively. The corresponding ranges for the selectivity S_{st} are [85.06, 94.29] and [84.99, 95.16] %.

The values of the decision variables (T_{eb}, P, SOR, F_{eb}^{o}, δ, and λ) corresponding to the Pareto domains were plotted as a function of the productivity F_{st} and the results are shown in Figures 2.4b-g. It was observed that the values of P, SOR and F_{eb}^{o} were constant for the range of F_{st} from 8 to 14 kmol/h, which is in accordance with previously published results by Yee et al. (2003) and Babu et al. (2005). Outside that range of F_{st} values, the optimal operating conditions started to vary. It was also observed that the temperature of ethyl benzene entering the reactor had an opposing effect on F_{st} and S_{st}. On one hand, increasing the temperature of ethyl benzene entering the reactor increased the productivity F_{st} because of the higher reaction rate. On the other hand, a higher reaction rate for the other reactions led to a decrease of selectivity S_{st}. As shown in Figure 2.4e, the ethyl benzene inlet flow rate F_{eb}^{o} reached the upper bound value. It was also observed that the isothermal configuration has the smallest SOR optimal values followed by steam-injected and adiabatic configurations, respectively. For the isothermal reactor, an additional source of heat would be required to maintain the temperature constant and, as a result, less steam is required for optimal operation. Given that the isothermal configuration is theoretical and not physically feasible, the steam-injected configuration is considered the best alternative. Concerning the steam-injected configuration, the values of δ and λ were found to decrease with the production rate, then to increase at F_{st} above 14.95 kmol/h as shown in Figures 2.4f-g.

For this case study, a simple profit function was used to rank the Pareto domain. It is defined as the difference between the revenue generated from selling the desired product styrene and the benzene and toluene by-products minus the cost of the raw material ethyl benzene and steam. This method has been used in previous studies to rank the Pareto domain of the adiabatic and steam-injected styrene reactors (Yee et al., 2003; Babu et al., 2005; Gujarathi and Babu, 2010). The simple profit function serves as a rapid guideline for the decision maker. It does not include the operating costs and separation costs involved downstream of the reactor to purify styrene from the by-products and unreacted feed. The cost function is given by:

$$Profit = F_{st}C_{st} + F_{bz}C_{bz} + F_{tol}C_{tol} - \left(F_{eb}^{o} - F_{eb}\right)C_{eb} - F_{steam}C_{steam} \qquad (2.22)$$

where C_{st}, C_{bz}, C_{tol}, C_{eb} and C_{steam} are the cost of styrene ($103/kmol), benzene ($30.8/kmol), toluene ($33.9/kmol), ethyl benzene ($45.6/kmol) and high pressure steam ($0.36/kmol), respectively. F_{st}, F_{bz}, $F_{tol,}$ and F_{steam} are the molar flow rates of styrene, benzene, toluene, and steam, respectively. In order to compare the optimization results of this study with previously published data, identical prices were used (Yee et al., 2003; Babu et al., 2005).

Table 2.4 - Comparison of the optimal operating conditions for the adiabatic reactor with previously published results using the profit function.

Parameter	Case 1			Case 2		Case 3	
	Yee et al. (2003)	Babu et al. (2005)	Present study	Yee et al. (2003)	Present study	Yee et al. (2003)	Present study
T_{eb}(K)	799.98	799.58	795.74	800.00	784.40	776.13	795.74
P (bar)	2.03	1.76	1.98	2.45	2.27	1.99	2.50
SOR	10.94	10.60	10.74	12.47	11.52	13.16	10.70
F^o_{eb} (kmol/h)	40.74	39.87	39.71	35.49	38.86	34.24	39.71
F_{st} (kmol/h)	16.52	15.57	15.92	15.70	16.03	14.51	16.28
S_{st} (%)	86.20	87.58	86.76	83.20	85.61	86.74	83.68
Y_{st} (%)	38.90	37.36	38.41	42.34	39.53	40.44	39.32
F_{bz} (kmol/h)	1.62	1.47	1.49	1.73	1.52	1.46	1.56
F_{tol} (kmol/h)	1.91	1.64	1.83	2.30	2.05	1.65	2.47
Profit ($/h)	817.18	776.23	792.69	764.88	788.07	705.86	805.36

Table 2.5 - Comparison of the optimal operating conditions for the steam-injected reactor with previously published results using the profit function.

Parameter	Case 1		Case 2		Case 3	
	Yee et al. (2003)	Present study	Yee et al. (2003)	Present study	Yee et al. (2003)	Present study
T_{eb}(K)	795.08	794.50	800.00	799.99	791.41	798.95
P (bar)	2.59	2.55	2.63	2.45	2.54	2.57
SOR	10.89	10.89	11.06	11.28	11.30	10.91
F^o_{eb} (kmol/h)	40.36	40.36	40.29	39.09	35.27	40.27
δ	0.52	0.52	0.97	0.54	0.57	0.52
λ	0.30	0.30	0.11	0.17	0.24	0.29
F_{st} (kmol/h)	16.90	16.88	16.79	16.88	15.21	17.00
S_{st} (%)	85.13	85.46	82.60	85.46	85.16	84.99
Y_{st} (%)	40.21	40.18	40.00	41.47	41.23	40.56
F_{bz} (kmol/h)	1.12	1.11	1.71	1.313	1.06	1.15
F_{tol} (kmol/h)	2.71	2.64	2.68	2.43	2.46	2.72
Profit ($/h)	839.23	839.35	822.26	837.80	760.76	844.53

Table 2.6 - Summary of the optimization results for the isothermal reactor using the profit function.

Parameter	Case 1	Case 2	Case 3
T_{eb}(K)	783.94	786.48	783.26
P (bar)	2.16	2.25	2.30
SOR	10.69	10.98	10.60
F^o_{eb} (kmol/h)	40.10	40.09	40.54
F_{st} (kmol/h)	22.25	22.47	22.49
S_{st} (%)	78.36	77.12	77.02
Y_{st} (%)	53.81	54.38	53.83
F_{bz} (kmol/h)	3.53	3.78	3.64
F_{tol} (kmol/h)	3.42	3.68	3.86
Profit ($/h)	1106.11	1108.11	1113.05

Based on the profit function, the optimal solution in the Pareto domain of the adiabatic reactor with the highest profit is \$805.36/kmol where F_{st} is 16.28 kmol/h and S_{st} is 83.68% and Y_{st} is 39.32% whereas for the steam-injected reactor the highest profit is \$844.53 where F_{st} is 17.00 kmol/h and S_{st} is 84.99% and Y_{st} is 40.56%. For the isothermal reactor, it is \$1113.05where F_{st} is 22.49 kmol/h and S_{st} is 77.02% and Y_{st} is 53.83%.. The optimal operating conditions for the adiabatic, steam-injected, and isothermal reactors are listed in Tables 2.4, 2.5, and 2.6, respectively. Results of this investigation show an overall increase in the profitability compared to previously reported data (Yee et al., 2003; Babu et al., 2005). One reason for the higher profit obtained in this investigation is the population size. The large population size provided a better diversity and a more complete coverage of the Pareto domain such that the probability of finding a better solution increases with the population size.

It should be mentioned that the optimal operating conditions reported by Yee et al. (2003) for the first case study of the adiabatic reactor did not obey the constraint of the temperature T_1 at the inlet of the reactor and it was higher than 925 K, nonetheless these values were included for the sake of completeness.

2.3.2 Case 2: Maximization of F_{st} and Y_{st}

In the second case study, a two-objective optimization was carried out to maximize the productivity F_{st} and yield Y_{st}. The Pareto domains for the adiabatic, steam-injected and isothermal reactor configurations containing 2500 non-dominated solutions are plotted in Figure 2.6. Concerning the Pareto domain of the adiabatic configuration $F_{st} \in [12.96,16.03]$ kmol/h and $Y_{st} \in [39.53,43.63]$ %, whereas for the steam-injected configuration $F_{st} \in [14.07,16.88]$ kmol/h and $Y_{st} \in [41.46,47.66]$ %. These results complete the previously published results. Yee et al. (2003) obtained 20 non-dominated solutions for the adiabatic configuration after 100 generations using NGSA-II for a population size of 50 for the case of the adiabatic reactor configuration. On the other hand, Gujarathi and Babu (2010) obtained 14 non-dominated solutions for the adiabatic configuration and 3 non-dominated solutions for the steam-injected configuration after 50 generations using MODE with an initial population of 500.

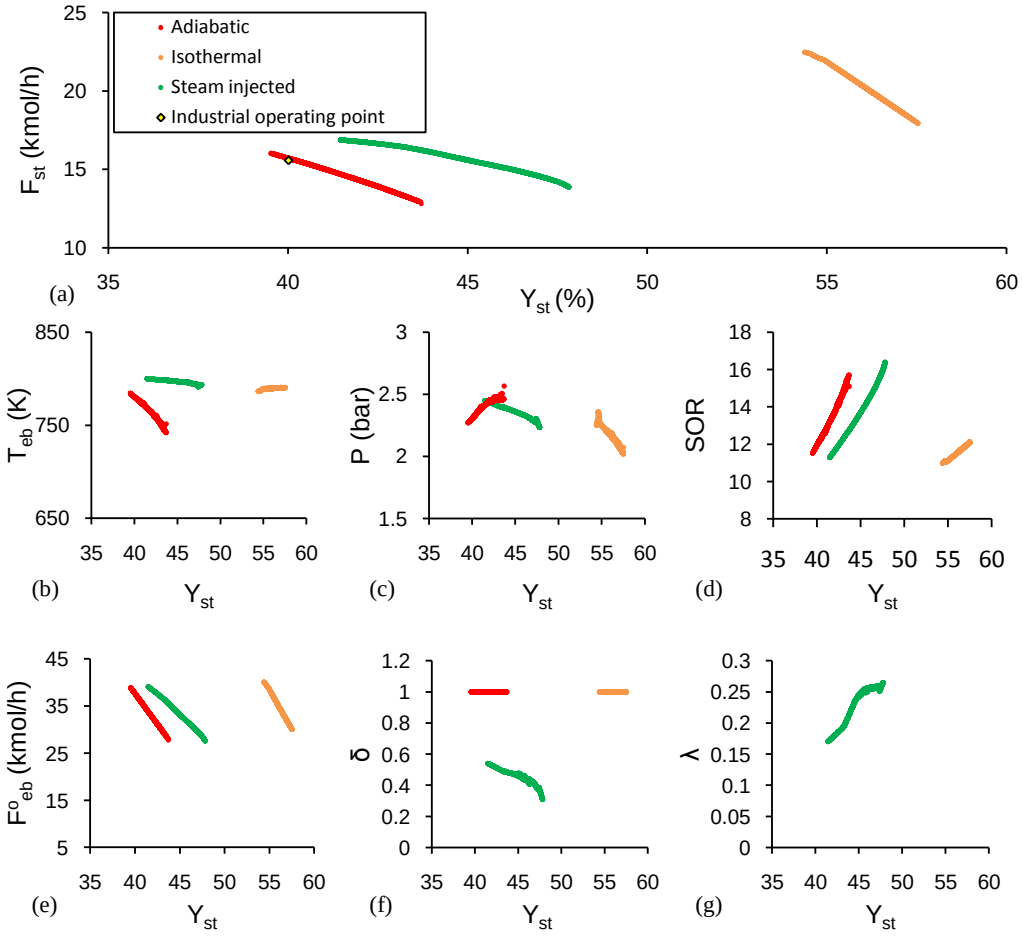

Figure 2.6 - (a) Pareto domains generated using DPEA for study case study 2; (b-g) values of the decision variables as a function the selectivity.

As shown in Figure 2.6, the solutions of the isothermal configuration had by a large margin the highest productivity and selectivity, followed by the steam-injected configuration, and lastly the adiabatic configuration. This was expected since the isothermal reactor is an ideal configuration where the reactor temperature is maintained constant, whereas in the adiabatic configuration the temperature of the reactor decreases continuously along the length of the reactor. The steam-injected is an intermediate in the sense that the temperature originally decreases and then increases sharply at the injection port. As a result, its optimal values are intermediate between those of isothermal and adiabatic configurations.

To understand the effect of decision variables (T_{eb}, P, SOR, F^{o}_{eb}, δ, and λ), their values are plotted against the objective Y_{st} as shown in Figures 2.6b-g. It was found that the value of

F_{eb}^{o} had a positive effect on the productivity and a negative one on the yield. This is expected given that increasing the ethyl benzene inlet flow rate results in a higher styrene production. However, this unfortunately increases the amount of by-products formed and results in a decreased yield. The optimal values of the *P* and *SOR* were also found to increase with the yield.

Furthermore, the adiabatic configuration had higher values for the pressure followed by the steam-injected and isothermal configurations, whereas the isothermal configuration had lower SOR values. The temperature of ethyl benzene feed T_{eb} was found to have a slightly negative correlation with yield of the adiabatic and steam-injected configurations. This is due to the fact that higher inlet temperature favours the formation of not only styrene but also side products such as benzene and toluene. By decreasing the inlet temperature, the reaction kinetics of the styrene side reactions also decrease and therefore the yield of styrene increases. Lower ethyl benzene flow rate F_{eb}^{o} values resulted in higher yields.

The Pareto domain was ranked with respect to the simple profit function (Eq. 2.22) and the best operating conditions are listed in Tables 2.4, 2.5, and 2.6 for the adiabatic, steam-injected and isothermal reactors, respectively. The results showed a small increase in the profit function compared to previously reported operating conditions.

2.3.3 Case 3: Maximization of F_{st}, Y_{st}, and S_{st}

The last case study consisted in the maximization of three objectives namely the productivity F_{st}, selectivity S_{st} and yield Y_{st} for the adiabatic, steam-injected and isothermal reactor configurations. The Pareto domain for the three-objective optimization is a three-dimensional surface. The three two-dimensional projections of the Pareto domains for the three reactor configurations are shown in Figure 2.7. The predicted results show that higher values of F_{st} and Y_{st} are obtained for the isothermal reactor configuration whereas the highest values of S_{st} were obtained for the steam-injected configuration. In addition, Y_{st} and F_{st} can be maximized simultaneously whereas an increase in productivity and yield leads to a decrease in selectivity such that a compromise solution must be found based on the preferences of the decision-maker. When all three objectives are simultaneously maximized, the industrial operating point is now located within the Pareto domain. When comparing the Pareto domain obtained for the adiabatic and steam-injected reactor configurations, higher selectivity, yield and productivity are obtained for the steam-injected configuration. Furthermore, the NFM was used to rank the three Pareto

domains using the parameters in Table 2.7. The choice of the relative weights and thresholds are expert-dependent. It depends on the importance that one would give to each objective and the degree of precision and tolerance relative to each objective. It has a certain level of subjectivity. Slightly higher relative weights were given for the productivity and yield is because they have a greater impact on the profit than selectivity. With respect to the selection of thresholds, the range of values of each objective was used to make an appropriate choice. Results of the ranking are shown in Figure 2.7. The best solutions corresponding to each configuration are listed in Table 2.8.

Table 2.7 - Parameters used for ranking the Pareto domain using the net flow method (NFM).

m	Objective	W_m	Q_m	P_m	V_m
1	F_{st}	0.35	0.5	2	5
2	S_{st}	0.3	0.5	2	5
3	Y_{st}	0.35	1	4	12

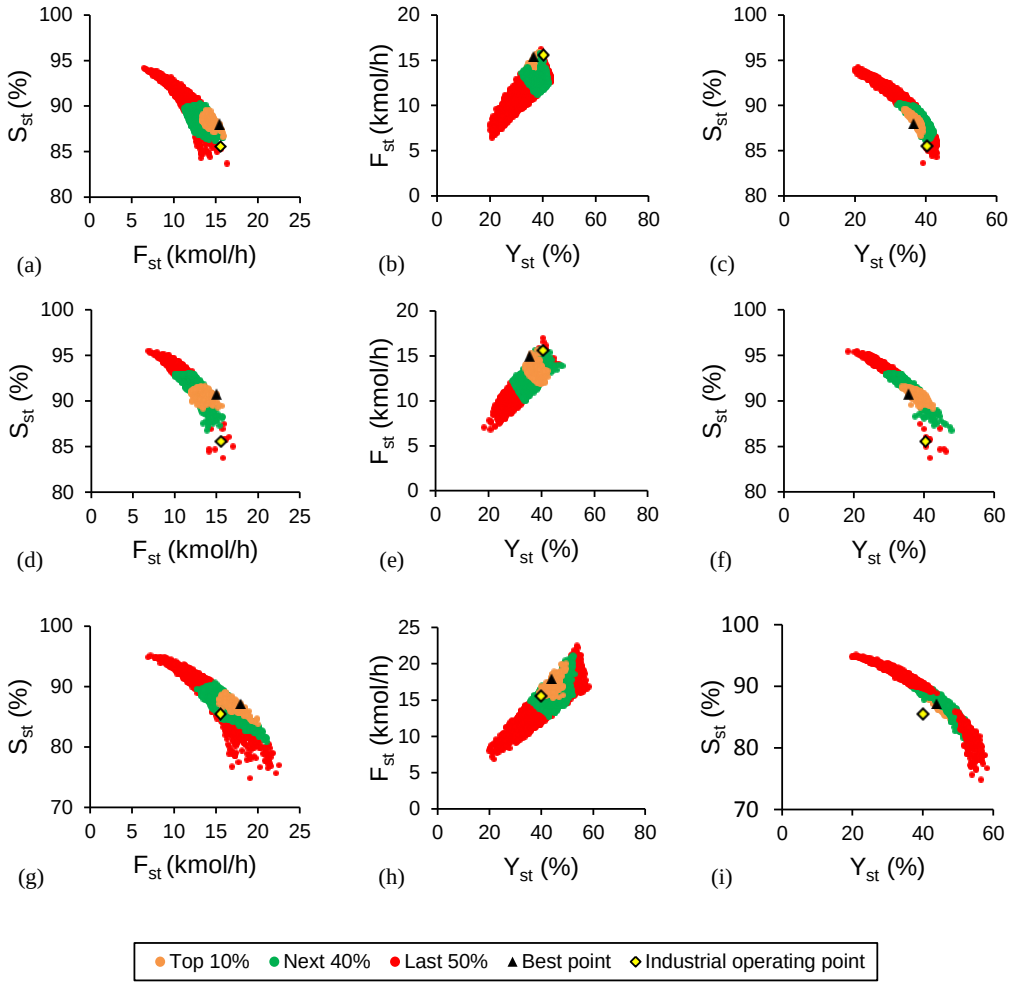

Figure 2.7 - Pareto domains ranked using the net flow method (NFM) for (a-c) adiabatic (d-f) steam-injected and (g-i) isothermal reactors for case study 3.

Table 2.8 - Summary of the optimization results for case study 3 reactor using NFM.

Parameter	Adiabatic	Steam injected	Isothermal
T_{eb} (K)	791.05	785.38	781.31
P (bar)	1.76	1.63	1.35
SOR	10.85	10.93	7.01
F^{o}_{eb} (kmol/h)	38.16	40.31	39.35
δ	-	0.44	-
λ	-	0.28	-
F_{st} (kmol/h)	14.91	15.01	17.94
S_{st} (%)	87.94	90.74	87.15
Y_{st} (%)	37.30	35.57	43.89
F_{bz} (kmol/h)	1.36	0.95	1.62
F_{tol} (kmol/h)	1.58	1.50	1.91

In order to better compare the adiabatic and steam-injected configurations, the decision variables (T_{eb}, P, SOR, F_{eb}^{o}, δ, and λ) corresponding to the ranked Pareto domains were plotted as a function the objective Y_{st} as shown in Figures 2.8 and 2.9.

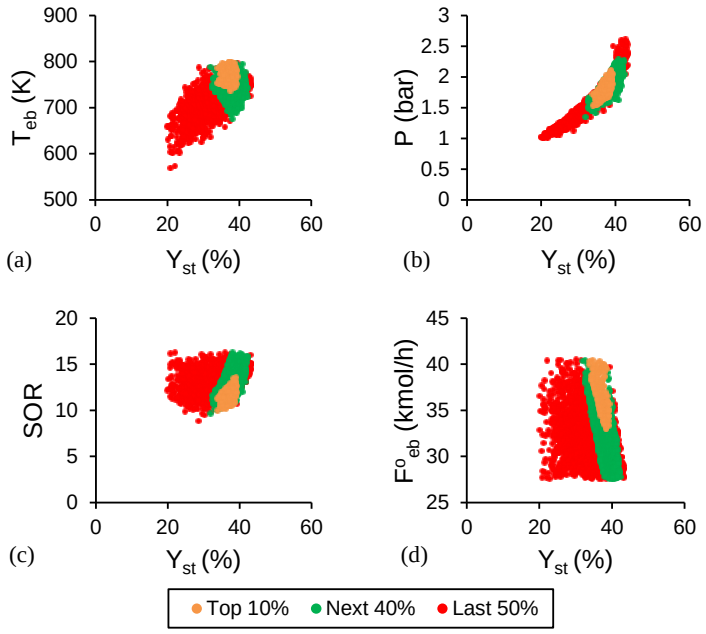

Figure 2.8 - Values of the decision variables as a function of the objective variable Y_{st} for the adiabatic configuration ranked using the net flow method (NFM).

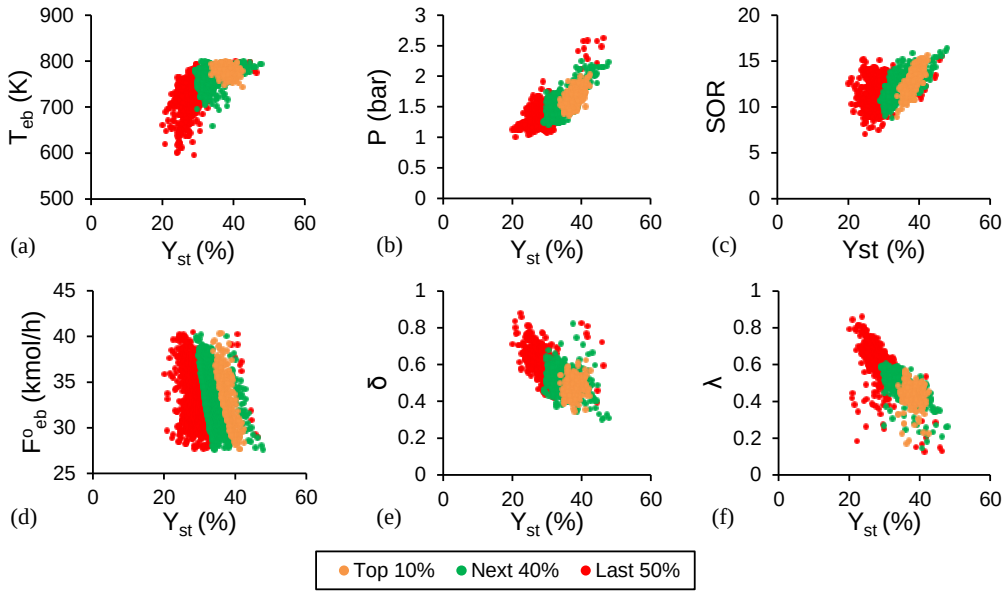

Figure 2.9 - Values of the decision variables as a function of the objective variable Y_{st} for the steam-injected configuration ranked using the net flow method (NFM).

The value of Y_{st} was found to increase with the ethyl benzene temperature T_{eb} and pressure P whereas the values of initial flow rate of ethyl benzene F^o_{eb} remained uniformly scattered. This originally came as a surprise given that high F^o_{eb} values were required to maximize both F_{st} and S_{st} in Case 1 and F_{st} and Y_{st} in Case 2. Even though when the three-objective optimization is considered, the values of F^o_{eb} are scattered with no clear trend. This is due to the fact that low and constant values of F^o_{eb} are required to maximize S_{st} and Y_{st} in case study 2.

As shown in Figures 2.8 and 2.9, the steam-injected Pareto domain reached a higher average operating value of T_{eb} in comparison with the adiabatic configuration. This is due to splitting the steam for later injection which lowered the temperature at the feed at the inlet of the reactor T_1 below the bound of 850 K and therefore higher values of T_{eb} are required. On the other hand, the steam-injected configuration had lower *SOR* values for the optimal operating conditions compared to the adiabatic configuration. In the case of the steam-injected configuration, the values of δ were found to range from 0.30 to 0.87 and λ from 0.12 to 0.86.

The Pareto domains were also ranked taking into account the simple profit function, and the solutions leading to the higher profit are listed in Tables 2.4, 2.5, and 2.6 along with the corresponding design variables.

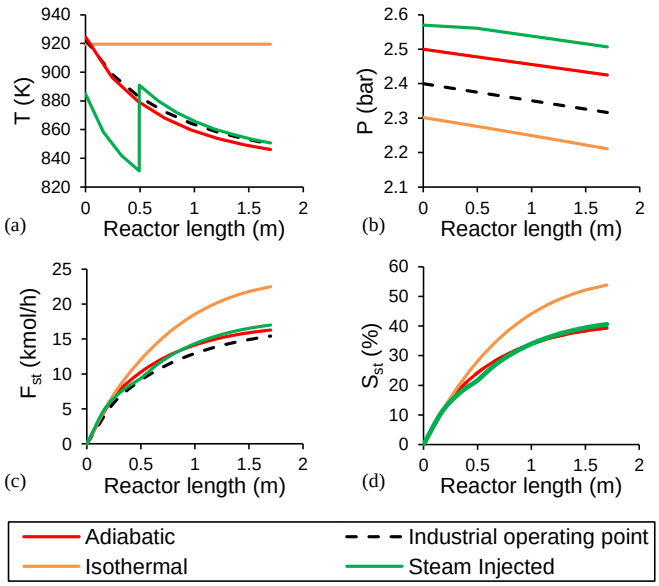

Figure 2.10 - Temperature, pressure, production rate and conversion profiles of styrene along the reactor for the adiabatic, steam-injected and isothermal reactor configurations at the most profitable operating conditions. The profiles under industrial conditions are also provided.

As shown in Figure 2.10, the most profitable individuals for the three-objective optimization for each configuration are compared with the industrial operating point. There is an improvement in the productivity for the steam-injected reactor configuration by 10.24 % and for adiabatic reactor configuration by 5.59 %.

2.4 Conclusion

This paper presented the dual population evolutionary algorithm (DPEA) as a method for the optimization of multiple conflicting design objectives of an industrial styrene reactor. The objectives were the maximization of the selectivity, productivity and yield. The Pareto domain was successfully obtained for two- and three-objective optimization case studies for the adiabatic, steam-injected and isothermal reactor models. It was found that DPEA led to Pareto domains for which the spread of each objective covers a wider range of values of non-dominated

solutions compared to those reported by Yee et al. (2003) and Babu et al. (2005). In addition, it was found that the industrial operating conditions led to a dominated solution.

In order to compare our proposed operating conditions with previously published results, a profit function was used with the same raw material and product prices taken by Yee et al. (2003) and Babu et al. (2005). It was found that the new operating conditions achieve a higher profit than previously published in the literature. In addition, an alternative ranking method, NFM was used to incorporate the preferences of the expert into the optimization strategy.

Although DPEA has been successful for the mutli-objective optimization of the styrene reactor, different constraint handling methods such as the penalty functions and constraint domination approach could be used for future work. In addition, multiple steam injections could be investigated and optimized in order to achieve the limiting case of isothermal reactor configuration.

2.5 Appendix A: Model, design and operating conditions for a styrene reactor

The six main reactions occurring in the styrene reactor were presented in Equations (A1)-(A6). The rates of reactions for the pseudo-homogenous model listed below were obtained from Sheel and Crowe (1969) and Elnashaie and Elshishini (1994).

$$r_1 = k_1\left(p_{EB} - p_{ST}\, p_{H_2} / K_{EB}\right) \quad \text{(A1)}$$

$$r_2 = k_2\left(p_{EB}\right) \quad \text{(A2)}$$

$$r_3 = k_3\left(p_{EB}\, p_{H_2}\right) \quad \text{(A3)}$$

$$r_4 = k_4\left(p_{H_2O}\, p_{ETH}^{0.5}\right) \quad \text{(A4)}$$

$$r_5 = k_5\left(p_{H_2O}\, p_{MET}\right) \quad \text{(A5)}$$

$$r_6 = k_6\left(p_{H_2O}\, p_{CO}\right)\left(P/T^3\right) \quad \text{(A6)}$$

The rate constants k_i of the reaction are given by:

$$k_i = \exp\left[A_i - \left(E_i / RT\right)\right] \quad \text{(A7)}$$

Where A_i and E_i are the apparent frequency factor and activation energy of reaction i. These constants are given in Table A.1.

Table A.1 - Original values of frequency factors and activation energies of the reactions from Sheel and Crowe (1969) and their converted SI values.

Reaction No.	A_i (dimensionless)	E_i (PCU/lb mole)	E_i (kJ/kmol)
1	−0.0854[a]	21708	90887
2	13.2392	49675	207979
3	0.2961	21857	91511
4	−0.0724	24838	103992
5	−2.9344	15697	65720
6	21.2402	17585	73625

[a] Corrected by Crowe in 1989 (Elnashaie and Elshishini, 1994)

Equilibrium constant $K_{EB} = \exp\left(-\Delta G_0 / RT\right)$ bar; $\Delta G_0 = a + bT + cT^2$ (kJ/kmol), where a = 122725.157 kJ/kmol; b = -126.267 kJ/kmol·K; and $c = 2.194 \cdot 10^{-3}$ kJ/kmol·K^2.

The mass balances are given by:

$$\frac{dX_i}{dz} = \frac{\rho_b A_t r_i}{F_{eb}^o} \tag{A8}$$

Where, X_i is the fractional conversion of ethyl benzene in each of the first three reactions, i = 1, 2, 3. For the other three reactions, i = 4, 5, and 6, X_i is given by:

$$\frac{dX_i}{dz} = \frac{\rho_b A_t r_i}{F_{steam}^o} \tag{A9}$$

Reactions 1, 2, and 3 are expressed in terms of ethyl benzene conversion. The sum of these conversions gives the total conversion of ethyl benzene.

$$X_{EB_{ST}} = \frac{F_{ST} - F_{ST}^o}{F_{EB}^o} \tag{A10}$$

$$X_{EB_{BZ}} = \frac{F_{BZ} - F_{BZ}^o}{F_{EB}^o} \tag{A11}$$

$$X_{EB_{TOL}} = \frac{F_{TOL} - F_{TOL}^o}{F_{EB}^o} \tag{A12}$$

$$X_{EB} = \frac{F_{EB}^o - F_{EB}}{F_{EB}^o} \tag{A13}$$

$$X_{EB} = X_{EB_{ST}} + X_{EB_{BZ}} + X_{EB_{TOL}} \tag{A14}$$

Reactions 4, 5, and 6 are expressed in terms of steam conversion (Eqs. A15-A17). The sum of these conversions gives the total conversion of steam.

$$X_{H_2O_{COI}} = \frac{F_{COI} - F^o_{CO}}{F^o_{H_2O}} \tag{A15}$$

$$X_{H_2O_{COII}} = \frac{F_{COII} - F^o_{CO}}{F^o_{H_2O}} \tag{A16}$$

$$X_{H_2O_{CO_2}} = \frac{F_{CO_2} - F^o_{CO_2}}{F^o_{H_2O}} \tag{A17}$$

$$X_{H_2O} = \frac{F^o_{H_2O} - F_{H_2O}}{F^o_{H_2O}} \tag{A18}$$

$$X_{H_2O} = X_{H_2O_{COI}} + X_{H_2O_{COII}} + X_{H_2O_{CO_2}} \tag{A19}$$

The molar flow rate of the components in the reactor can be found as follows:

For the ethyl benzene $$\left(F_{EB}\right) = F^o_{EB} - X_{EB}F^o_{EB} \tag{A20}$$

For the styrene $$\left(F_{ST}\right) = F^o_{ST} + X_{EB_{ST}}F^o_{EB} \tag{A21}$$

For the benzene $$\left(F_{BZ}\right) = F^o_{BZ} + X_{EB_{BZ}}F^o_{EB} \tag{A22}$$

For the toluene $$\left(F_{TOL}\right) = F^o_{TOL} + X_{EB_{TOL}}F^o_{EB} \tag{A23}$$

For the ethylene $$\left(F_{ETH}\right) = F^o_{ETH} + X_{EB_{BZ}}F^o_{EB} - 0.5X_{H_2O_{COI}}F^o_{H_2O} \tag{A24}$$

For the methane $$\left(F_{MET}\right) = F^o_{MET} + X_{EB_{TOL}}F^o_{EB} - X_{H_2O_{COII}}F^o_{H_2O} \tag{A25}$$

For the steam $$\left(F_{H_2O}\right) = F^o_{H_2O} + X_{H_2O}F^o_{H_2O} \tag{A26}$$

For the hydrogen $$\left(F_{H_2}\right) = F^o_{H_2} + \left(X_{EB_{ST}} - X_{EB_{TOL}}\right)F^o_{EB} + \left(2X_{H_2O_{COI}} + 3X_{H_2O_{COII}} + X_{H_2O_{CO_2}}\right)F^o_{H_2O} \tag{A27}$$

For the carbon monoxide

$$\left(F_{CO}\right) = F^o_{CO} + \left(X_{H_2O_{COI}} + X_{H_2O_{COII}} - X_{H_2O_{CO_2}}\right)F^o_{H_2O} \tag{A28}$$

For the carbon dioxide $$\left(F_{CO_2}\right) = F^o_{CO_2} + X_{H_2O_{CO_2}}F^o_{H_2O} \tag{A29}$$

The pressure drop along the length of the reactor is given by the Ergun equation (Elnashaie and Elshishini, 1994):

$$\frac{dP}{dz} = 1 \cdot 10^{-5} \frac{(1-\varepsilon) G_o}{D_p \varepsilon^3 \rho_G} \left[\frac{150(1-\varepsilon)\mu_G}{D_p} + 1.75 G_o \right] \tag{A30}$$

where the gas density ρ_G was calculated using the ideal gas law. Given that the reactor is adiabatic, no heat is transferred to the surroundings. The temperature profile along the reactor is given by:

$$\frac{dT}{dz} = \frac{\sum_{i=1}^{6} (-\Delta H_i) \rho_b A_t r_i}{\sum_{j=1}^{10} F_j Cp_j} \tag{A31}$$

The heats of reactions are taken from Sheel and Crowe (1969):

$$\Delta H_i = a_i + b_i T \tag{A32}$$

The values of a_i and b_i are listed in Table A.2.

Table A.2 - Initial values of the constants a_i and b_i for the heat of reaction from Sheel and Crowe (1969) and their values converted to SI units.

	a		***b***	
Reaction No.	(PCU/lbmole)	(kJ/kmol)	(PCU/lbmole.K)	(kJ/kmol.K)
1	28843	120760	1.09	4.56361
2	25992	108823	-1.9	-7.95492
3	-12702	-53181	-3.15	-13.18840
4	19602	82070	2.11	8.83415
5	50460	211266	3.96	16.57973
6	-10802	-45226	2.5	10.46700

The molar heat capacities C_{pj} are obtained from Smith et al. (2005):

$$\frac{C_{pj}}{R} = a_j + b_j T + c_j T^2 + d_j T^{-2} \tag{A33}$$

The values of the constants for the molar heat capacities are listed in Table A.3.

Table A.3 - Values of the constants for the molar heat capacity (Smith et al., 2005).

Component	*a*	*b* (10^3)	*c* (10^6)	*d* (10^{-5})
Ethyl benzene	1.124	55.38	-18.476	-
Styrene	2.05	50.192	-16.662	-
Benzene	-0.206	39.064	-13.301	-
Toluene	0.29	47.052	-15.716	-
Ethylene	1.424	14.394	-4.392	-
Methane	1.702	9.081	-2.164	-
Water	3.47	1.45	-	0.121
Hydrogen	3.249	0.422	-	0.083
Carbon monoxide	3.376	0.557	-	-0.031
Carbon dioxide	5.457	1.045	-	-1.157

The design and operating conditions of the industrial reactor are listed in Table A.4.

Table A.4 - Design and operating conditions of the industrial styrene packed bed reactor.

Parameter	Value
Reactor diameter D (m)	1.95
Reactor length L (m)	1.7
Catalyst bulk density ρ_b (kg/m^3)	2146
Bed void fraction ε	0.445
Catalyst composition	62% Fe_2O_3, 36% K_2CO_3, 2% Cr_2O_3
Inlet pressure P (bar)	2.4
Inlet temperature T_1 (K)	922.59
Ethyl benzene in the feed (kmol/h)	36.87
Styrene in the feed (kmol/h) [a]	0.67
Benzene in the feed (kmol/h) [a]	0.11
Toluene in the feed (kmol/h) [a]	0.88
Steam (kmol/h)	453.1
Total molar feed (kmol/h)	491.63

[a] Components present as impurities in the ethyl benzene feed.

2.6 Notation

A	frequency factor (dimensionless); cross-section area of reactor (m^2)
c	individual concordance index
C	molar concentration, kmol/m^3; cost factor, \$/kmol; global concordance index
C_p	molar heat capacity, kJ/kmol·K
D	diameter, m; discordance index
E	activation energy, kJ/kmol
f	objective function
F	molar flow rate, kmol/h
F_S	survival fraction in DPEA
G	mass flux of the gas mixture, kg/m^2·h
G_0	Gibbs free energy (kJ/kmol)
k	reaction rate constant, kmol/kg·h·bar^n; index for objective function
K	equilibrium rate constant, bar
L	length of the reactor, m
M	number of objectives
N	total number of points in population
p	partial pressure, bar
P	total pressure, bar; preference threshold
Q	indifference threshold
r	reaction rate, kmol/kg·h
S	selectivity, %
SOR	steam over reactant (ethyl benzene) molar ratio, dimensionless
T	temperature, K
U	decision variable
V	veto threshold
W	relative weight, dimensionless
x	mole fraction
X	conversion, %
Y	yield, %
z	axial coordinate along length of the reactor, m

Greek letters

δ	fraction of injected steam flow rate, dimensionless
Δ	difference between objective function
ΔH	heat of reaction, kJ/kmol
ε	void fraction, dimensionless

λ	fraction of reactor bed where steam is injected, dimensionless
μ	viscosity, kg/m·s
ρ	density, kg/m^3
σ	outranking matrix
ϕ	random number

Subscripts

1	feed; first objective function
2	inter-reactor for steam-injected; second objective function
3	third objective function
o	initial
a	activation
b	bulk
bz	benzene
C	catalyst
eb	ethyl benzene
eth	ethylene
G	gas
gen	generation
i	reaction i
j	component j
m	objective variable *m*
meth	methane
p	particle
st	styrene
steam	steam
tol	toluene
v	decision variable *v*

Superscript

I	iteration number

2.7 References

1. Abdallah, B., Elnashaie, S., Alkhowaiter, S., and Elshishini, S. (1994). Intrinsic kinetics and industrial reactors modeling for the dehydrogenation of ethyl benzene to styrene on promoted iron oxide catalysts. *Applied Catalysis A: General* (113), pp. 89-102.
2. Abdollahi, F., Mostoufi, N., and Sotudeh-Gharebagh, R. (2007). Optimization of radial flow reactors of styrene production. *Internation Journal of Chemical Reactor Engineering* 5 (A75).
3. Babu, B. V., Pallavi, G., Chakole, J. H., and Mubeen, S. (2005). Multiobjective differential evolution (MODE) for optimization of adiabatic styrene reactor. *Chemical Engineering Science* (60), pp. 4822-4837.
4. Bhaskar, V., Gupta, S., and Ray, A. (2000). Application of multi-objective optimization in chemical engineering. *Reviews in Chemical Engineering* 16 (1), pp. 1-54.
5. Brans, J., Mareschal, B., and Vincke, P. (1984). PROMETHEE: A new family of outranking methods in multicriteria decision making. *Operations Research* (84), pp. 477-498.
6. Chen, S., and Updated by Staff. (2006). Styrene. In *Kirk Othmer Encyclopedia of Chemical Technology*, pp. 956-994. New York: Wiley.
7. Clough, D., and Ramirez, W. (1976). Mathematical modeling and optimization of the dehydrogenation of ethyl benzene to form styrene. *American Institute of Chemical Engineering* (22), pp. 1097-1105.
8. Deb, K. (2001). *Multi-objective optimization using evolutionary algorithms*. New York: Wiley.
9. Denis, H.J., and Castor, W. M. (1992). Styrene. In B. Elvers, S. Hawkin and W. Russey (Eds.) *Ullmann's encyclopedia of industrial chemistry* (25), pp. 325-335. New York: Wiley.
10. Derot, B., Gareau, J., Kiss, L., and Martel, J. (1997). In J. Climaio (Ed.), *The Solver of the Volvox Multicriteria Table. Multicriteria Analysis*, pp. 113-126. Springer-Verlag.
11. Doumpos, M., and Zopounidis, C. (2002). Multicriteria decision aid classification methods. *Applied Optimization* (73).

12. Elnashaie, S., and Elshishini, S. (1994). *Modelling, simulation and optimization of industrial fixed bed catalytic reactors*. London: Gordon and Breach Science Publisher.

13. Elnashaie, S., Abdalla, B., and Hughes, R. (1993). Simulation of the industrial fixed bed catalytic reactor for the dehydrogenation of ethyl benzene to styrene: heterogeneous dusty gas model. *Industrial and Engineering Chemistry Research* (32), pp. 2537-2541.

14. Gujarathi, A. M., and Babu, B. (2010). Multi-objective optimization of industrial styrene reactor: Adiabatic and pseudo-isothermal operation. *Chemical Engineering Science* (65), p. 2009.

15. Halsall-Whitney, H. (2004). *The devopment and application of a multi-objective optimization technique for chemical processes and controller design*. Masters of Applied Science in Chemical Engineering Thesis, Ottawa, Canada: University of Ottawa.

16. Halsall-Whitney, H., Taylor, D., and Thibault, J. (2003). Multicriteria optimization of gluconic acid production using net flow. *Bioprocess and Biosystems Engineering* 25 (5), pp. 299-307.

17. Hermann, C., Quicker, P., and Dittmeyer, R. (1997). Mathematical simulation of catalytic dehydrogenation of ethylbenzene to styrene in a composite palladium membrane reactor. *Journal of Membrane Science* (136), pp. 161-172.

18. Kiss, L.N., Zaras, K., Fonteix, C. and Dominique, R. (2002). Multicriteria modelling and decision engineering of a chemical extrusion process. *Australian Society for Operations Research Bulletin* 21 (2) pp. 2-8.

19. Lee, W. J., and Froment, G. F. (2008). Ethylbenzene Dehydrogenation into Styrene: Kinetic Modeling and Reactor Simulation. *Ind. Eng. Chem. Res.* (47), pp. 9183-9194.

20. Li, C., and Hubbell, O. (1982). Styrene. In J. Mcketta, and G. Weismantel (Eds.), *Encyclopedia of chemical processing and design* (55), pp. 197-217. New York: Wiley.

21. Li, C., Maier, E., and Caram, H. (1986). Ethyl benzene dehydrogenation reactor model. *Industrial and Engineering Chemical Process Design Development* (25), pp. 207-210.

22. Miettinen, K. (1999). *Nonlinear Multiobjective Optimization*. Boston: Kluwer.

23. Pawlak, Z. (1997). Rough set approach to knowledge-based decision support. *European Journal of Operational Research* (99), pp. 48-57.

24. Pawlak, Z. (1982). Rough sets. *International Journal of Computer and Information Sciences* (11), pp. 341-356.

25. Polkowski, L., and Skowron, A. (1998). *Rough sets in knowledge discovery (Vol. 2)*. Heidelberg: Physica-Verlag.

26. Rajesh, J., Gupta, S., Rangaiah, G., and Ray, A. (2000). Multiobjective optimization of steam reformer using genetic algorithm. *Industrial and Engineering Chemistry Research* 39 (3), pp. 706-717.

27. Roy, B. (1978). ELECTRE II: Algorithme de classement base sur une representation floue des preferences en presence de criteres multiples. *Cahiers du CERO* (20), pp. 3-24.

28. Savoretti, A., Borio, D., Bucala, V., and Porras, J. (1999). Non-adiabatic radial-flow reactor for styrene production. *Chemical Engineering Science* (54), pp. 205-213.

29. Scarelli, A., and Narula, C. (2002). A multicriteria assignment problem. *Journal of Multi-Criteria Decision Analysis* (11), pp. 65-74.

30. Sheel, J., and Crowe, C. (1969). Simulation and optimization of an existing ethyl benzene dehydrogenation reactor. *Canadian Journal of Chemical Engineering* (47), pp. 183-187.

31. Sheppard, C., Maier, E., and Caram, H. (1986). Ethyl benzene dehydrogenation reactor model. *Industrial and Engineering Chemistry Process Design Development* (25), pp. 207-210.

32. Smith, J., and Van Ness, H. (1975). *Introduction to Chemical Engineering Thermodynamics.* (3rd Edition ed.). New York: McGraw-Hill.

33. Smith, J., Van Ness, H., and Abbott M. (2005). *Introduction to Chemical Engineering Thermodynamics.* (7th Edition ed.). New York: McGraw-Hill.

34. Srinivas, N., and Deb, K. (1995). Multiobjective function optimization using nondominated sorting genetic algorithms. *Evolutionary Computation* (2), pp. 221-248.

35. Sundaram, K., Sardina, H., Fernandez-Baujin, J., and Hilderth, J. (1991). Styrene plant simulation and optimization. *Hydrocarbon Processing* (70), pp. 93-97.

36. Tarafdar, A., Rangaiah, G. P., and Ray, A. (2005). Multi-objective optimization of an industrial styrene monomer manufacturing process. *Chemical Engineering Science* (60), pp. 347-363.

37. Thibault, J. (2008). Net flow and rough sets: Two methods for ranking the pareto domain. In G. Rangaiah (Ed.), *Multi-Objective Optimization: Techniques and Applications in Chemical Engineering*. World Scientific Publishing.

38. Viennet, R., Fonteix, C. and Marc I. (1996). Multicriteria optimization using a genetic algorithm for determining a Pareto set. *International Journal of Systems Science* 27 (2), pp. 255-260.

39. Wenner, R., and Dybdal, E. (1948). Catalytic dehydrogenation of ethyl benzene. *Chemical Engineering Progress* (44), pp. 275-286.

40. Yee, A. K., Ajay, K. R., and Rangaiah, G. P. (2003). Multi-objective optimization of industrial styrene reactor. *Computers and Chemical Engineering* (27), pp. 111-130.

41. Yu, P. L. (1973) A class of solutions for group decision problems. *Management Science* 19 (8), pp. 936-946.

42. Zeleny, M. (1973). Compromise programming. In J.L Cochrane and M. Zeleny (Eds), *Multiple Criteria Decision Making*. University of South Carolina Press.

Chapter 3: Design of shell-and-tube heat exchangers using multiobjective optimization

Salim Fettaka, Jules Thibault and Yash Gupta
Department of Chemical and Biological Engineering
University of Ottawa

Abstract

In this paper, a multiobjective optimization of the heat transfer area and pumping power of a shell-and-tube heat exchanger is presented to provide the designer with multiple Pareto-optimal solutions which capture the trade-off between the two objectives. Nine decision variables were considered: tube layout pattern, number of tube passes, baffle spacing, baffle cut, tube-to-baffle diametrical clearance, shell-to-baffle diametrical clearance, tube length, tube outer diameter, and tube wall thickness. The optimization was performed using the fast and elitist non-dominated sorting genetic algorithm (NSGA-II) available in the multiobjective genetic algorithm module of MATLAB®. In order to verify the improvements in design that the method offers, two case studies from the open literature are presented. The results show that for both case studies, better values of the two objective functions can be obtained than the ones previously published. In addition, NSGA-II provides a Pareto front with a wider range of optimal decision variables. Ranking the Pareto-optimal solutions using a simple cost function shows that the costs for optimal design are lower than those reported in the literature for both case studies. The algorithm was also used to determine the impact of using discrete standard values of the tube length, diameter and thickness rather than using continuous values to obtain the optimal heat transfer area and pumping power. Results show that the use of continuous values of these three decision variables only lead to marginally improved performance than the use of discrete values.

Keywords: Optimization, Shell-and-Tube Heat Exchanger, Pareto domain, Surface area, Total Power Consumption

Publication Status: International Journal of Heat and Mass Transfer, submitted.

3.1 Introduction

Heat exchangers are ubiquitous pieces of equipment in the process industry. Several types and designs of heat exchangers are used in industrial processes. These include double pipe heat exchangers, shell-and-tube exchangers, plate and frame exchangers and many others. However the more common type of heat exchangers is by far the shell-and-tube heat exchanger. Significant effort has been devoted in recent decades to improve their efficiency in order to conserve energy and render processes more profitable. As energy continues to become more expensive with decreasing fossil fuel resources, optimal design and operation of heat exchangers is required. Improvements in heat exchanger design can have significant advantages such as decreasing the amount of external utilities used which would reduce operating costs and increase profits, in addition to lowering the environmental footprint of the process.

Many handbooks covering the design of shell-and-tube heat exchangers are available. These include the compilation edited by Schlunder [1], Hewitt [2], Saunders [3], and Shah and Sekulic [4]. These references are recommended as a good source of information on heat exchanger design, especially for shell-and-tube heat exchangers.

The design method of segmented baffle shell-and-tube heat exchangers involves an iterative algorithm where several configurations are tested by trial and error until the convergence of the heat transfer coefficient and the tube and shell-side pressure drops are within the maximum allowable values. However, this method often results in oversized equipment without being garanteed to be optimal [5].

Over the last years, genetic algorithms (GAs) have received a lot of attention as an optimization method in heat transfer and shell-and-tube heat exchanger design in particular. GAs mimic nature's evolutionary process to find an optimal solution. A recent review on the application of GAs in heat transfer reported interesting optimization studies on the design of heat exchangers [6]. Optimization algorithms can be divided into two categories. The first category, known as single objective optimization, consists of finding the global minimum or maximum of an aggregating function normally composed of the weighted sum of the individual objectives. The second category is multiobjective optimization, which involves the simultaneous optimization of multiple, often conflicting, objectives. Instead of finding a unique optimal solution, a set of optimal non-dominated solutions is generated; this set is referred to as the

Pareto domain. A solution (A) is said to dominate a solution (B) when (A) is not worse than (B) in any of its objective function values and it is better with respect to at least one objective [7].

A number of earlier optimization studies using GAs only considered a single objective. Selbas et al. used a binary-coded GA to minimize a cost function [8]. Their decision variables were the tube diameter, tube pitch, number of passes, shell outer diameter and baffle cut. Wildi-Tremblay and Gosselin performed an optimization study on a heat exchanger with a given heat duty by minimizing a cost function [9]. A binary-coded GA was employed to carry the optimization with 11 discrete decision variables: the tube pitch, tube layout pattern, number of tube passes, baffle spacing at the centre, baffle spacing at the inlet and outlet, baffle cut, tube-to-baffle diametrical clearance, shell-to-baffle diametrical clearance, tube bundle outer diameter, shell diameter and tube outer diameter. Results indicated that the GA identified the optimal results much faster than evaluating all possible combinations of decision variables.

Later Allen and Gosselin expanded this optimization work to consider a condenser shell-and-tube heat exchanger, using the identical cost function [10]. The decision variables were augmented by one to include the heat exchanger side where condensation occurs (shell or tube side).

Babu and Munawar used differential evolution (DE) optimization for the design of a heat exchanger [11]. They chose the minimization of a cost function as their objective and seven decision variables: the tube outer diameter, tube pitch, shell type, number of tube passes, tube length, baffle spacing and baffle cut.

Ozcelik used GA to minimize the exergetic cost of a heat exchanger with the following decision variables: tube length, outer tube diameter, pitch type, pitch ratio, tube layout angle, number of tube passes, baffle spacing ratio, and the mass flowrate of the utility [12].

Caputo et al. employed the MATLAB® genetic alogorithm toolbox to minimize the cost of a shell-and-tube heat exchanger [13]. They chose a cost function which was the sum of the capital investment and the discounted annual energy for pumping as their objective and used three decision variables: shell diameter, tube diameter, and baffle spacing. Their results indicated a reduction in cost when compared to exchangers designed using traditional methods [13].

Hajabdollahi et al. [14] have performed a thermoeconomic optimization of a shell-and-tube condenser. They employed both genetic algorithm and particle swarm algorithms to minimize a cost function which included the investment and operating cost of the condenser. The

decision variables were the number of tubes, number of tube passes, inlet and outlet tube diameters, tube pitch ratio and tube layout. Results indicated that the optimal shell diameter was less than 7 m and the optimal tube length less than 15 m, the ratio of diameter to tube length varied between 1/12 to 1/3, and GA has a lower CPU time compared to particle swarm.

Although single-objective optimization has been often used in the literature, this method does not provide any information about the trade-off between various competing objectives and may converge on a local instead of a global optimum in complex problems. Furthermore the results obtained by using single-objective optimization are sensitive to the relative weighting of the individual objectives in a single aggregating function [7, 15].

Research in the field of multiobjective optimization in heat transfer has been very diverse. In 2006, Hilbert et al. [16] carried out a multiobjective optimization of the blade shape of a tube bank heat exchanger based on GAs and computational fluid dynamics (CFD) codes. Their objective variables were the maximization of the average temperature difference ΔT and minimization of the pressure difference ΔP by considering the coupled solution of the flow and heat transfer processes. The shape of the blade geometry was modeled using non-uniform rational basic splines (NURBS), where four independent parameters describe half of the blade shape. The authors established the proof of concept and obtained a Pareto front associated with this problem.

Pouria et al. [17] used NSGA-II for the optimal design of a plate-and-fin heat exchanger using the fast and elitist non-dominated sorting genetic algorithm (NSGA-II). The heat exchanger was modeled using ε-NTU method. The objective variables were the minimization of the cost and entropy generation, and the decision variables were the fin pitch, fin height, fin offset length, cold stream flow length, no-flow length, and hot stream flow length. They generated a Pareto domain which showed the trade-off between entropy generation and total cost and reported the optimal decision variables.

Hajabdollahi et al. [18] used NSGA-II for the optimal design of a compact heat exchanger and developed a CFD analysis with artificial neural network. The objectives were the maximization of the effectiveness and the minimization of the total pressure drop. The decision variables were the fin pitch, fin height, cold stream flow length, no-flow length and hot stream flow length. Their results showed the trade-off between pressure drop and effectiveness.

Belanger and Gosselin [19] optimized the design of a cross-flow heat exchanger with embedded thermoelectric generators using a multiobjective GA. Their objective variables were the maximization of the net power output, the minimization of the volume, and the number of thermoelectric modules. The decision variables consisted of the local distribution of thermoelectric modules and of current, the shape of the fins, and the division of the heat exchanger in sub-channels. It was found that that the number of sub-channels in the heat exchanger had a larger impact on the overall performance than the fin geometry for this particular problem. In addition, there is a correlation between the net power output and the number of thermoelectric modules, and to a lesser extent with the heat exchanger volume. Although, there is no mention of the multiobjective optimization algorithm used in their paper.

Recently, Sanaye and Hajabdollahi conducted a multiobjective optimization of an industrial shell-and-tube heat exchanger using the ε-NTU method and the Bell-Delaware method for estimating the shell-side heat transfer coefficient and pressure drop [20]. The objectives were to maximize the effectiveness and minimize the cost of the heat exchanger. They chose seven decision variables: the tube arrangement, baffle cut ratio, tube pitch ratio, tube length, number of tubes, baffle spacing ratio and the tube diameter. Their results indicated that the tube pitch ratio, tube length, number of tubes and the baffle spacing ratio were responsible for the trade-off in the Pareto domain between the effectiveness and cost [20]. However, the use of cost as an objective can present a number of potential disadvantages such as determining the relative weighting of the fixed capital cost to the operational cost in the total cost function. This approach requires an assumption on the purchase cost and cost of utilities prior to running the GA. As a result, Pareto-optimal solutions are based on the assigned weights in the cost function and may not be the best when the economic situation varies.

This paper aims at performing a multiobjective optimization of the design of a shell-and-tube heat exchanger. A summary of the primary objectives of this paper and contributions to the subject are as follow:

- Multiobjective optimization of shell-and-tube heat exchanger to minimize the area and total pressure drop using NSGA-II.
- Selecting the tube layout pattern, number of tube passes, baffle spacing, baffle cut, tube-to-baffle diametrical clearance, shell-to-baffle diametrical clearance, tube length, tube outer diameter, and tube wall thickness as the nine decision variables.

- Determining the impact on the objective variables (area and pumping power) when using discrete or continuous values of the tube length, diameter and thickness and examine the trade-off that is made when standard commercial tube sizes have to be used.

This paper briefly describes in Section 3.2 the Bell-Delaware method used for modeling the heat exchanger. Then, the multiobjective optimization method using NSGA-II available in the `gamultiobj` toolbox in MATLAB® is covered in Section 3.3. The heat exchanger model is validated in Section 3.4. Results of the optimization study for the discrete and continuous tube length, diameter and thickness are compared and discussed in Section 3.5. To the best of our knowledge this is the first attempt to study multiobjective optimization of a shell-and-tube heat exchanger with area and pumping power as objective variables, in addition to providing quantitative results useful for understanding the impact of using or not using discrete standard values for the length, diameter and thickness in the optimization of a heat exchanger design.

3.2 Heat exchanger model and simulation

The shell-and-tube heat exchanger is modeled using the Bell-Delaware method for the shell-side heat transfer coefficient and pressure drop. On the tube-side, the heat transfer coefficient and pressure drop are determined from empirical correlations [4, 21]. Figure 3.1 presents the schematic of a shell-and-tube heat exchanger where T_{hi} and T_{ho} are the inlet and outlet temperatures of the hot stream and T_{ci} and T_{co} are the inlet and outlet temperatures of the cold stream.

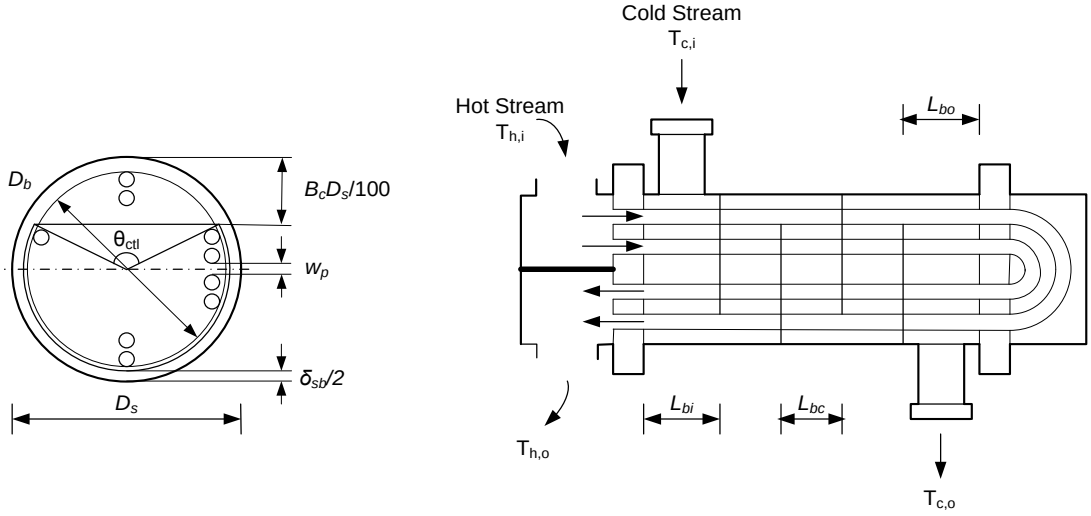

Figure 3.1 - Schematic of a shell-and-tube heat exchanger.

The design of a heat exchanger is normally performed using a trial and error iterative approach. In order to properly size a heat exchanger, three important parameters must be determined carefully: the overall heat transfer coefficient (U_o), the tube-side pressure drop (ΔP_t), and the shell-side pressure drop (ΔP_s).

The overall heat transfer coefficient based on tube outer diameter, U_o, is given by Equation (3.1) [4]:

$$U_o = \frac{1}{\frac{1}{h_o} + R_s + \frac{d_o \ln(d_o / d_i)}{2k_w} + R_t \frac{d_o}{d_i} + \frac{1}{h_i}\frac{d_o}{d_i}} \tag{3.1}$$

where h_o and h_i are the shell-side and tube-side heat transfer coefficients, d_o and d_i are the outer and inner tube diameters, R_s and R_t are fouling resistances on the tube and shell sides, and k_w is the tube wall thermal conductivity.

The value of U_o is not known a priori and must be initially guessed. However, typical values of heat transfer and fouling coefficients for different fluids are available in the literature and can be used as initial guesses [4, 21, 22]. Furthermore, the system must satisfy the equation governing heat exchangers, defined as:

$$A_o = \frac{Q}{U_o \Delta T_{lm} F} \tag{3.2}$$

where A_o is the heat transfer area based on the outer tube diameter, Q is the heat duty, ΔT_{lm} is the log mean temperature difference, and F is the correction factor for multiple pass layout. The latter variable is due to the reduction of the effective temperature difference in the heat exchanger when there is more than one tube pass.

The heat duty is obtained by doing a simple energy balance on one of the streams:

$$Q = \dot{m}_h c_{p,h}\left(T_{h,i} - T_{h,o}\right) = \dot{m}_c c_{p,c}\left(T_{c,o} - T_{c,i}\right) \tag{3.3}$$

In Equation (3.3), either T_{ho} or T_{co} will need to be solved, depending on the problem. Furthermore, it is important to note that all stream properties will be calculated using the average temperature of the inlet and outlet temperatures of the streams.

The log mean temperature difference for a shell-and-tube heat exchanger can be calculated from the following expression.

$$\Delta T_{lm} = \frac{\left(T_{h,i} - T_{c,o}\right) - \left(T_{h,o} - T_{c,i}\right)}{\ln\left(\frac{T_{h,i} - T_{c,o}}{T_{h,o} - T_{c,i}}\right)} \tag{3.4}$$

The correction factor for a layout having an even number of tube passes is given by Equation (3.5) [4]:

$$F = \frac{\sqrt{\left(R^2+1\right)\ln\left(\frac{1-S}{1-RS}\right)}}{\left(R-1\right)\ln\left[\frac{2-S\left(R+1-\sqrt{R^2+1}\right)}{2-S\left(R+1+\sqrt{R^2+1}\right)}\right]} \tag{3.5}$$

where

$$R = \frac{T_{h,i} - T_{h,o}}{T_{c,o} - T_{c,i}} \tag{3.6}$$

and

$$S = \frac{T_{c,o} - T_{c,i}}{T_{h,i} - T_{c,i}} \tag{3.7}$$

A series of other key parameters must be determined to satisfy the estimated surface area: the tube length and the tube outer diameter. The exchanger layout and the number of passes must also be specified. Three main layouts are commonly used for shell-and-tube heat exchangers, namely triangular, square, and rotated square. In this investigation, the tube pitch was maintained constant at 1.25:

$$P_t = 1.25 d_o \tag{3.8}$$

Based on the selected tube and shell specifications, the number of tubes N_t that satisfies the heat transfer area can be determined:

$$N_t = \frac{A}{\pi\ d_o L_t} \tag{3.9}$$

where d_o is the tube outer diameter and L_t is the tube length.

The tube bundle outer diameter can be determined from Equation (3.10):

$$D_{otl} = d_o \left(\frac{N_t}{K_1} \right)^{\frac{1}{n_1}} \tag{3.10}$$

Values of K_1 and n_1 for different tube configurations are given in Table 3.1 [22].

Table 3.1 - Parameters used in the calculation of tube bundle diameter [22].

Number of passes	Triangular Pitch		Square and Rotated Square	
	K_1	n_1	K_1	n_1
1	0.319	2.142	0.215	2.207
2	0.249	2.207	0.156	2.291
4	0.175	2.285	0.158	2.263

The shell diameter is given by:

$$D_s = \frac{D_{otl}}{0.95} + \delta_{sb} \tag{3.11}$$

where δ_{sb} is the shell-to-baffle clearance.

3.2.1 Shell-side heat transfer

The Bell-Delaware method is used to determine the shell-side heat transfer coefficient h_o as per Equation (3.12). This equation uses a heat transfer coefficient with five correction factors to account for the shell geometry, leakage, and bypass streams. An excellent review of the Bell-Delaware method is found in Shah and Sekulic [4]:

$$h_o = h_{id} J_c J_l J_b J_s J_r \tag{3.12}$$

The ideal heat transfer coefficient (h_{id}) on the shell-side is obtained using the Chilton and Colburn *j*-factor. Many correlations were developed in the literature for evaluating h_{id}, but the equation suggested by Shah and Sekulic [4] is used.

$$h_{id} = \frac{j \, \dot{m}_s \, c_{ps} \, \mathrm{Pr}^{-2/3}}{A_{o,cr}} \tag{3.13}$$

where j is the Colburn factor, c_{ps} is the heat capacity of the fluid in the shell-side and $A_{o,cr}$ is the cross flow area at the shell centreline for one cross-flow between two subsequent baffles. The *Prandtl* number Pr is given by Equation (3.14).

$$\mathrm{Pr} = \frac{c_{ps} \, \mu_s}{k_s} \tag{3.14}$$

Although the values of j are available in graphical form, a series of representative correlations were used for computer simulations [4, 9]:

$$j = a_1\left(\frac{1.33}{P_T / d_o}\right)^a \left(\mathrm{Re}_s\right)^{a_2},\ a = \frac{a_3}{1+0.14\left(\mathrm{Re}_s\right)^{a_4}} \tag{3.15}$$

where a_1, a_2, a_3 and a_4 are coefficients listed in Table 3.2. Re_s is the shell-side Reynolds number given by [4]:

$$\mathrm{Re}_s = \frac{\dot{m}_s\ d_o}{\mu_s\ A_{o,cr}} \tag{3.16}$$

Table 3.2 - The Colburn factor j coefficients and ideal friction factor f_{id} [4].

Layout angle	Reynolds number	a_1	a_2	a_3	a_4	b_1	b_2	b_3	b_4
30°	10^5-10^4	0.321	-0.388	1.450	0.519	0.372	-0.123	7.00	0.500
	10^4-10^3	0.321	-0.388	-	-	0.486	-0.152	-	-
	10^3-10^2	0.593	-0.477	-	-	4.570	-0.476	-	-
	10^2-10^1	1.360	-0.657	-	-	45.100	-0.973	-	-
	< 10	1.400	-0.667	-	-	48.000	-1.00	-	-
45°	10^5-10^4	0.370	-0.396	1.930	0.500	0.303	-0.126	6.59	0.520
	10^4-10^3	0.370	-0.396	-	-	0.333	-0.136	-	-
	10^3-10^2	0.730	-0.500	-	-	3.500	-0.476	-	-
	10^2-10^1	0.498	-0.656	-	-	26.200	-0.913	-	-
	< 10	1.550	-0.667	-	-	32.00	-1.000	-	-
90°	10^5-10^4	0.370	-0.395	1.187	0.370	0.391	-0.148	6.30	0.378
	10^4-10^3	0.107	-0.266	-	-	0.0815	0.022	-	-
	10^3-10^2	0.408	-0.460	-	-	6.0900	-0.602	-	-
	10^2-10^1	0.900	-0.631	-	-	32.1000	-0.963	-	-
	< 10	0.97	-0.667	-	-	35.000	-1.000	-	-

The correction factor for the baffle cut and spacing J_c is calculated by:

$$J_c = 0.55 + 0.72F_c \tag{3.17}$$

where F_c represents the fraction of the total number of tubes in the cross-flow section [4].

The tube-to-baffle and baffle-to-shell leakage correction factor J_1 is given by:

$$J_1 = 0.44\left(1-r_s\right) + \left[1-0.44\left(1-r_s\right)\right]\exp\left(-\frac{2.2}{r_{lm}}\right) \tag{3.18}$$

$$\text{where } r_s = \frac{A_{o,sb}}{A_{o,sb}+A_{o,tb}} \text{ and } r_{lm} = \frac{A_{o,sb}+A_{o,tb}}{A_{o,cr}} \tag{3.19}$$

$A_{o,sb}$ is the shell-to-baffle leakage flow area and $A_{o,tb}$ is the tube-to-baffle leakage flow area [4].

The bundle and pass partition bypass stream correction factor J_b is a function of the cross flow area bypass N_{ss} and the number of tube rows crossed during flow through one cross-flow section between baffle tips $N_{r,cc}$ and is given by Eqs. (3.20-3.23):

$$J_b = \begin{cases} 1 & \text{for } N_{ss}^{+} \geq 1/2 \\ \exp\left[-C \cdot r_b \left(1-\left(2N_{ss}^{+}\right)^{1/3}\right)\right] & \text{for } N_{ss}^{+} \leq 1/2 \end{cases} \tag{3.20}$$

$$\text{where } r_b = \frac{A_{o,bp}}{A_{o,cr}} \tag{3.21}$$

$$N_{ss}^{+} = \frac{N_{ss}}{N_{r,cc}} \tag{3.22}$$

$$C = \begin{cases} 1.35 & \text{for } \mathrm{Re_s} \leq 100 \\ 1.25 & \text{for } \mathrm{Re_s} > 100 \end{cases} \tag{3.23}$$

The correction factor J_s for large baffle spacing at the inlet and outlet sections compared to the central baffle spacing is calculated by [4]:

$$J_s = \frac{N_b - 1 + \left(L_i^{+}\right)^{1-n} + \left(L_o^{+}\right)^{1-n}}{N_b - 1 + L_i^{+} + L_o^{+}} \tag{3.24}$$

where

$$L_i^{+} = \frac{L_{b,i}}{L_{b,c}} \tag{3.25}$$

$$L_o^{+} = \frac{L_{b,o}}{L_{b,c}} \tag{3.26}$$

N_b is the number of baffles. Under turbulent flow on the shell-side (Re_s > 100), n is set to 0.6 whereas it is set to 1/3 for laminar flow ($Re_s \leq 100$). In this study, it was assumed that $L_{b,c} = L_{b,i} = L_{b,o}$ and thus J_s = 1. The correction factor for adverse temperature gradient build-up in laminar flows J_r was not taken into consideration in this study and was set to 1.

3.2.2 Tube-side heat transfer

For the tube-side, the heat transfer coefficient h_i is given by Equation (3.27) [4]:

$$h_i = 0.023 \frac{k_t}{d_i} \mathrm{Pr}_t^{1/3} \mathrm{Re}_t^{0.8} \left(\frac{\mu_t}{\mu_{tw}}\right)^{0.14} \tag{3.27}$$

where the tube-side Reynolds number is:

$$\mathrm{Re}_t = \frac{\rho_t V_t d_i}{\mu_t} \tag{3.28}$$

and the Prandlt number of the liquid in the tube-side is:

$$\mathrm{Pr}_t = \frac{c_{pt}\mu_t}{k_t} \tag{3.29}$$

The velocity of the fluid in the tubes V_t is calculated with the following equation:

$$V_t = \frac{N_p}{N_t}\frac{\dot{m}_t}{\pi\left(d_i^2/4\right)\rho_t} \tag{3.30}$$

where N_p is the number of tube passes and N_t is the total number of tubes.

Once the heat transfer coefficients on the shell-side and tube-side, h_o and h_i, are determined, the overall heat transfer coefficient based on tube outer diameter, U_o, is determined using Equation (3.1). If the calculated overall heat transfer coefficient is not within 10% of the value initially assumed, the value of U_o is updated and a new value is calculated until convergence is achieved with the pre-specified tolerance.

3.2.3 Shell-side pressure drop

The shell-side pressure drop is calculated using the Bell-Delaware method given by Equation (3.31) [4]:

$$\Delta P_S = \left[\left(N_b - 1\right)\Delta P_{b,id}\zeta_b + N_b \Delta P_{w,id}\right]\zeta_l + 2\Delta P_{b,id}\left(1 + \frac{N_{r,cw}}{N_{r,cc}}\right)\zeta_b \zeta_s \tag{3.31}$$

where $N_{r,cw}$ is the number of effective tube rows in cross-flow in each window, and $\Delta P_{b,id}$ is the pressure drop for liquid flow in an ideal cross flow between two baffles and is calculated by:

$$\Delta P_{b,id} = \frac{4 f_{id} G_s^2 N_{r,cc}}{2\rho_s}\left(\frac{\mu_{sw}}{\mu_s}\right)^{0.25} \tag{3.32}$$

The friction factor f_{id} associated with the ideal cross flow is expressed as:

$$f_{id} = b_1\left(\frac{1.33}{P_T/d_o}\right)^b \left(\mathrm{Re}_s\right)^{b_2} \tag{3.33}$$

and $$b = \frac{b_3}{1 + 0.14\left(\mathrm{Re}_s\right)^{b_4}} \tag{3.34}$$

Coefficients b_1, b_2, b_3, and b_4 are given in Table 3.2. The pressure drop associated with an ideal one-window section $\Delta P_{w,id}$ for turbulent flow on the shell-side ($Re_s > 100$) is:

$$\Delta P_{w,id} = \frac{\left(2 + 0.6 N_{r,cw}\right) \dot{m}_s^2}{2 \rho_s A_{o,cr} A_{o,w}} \tag{3.35}$$

where $N_{r,cw}$ is the number of effective tube rows crossed during flow through one window zone and $A_{o,w}$ is the net flow area in one window section.

The correction factor ζ_b is calculated as:

$$\zeta_b = \begin{cases} \exp\left(-3.7 r_b \left[1 - \left(2N_s^{++}\right)^{1/3}\right]\right) & \text{for } N_s^{++} < 1/2 \\ 1 & \text{for } N_s^{++} \geq 1/2 \end{cases} \tag{3.36}$$

The second correction factor ζ_l is [4]:

$$\zeta_l = \exp\left[-1.33(1 + r_s) r_{lm}^p\right] \tag{3.37}$$

where $p = \left[-0.15(1 + r_s) + 0.8\right]$ (3.38)

The correction factor ζ_s is given by [4]:

$$\zeta_s = \left(\frac{L_{b,c}}{L_{b,o}}\right)^{1.8} + \left(\frac{L_{b,c}}{L_{b,i}}\right)^{1.8} \tag{3.39}$$

It should be noted that lower values for ζ_b, ζ_l and ζ_s are desired to reduce the total pressure drop, while higher values for J_b, J_l and J_s are desired to increase the heat transfer coefficient on the shell-side. Thus, one can already appreciate the trade-off between the heat transfer coefficients and the pressure drop when designing a heat exchanger.

3.2.4 Tube-side pressure drop

The tube-side pressure drop is calculated from the following expression [21]:

$$\Delta P_t = N_p \left(\frac{4 f \ L}{d_i} + 2.5\right) \frac{\rho_t V_t^2}{2} \tag{3.40}$$

where f is the friction factor for turbulent flow and is given by:

$$f = 0.046 \left(\mathrm{Re}_t\right)^{-0.2} \tag{3.41}$$

The pumping power for the tube and shell sides is calculated similarly on both sides [22]:

$$P_{s,t} = \frac{\Delta P_t \dot{m}_t}{\rho_t \eta} + \frac{\Delta P_s \dot{m}_s}{\rho_s \eta} \tag{3.42}$$

where η is the pump efficiency. In this case, η is assumed to be constant (η = 0.85) for the tube and shell sides.

3.2.5 Cost estimation

The total cost associated with the heat exchanger is the sum of the initial capital cost to purchase the heat exchanger and the operating cost. The purchase cost is obtained from the following correlation for ambient operating pressure and carbon steel material [23]:

$$\log_{10} C_p = K_1 + K_2 \log_{10} A_o + K_3 (\log_{10} A_o)^2 \tag{3.43}$$

Parameters K_1, K_2 and K_3 were determined for a shell-and-tube heat exchanger at one point in time. As a result, the purchase cost has to be corrected for the effect of changing economic conditions and inflation with the following correlation:

$$C_2 = C_1 \left(\frac{I_2}{I_1} \right) \tag{3.44}$$

where C is the purchase equipment cost, I is the cost index, 1 indicates the base time when the cost was determined and 2 the time when the cost is desired. All costs were reported for 2010 using the Chemical Engineering Plant Cost Index (CEPCI). The 1996 CEPCI was 382 and 2010 CEPCI was 556.4.

The bare module cost C_{BM} of the heat exchanger which includes the direct and indirect costs for non-base conditions such as non-ambient pressure and materials of construction other than carbon steel is given by the following correlation:

$$C_{BM} = C_P F_{PM}^o = C_P (B_1 + B_2 F_M F_P) \tag{3.45}$$

The pressure factor F_P is given by:

$$\log_{10} F_p = C_1 + C_2 \log_{10} P + C_3 (\log_{10} P)^2 \tag{3.46}$$

The units of pressure P are in bar gauge, the material factor F_M , as well as the C_1, C_2, and C_3 coefficients are listed in Table 3.3.

Table 3.3 - Capital cost factors [23].

Correlation factor	Value
K_1 [a]	3.2138
K_2 [a]	0.2688
K_3 [a]	0.07961
C_1	0
C_2	0
C_3	0
F_M (Shell-CS Tube-Cu)	1.25
F_M (Shell-CS Tube-SS)	1.70
B_1	1.80
B_2	1.50

[a] P < 10 barg
Cu: Copper
CS: Carbon steel
SS: Stainless steel
All data are for mid-1996, for which CEPCI = 382

The annual operating cost is obtained from the total pumping power ($P_{s,t}$) on the tube and shell sides:

$$OC = 8232\ P_{s,t}\ ec \tag{3.47}$$

where *ec* is the electricity cost. In this paper, *ec* is assumed to be \$0.1 $kW^{-1}h^{-1}$. The factor 8232 accounts for the number of hours of operation assuming the heat exchanger is operating 49 weeks during the year.

The total annual cost of the heat exchanger is expressed in terms of equal annuities of the bare module cost and annual operating cost:

$$TC = C_{BM}\frac{i(1+i)^n}{(1+i)^n - 1} + OC \tag{3.48}$$

where i is the fractional interest rate per year (i = 0.05) and n is the expected lifetime of the heat exchanger which was taken to be 20 years, in order to compare the results with previously published design of Wildi-Tremblay and Gosselin [9].

3.3 Multiobjective optimization

The purpose of the multiobjective optimization of the shell-and-tube heat exchanger is the minimization of the heat transfer area (A_o) and pumping power ($P_{s,t}$) on the tube and shell

sides. Low values of area and pumping power are desired to reduce the capital and operating costs. These two objective functions are defined by Eqs. (3.49) and (3.50):

$$\text{Minimize } f_1 = A_o \tag{3.49}$$

$$\text{Minimize } f_2 = P_{s,t} \tag{3.50}$$

This study considers discrete and continuous decision variables to find the optimal operating conditions for two different case studies. The specifications of the discrete variables are as follow:

1. The tube layout can adopt three discrete values: triangular (30^o), rotated square (45^o) or square (90^o).
2. The number of tube passes (N_p) can have three discrete values: 1, 2 or 4.
3. The baffle spacing at the centre, inlet and outlet ($L_{bc} = L_{bo} = L_{bi}$) varies from the minimum baffle spacing of 0.0508 m to the maximum unsupported tube span of $29.5d_o^{0.75}$ where d_o is in meters [24].
4. The baffle cut (B_c) can vary from 15% to 45%.
5. Tube-to-baffle diameter clearance (δ_{tb}) can take values between $0.01d_o$ and $0.1d_o$.
6. Shell-to-baffle diametrical clearance (δ_{sb}) in accordance with the standards of the Tubular Exchanger Manufacturers Association (TEMA) can take values between 0.0032 m and 0.011 m [25].
7. The tube length (L) can adopt ten discrete values: 2.438 m, 3.048 m, 3.658 m, 4.877 m, 6.096 m, 7.32 m, 8.53 m, 9.75 m, 10.7 m, 11.58 m [25].
8. The tube outer diameter (d_o) can have seven values: 0.01588 m, 0.01905 m, 0.02223 m, 0.0254 m, 0.03175 m, 0.0381 m, 0.0508 m [25].
9. The tube wall thickness can assume discrete values based on the Birmingham Wire Gauge (BWG) and were used for each pipe diameter according to the recommendations of Tubular Exchanger Manufacturers Association (TEMA). The range of thicknesses is presented in Table 3.4 [25].

Table 3.4 - Values of the BWG wall thicknesses [25].

BWG	7	8	9	10	11	12	13	14	15	16
t (mm)	4.572	4.191	3.759	3.404	3.048	2.769	2.413	2.108	1.829	1.651

The decisions variables for the continuous case, three variables were made continuous rather than discrete. The tube length, diameter and thickness were allowed to vary respectively over the ranges of [2.438, 11.58] m, [0.01588, 0.0508] m and [1.651, 4.572] mm. It is assumed that the width of the pass divider lane w_p is 0.05 D_s and the number of pass divider lanes is 0, 1, and 2 for 1, 2, and 4 tube passes, respectively. In addition to the above constraints on the decision variables, there are three inequality constraints involving the allowable pressure drop on the tube and shell sides, as well as the maximum area of the heat exchanger.

$$\begin{cases} g_1(x) = \Delta P_{ct} - \Delta P_t \geq 0 \\ g_2(x) = \Delta P_{cs} - \Delta P_s \geq 0 \\ g_3(x) = A_{o,\max} - A_o \geq 0 \end{cases} \tag{3.51}$$

The constraints are incorporated in both objective functions using penalty functions [9]:

If $\Delta P_t > \Delta P_{ct}$ or $\Delta P_s > \Delta P_{cs}$ or $A_o > A_{o,\max}$

$$f_1 = A_o + 10^9 \cdot |g_3(x)|$$

$$f_2 = P_{s,t} + 10^9 \cdot (|g_1(x)| + |g_2(x)|)$$

else

$$f_1 = A_o$$

$$f_2 = P_{s,t}$$

end

In this paper, the maximum allowable pressure drop for both the tube ΔP_{ct} and shell side ΔP_{cs} was 7 x 10^4 Pa, and the maximum area was 60 m^2. The elitist non-dominated sorting genetic algorithm (NSGA-II) was used. For more information about NSGA-II, a number of references are available to provide a complete picture of the field of multiobjective GAs [7, 15, 26]. The GA was used to circumscribe the Pareto domain for both discrete and continuous tube length, tube outer diameter and tube wall thickness values.

The optimization was performed on a personal computer with Intel Core 2 Duo CPU T5450 of 1.66 and 1.33 GHz and 2.00 GB of RAM using the multiobjective genetic algorithm toolbox `gamultiobj` solver in MATLAB® which is based on NSGA-II. To use the `gamultiobj`

MATLAB® toolbox, some parameters need to be set. These include the number of variables, the objective functions and constraints. For the fitness function, the Bell-Delaware heat exchanger model was used to return the area and pumping power in vector form. Given that the decision variables are constrained, lower and upper bounds had to be specified. Table 3.5 shows the values of the parameters used in the optimization. These parameters were chosen after trial and error to improve the smoothness and spread of the Pareto optimal solutions.

Table 3.5 - NSGA-II optimization parameters.

Parameter	Value
Number of generations	1200
Population size	200
Chromosome	Real coded
Crossover fraction	0.8
Mutation function	Adaptive feasible
Selection function	Stochastic uniform

3.4 Model validation

In order to validate the modeling results, the simulation ouputs and the corresponding values presented by Shah and Sekulic [4] and Wildi-Tremblay and Gosselin [9] for the same input values are presented in Table 3.6. Results show that the differences between the predicted and published values are quite reasonable and allow concluding that the developed code is valid and can be used with confidence for the optimization of heat exchangers.

Table 3.6 - Comparison between simulation code and the literature.

	Case Study 1		Case Study 2	
	Simulation	Shah and Sekulic [4]	Simulation	Wildi-Tremblay and Gosselin [9]
A_o (m^2)	26.69	26.18	37.14	37.14
ΔP_s, shell-side (Pa)	111397	111845	20620	2.26×10^4
ΔP_t, tube side (Pa)	21665	17582	8584	8.6×10^3

3.5 Results and discussion

In this study, a two-objective optimization with NSGA-II was carried out for two case studies selected from the open literature, to demonstrate the usefulness of multiobjective optimization to minimize simultaneously the heat transfer area and the power consumption of a shell-and-tube heat exchanger. In addition, it is desired to compare the results of this study with previous designs. For both case studies, the Pareto domains were obtained after 1200 generations with 200 chromosomes or sets of decision variables.

3.5.1 Case study 1

The first case study was taken from Shah and Sekulic [4] and the specifications of the problem are presented in Table 3.7. In the original problem, lubricating oil was cooled by seawater in a heat exchanger. Seawater is used on the tube-side given its greater tendency to foul. The total heat exchanger duty is 395.26 kW.

Table 3.7 - Design data for Case study 1 [4].

	Tube-side	Shell-side
Fluid	Seawater	Oil
Flow rate (kg/s)	18.10	36.3
Inlet temperature (ºC)	32.20	65.6
Outlet temperature (ºC)	37.42	60.4
Density (kg/m^3)	993	849
Heat capacity (kJ/kg·K)	4.187	2.094
Viscosity (mN·s/m^2)	0.723	64.6
Thermal conductivity (W/m·K)	0.63	0.14
Fouling Resistance (m^2·K/W)	0.000176	0.000088
Tube material of construction	Admiralty (70% Cu, 30% Ni)	
Wall Thermal Conductivity (W/m·K)	111	

This problem was solved for both discrete and continuous decision variables for L, d_o, and t. As shown in the Pareto domains of Figure 3.2(a), results reveal clearly the trade-off between the heat transfer area and the pumping power. If one desires to design a heat exchanger with a geometry that minimizes the heat transfer area, it must be achieved at the expense of the pumping power. Results also indicate that there is no apparent difference whether discrete or continuous decision variables are used to perform the optimization. It is also shown that the design of Shah and Sekulic attempts to minimize the area while accepting high pumping power [4]. In fact, their design is a dominated solution with respect to the Pareto domain obtained in this investigation. Indeed, there exists a solution in the Pareto domain having the same surface area but much lower total power consumption.

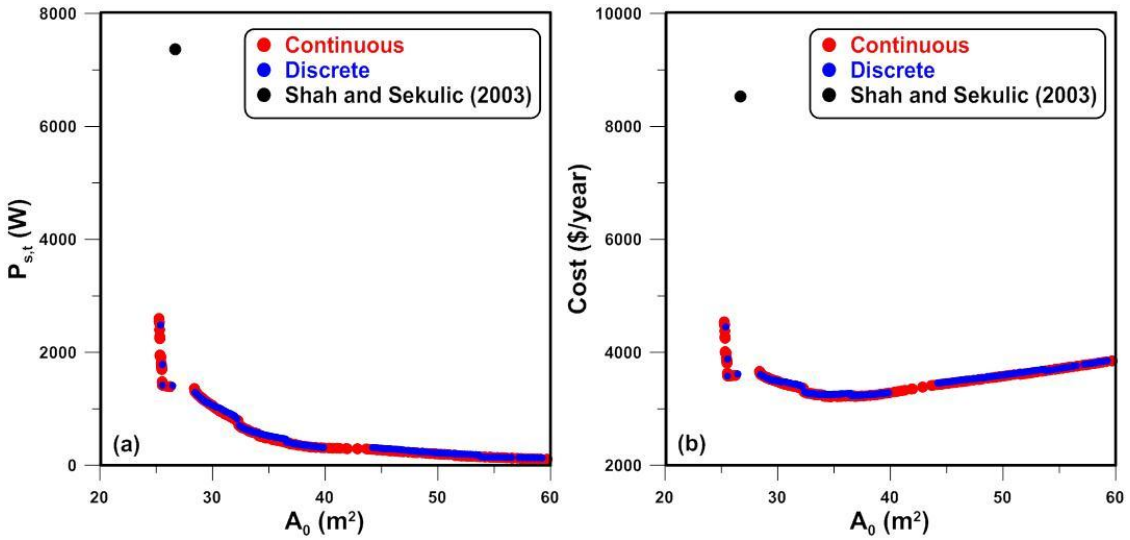

Figure 3.2 - (a) Pareto domains for case study 1 for continuous and discrete decision variables; and (b) simple cost function.

Using Eq. (3.48), the annual cost associated with each Pareto-optimal solution is plotted in Figure 3.2(b). It is observed that the cost function is concave down due to the capital cost which increases with the surface area and the operating cost which depends on the pumping power consumption. In Table 3.8, two designs with the minimum cost from the Pareto domains with discrete (Design 1) and continuous values of L, d_o, and t (Design 2), are compared with the design proposed by Shah and Sekulic [4]. A minimum cost of $ 3216/year was obtained with Design 2 for which A_o = 34.76 m^2 and $P_{s,t}$ = 482.45 W. This is slightly lower than the cost of $ 3233/year obtained with Design 1 with A_o = 36.56 m^2 and $P_{s,t}$ = 412.81 W. From Table 3.8, it can be observed that Design 1 not only decreases the cost by 62.11 %, but also the power consumption by 94.39 % compared to the design proposed by Shah and Sekulic [4].

Table 3.8 - Minimal cost design obtained by NSGA-II for discrete and continuous cases and compared with Shah and Sekulic [4].

	Shah and Sekulic [4]	Design 1 Discrete	Design 2 Continuous
Geometry			
1.Layout	Rotated square	Triangular	Triangular
2.Number of Pass N_P	2	1	1
3.Baffle spacing $L_{b,c}$ (m)	0.279	1.484	1.423
Inlet and outlet baffle spacing $L_{b,i}$ and $L_{b,o}$(m)	0.318	1.484	1.423
4.Baffle Cut B_c (%)	25.8	15.379	15.247
5.Shell-to-baffle clearance δ_{sb} (mm)	2.946	3.392	3.968
6.Tube to baffle clearance δ_{tb} (mm)	0.794	0.193	0.183
7.Tube length L_t (m)	4.3	3.658	3.463
8.Tube outer diameter d_o (mm)	19	19.050	17.559
9.Tube thickness t (mm)	1.2	1.651	1.665
Number of sealing strip pairs N_{ss}	1	2	2
Outer tube limit D_{otl} (m)	0.321	0.354	0.340
Shell diameter D_s (m)	0.336	0.376	0.362
Performance			
A_o (m^2)	26.69	36.56	34.76
ΔP_s, shell-side (Pa)	111397	6159.11	7117.15
ΔP_t, tube side (Pa)	21665	1406.01	1833.21
$P_{s,t}$ (W)	7368.29	412.81	482.45
Bare module cost C_{BM} ($)	30745.10	36058.10	35132.12
Operating cost ($/year)	6065.58	339.83	397.16
Annual cost ($/year)	8532.65	3233.22	3216.25

In addition, for the discrete design the number of tubes (N_t) and baffles (N_b) are 168 and 1, respectively, whereas they were respectively 104 and 14 for the solution obtained by Shah and Sekulic [4]. The above difference is due to the fact that the design by Shah and Sekulic minimizes A_o only. While Design 1 has a significantly higher surface area, it also has a drastically lower pressure drop on the tube and shell sides which leads to a more economical design.

To gain a greater insight on the underlying relationship of the decision variables with the two objective functions, the values of the decision variables corresponding to the Pareto domain of Figure 3.2(a) were plotted against the area of the heat exchanger in Figures 3.3(a)-3.3(h). It is observed that the optimal values for decision variables B_c, and t and the ratio of δ_{tb}/d_o are nearly constant over the range of the heat exchanger area. In addition, no clear pattern for the variation of δ_{sb} and L with the surface area is observed. The trade-off in the Pareto domain was due to the conflicting effects of the following decision variables: tube layout, N_p, L_{bc}, d_o, and δ_{tb}.

Figures 3.3(a) shows that as the area of the heat exchanger decreases, the tube layout changes from triangular to rotated square. A triangular pattern allows more tubes per unit area than a square pattern, and results in higher turbulence, hence increasing the heat-transfer coefficient on the shell side [22]. It is also seen in Figures 3.3(c), 3.3(f) and 3.3(h) that the values

of L_{bc}, δ_{tb} and d_o decrease as the surface area is minimized. A decrease in the baffle cut results in an increase in the shell-side heat transfer coefficient at the expense of a higher pressure drop through the shell. Lower values of d_o increase the tube-side velocity and thus the tube-side heat transfer coefficient, while lower L_{bc} values increase the shell side velocity and the shell side heat transfer rate. Although δ_{tb} can take values between $0.01d_o$ and $0.1d_o$, results indicate that the ratio δ_{tb}/d_o is close to the lower limit of 0.01, in order to reduce the shell-and-tube leakage and bypass effects. Likewise, the tube thickness t is nearly always at its lower limit to reduce the resistance to conduction through the tube wall. Although, it should be mentioned that the optimization did not take into consideration, hoop stress due to pressure and corrosion allowance for the wall thickness.

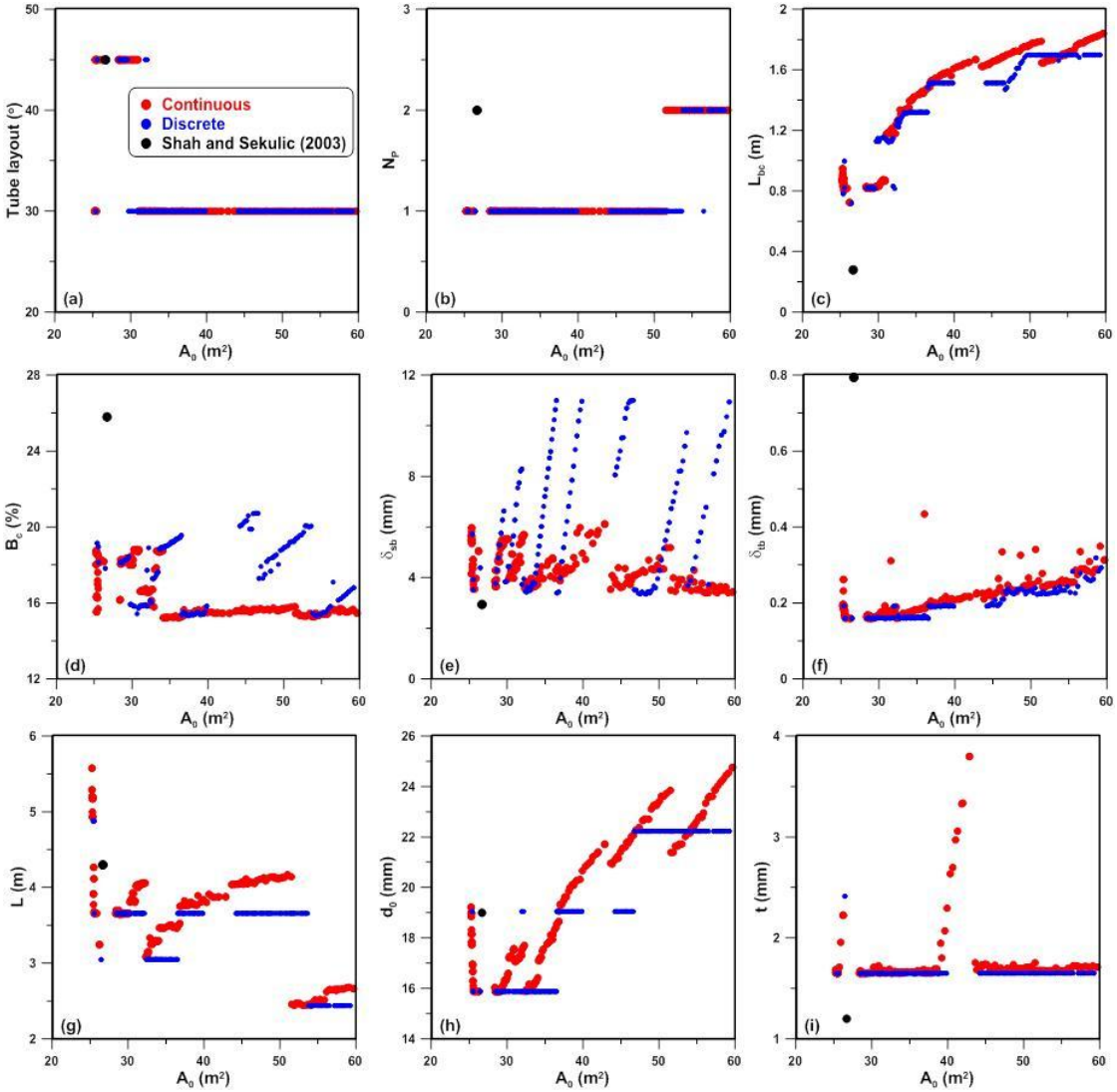

Figure 3.3 - Values of the decision variables as a function of heat transfer area for Pareto domains of case study 1.

3.5.2 Case study 2

The second case study was taken from Wildi-Tremblay and Gosselin [9]. This problem was originally proposed by Mukherjee [22]. Wildi-Tremblay and Gosselin obtained an optimal solution based on single-objective minimization of a cost function using a GA [9]. The problem considers the cooling of Naphtha using water in a shell-and-tube heat exchanger. The design specifications are given in Table 3.9.

Table 3.9 - Design data for case study 2 [9].

	Tube-side	Shell-side
Fluid	Cooling water	Naphtha
Flow rate (kg/s)	30	2.7
Inlet temperature (ºC)	33	114
Outlet temperature (ºC)	37.21	40
Density (kg/m^3)	1000	656
Heat capacity (J/kg·K)	4186.8	2646.06
Viscosity (N·s/m^2)	0.00071	3.70×10^{-4}
Thermal conductivity (W/m·K)	0.63	0.11
Design Pressure (Pa)	1278142	738767
Fouling Resistance (m^2·K/W)	0.0004	0.0002
Material of construction	Stainless steel	Carbon steel
Wall thermal conductivity (W/m·K)	16	55

In this case study, the same decision variables and constraints as in case study 1 were considered. Likewise, results reveal that using continuous and discrete decision variables for L, d_o, and t had a negligible effect on the Pareto-optimal solutions as shown in Figure 3.4(a). It can be seen that the point corresponding to the design found by Wildi-Tremblay and Gosselin [9] lies slightly above the Pareto domain and it is therefore dominated compared to the discrete and continuous Pareto domains of the present investigation. This means there is a solution in the Pareto domain that has the same surface area but with lower power consumption. Figure 3.4(b) shows that the cost of the design of Wildi-Tremblay and Gosselin [9] is marginally higher than the minimal cost function for the two designs in this case study (see Table 3.10). As indicated in Table 3.10, the minimum cost of $ 3391/year was obtained with Design 2 for which A_o =32.66 m^2 and $P_{s,t}$ = 193.25 W. This is slightly lower than the cost of $ 3405/year obtained with Design 1 with A_o = 32.40 m^2 and $P_{s,t}$ = 226.10 W. The discrete Design 1 lowers the cost by 11.69 %, and the power consumption by 53.77 % compared to the design proposed by Wildi-Tremblay and Gosselin [9].

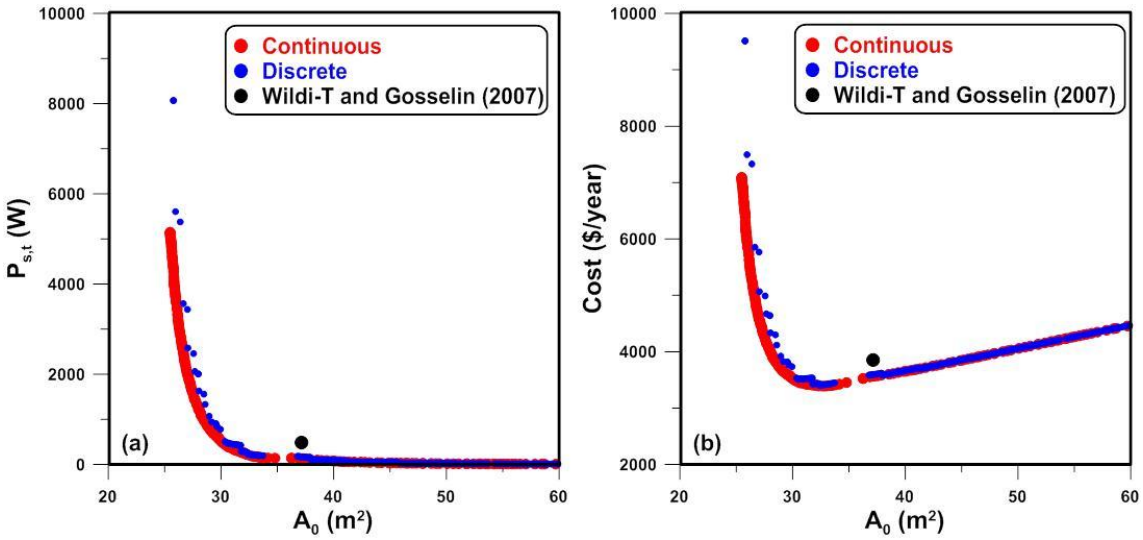

Figure 3.4 - (a) Pareto domains for case study 2 for continuous and discrete decision variables; and (b) the cost function associated with solutions of (a).

Interestingly in this second case study, the tube layout of the Pareto optimal solutions is square. This originally came as surprise since in the triangular pitch the tube are more closely packed in the bundle, which translates to higher heat transfer surface area in a given shell and somewhat higher pressure drop and heat-transfer coefficient. However, in this particular case, it is believed that the square layout is more optimal because it lowers the pressure drop without compromising too much on the heat transfer coefficient.

Table 3.10 - Minimal cost designs obtained by NSGA-II for discrete and continuous decision variables for case study 2 along with the design of Wildi-Tremblay and Gosselin [9].

	Wildi-Tremblay and Gosselin [9]	Design 1 Discrete	Design 2 Continuous
Geometry			
1.Layout	Square	Square	Square
2.Number of Pass N_P	1	1	1
3.Baffle spacing $L_{b,c}$ (m)	0.06	0.099	0.079
4.Baffle Cut B_c (%)	25	16.276	16.515
5.Shell-to-baffle clearance δ_{sb} (mm)	3	3.261	3.279
6.Tube to baffle clearance δ_{tb} (mm)	0.381	0.208	0.204
7.Tube length L_t (m)	10.7	3.658	3.426
8.Tube outer diameter d_o (mm)	38.1	19.050	19.578
9.Tube thickness (mm)	3.405	1.651	1.652
Number of sealing strip pairs N_{ss}	2	2	2
Outer tube limit D_{otl} (m)	0.238	0.368	0.379
Shell diameter D_s (m)	0.3	0.391	0.402
Performance			
A_o (m^2) (m^2)	37.14	32.40	32.66
ΔP_s, shell-side (Pa)	20620	5969.35	8329.87
ΔP_t, tube-side (Pa)	8584	4456.81	3366.43
$P_{s,t}$ (W)	489.12	226.10	193.25
Bare module cost C_{BM} ($)	43031.39	40114.37	40277.59
Operating cost ($/year)	402.64	186.13	159.09
Annual cost ($/year)	3855.59	3405.01	3391.06

For this second case study, Figures 3.5(a)-3.5(h) indicate that three decision variables, namely L, d_o, and δ_{tb}. are mainly responsible for the trade-off observed in the Pareto domain, while the other decision variables do not contribute significantly to this trade-off.

The Pareto-optimal value of L was found to decrease sharply and then level off to its minimum value as the heat exchanger surface area (A_o) increases. Although this observation might be counter-intuitive at first, this sharp decrease in tube length is accompanied by an increase of the number of tubes in such a way that the heat transfer area continues to increase. This sharp decrease is really prompted by the huge impact the tube length has on the pressure drop through the bundle of tubes, which also drastically decreases. Over the range where the length of the tubes drastically decreases, the tube diameter essentially remained constant. However, as the area continues to increase, the tube diameter and the number of tubes continue to increase in order to maintain a very low pressure drop in the tubes and the shell. However in order to maintain a high enough heat transfer coefficient on the shell side, the Pareto-optimal baffle spacing decreases so as to decrease the bypass and leakage flow areas. Similarly as in case study 1, that Pareto-optimal value of the tube thickness assumes its lowest value of 1.651 mm for both the continuous and discrete cases.

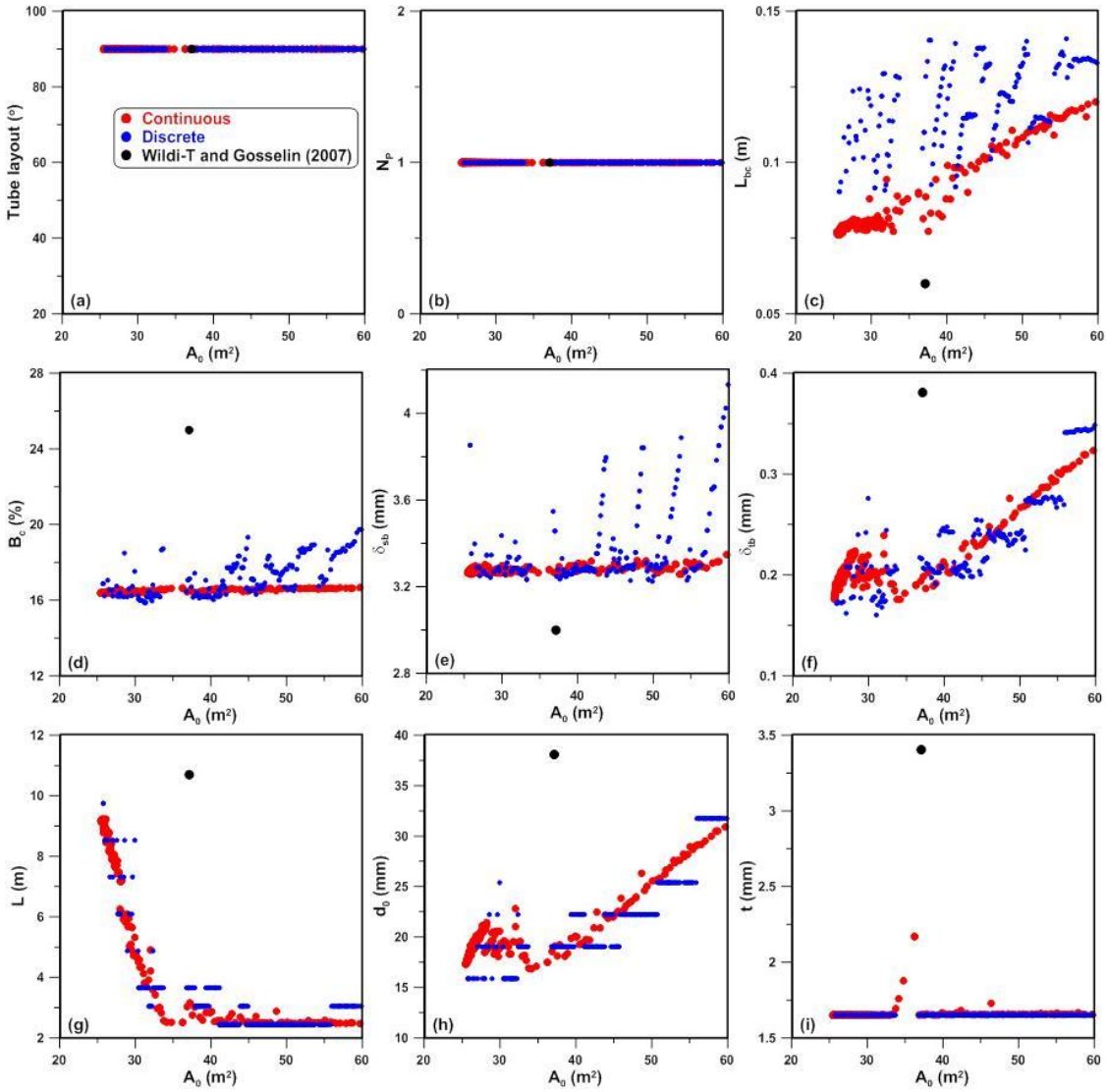

Figure 3.5 - Values of the decision variables as a function of the heat surface area corresponding to the Pareto domains of case study 2.

3.6 Conclusion

In this paper, the multiobjective optimization for two case studies of a shell-and-tube heat exchanger was performed using NSGA-II. The Pareto fronts for minimizing both the heat transfer area and pumping power of the shell-and-tube heat exchanger were obtained for both case studies and ranked using a simple cost function. The results indicate that one can achieve a lower value of the heat transfer area and the pumping power as compared to the previously published values. Furthermore, it was found that discretization of the tube length, diameter and thickness had a very minor effect on the optimal cost design. The value of L_{bc},, d_o, and δ_{tb}. are the decision variables that are responsible for the trade-off observed in the Pareto domain for both

cases studies, while for the first case study the tube layout and N_p were found to play a role, and the tube length had a significant effect in the second case study. The remaining decision variables did not affect significantly the trade-off.

It was shown that the approach of using multiobjective optimization for the design of a shell-and-tube heat exchanger allowed finding Pareto fronts with a wider range of optimal decision variables. The designer can choose one solution from all Pareto-optimal solutions based on his knowledge of the process as well as examining the cost of the design. The enviable advantages of the multiobjective optimization are the ability for the designer to readily visualize the trade-off being made in choosing a given design, in addition to finding the optimum heat exchanger configuration that can be counter-intuitive at times if one relies on heuristics.

3.7 Acknowledgments

Financial support was provided by the Ontario Ministry of Training, Colleges and Universities, Canada. Salim Fettaka was the holder of an Ontario Graduate Scholarship over the course of this work. Grants from the Natural Sciences and Engineering Research Council (NSERC) are also greatly appreciated.

3.8 Nomenclature

A_o heat transfer surface area (m^2)

$A_{o,cr}$ flow area at or near the shell centreline for one cross-flow section (m^2)

$A_{o,sb}$ shell-to-baffle leakage flow area (m^2)

$A_{o,tb}$ tube-to-shell leakage flow area (m^2)

B bare module factor

B_c baffle cut (%)

C purchase cost coefficient

C_{BM} bare module cost

c_p heat capacity (J kg^{-1} K)

C_p purchase cost of the exchanger ($)

d_i tube inside diameter (m)

d_o tube outside diameter (m)

D_{otl} tube bundle outer diameter (m)

D_s shell diameter (m)

ec electricity cost ($\$kW^{-1}$ h)

F correction factor for the number of tube passes

F_M material correction factor

G fluid mass velocity (kg m^2 s)

h heat transfer coefficient (W m^{-2} K)

i interest rate (%)

I cost index

J correction factor for the shell-side heat transfer

k thermal conductivity (W m^{-2} K)

K capital cost correlation factor

L_b distance between baffles (m)

$\dot{m}$ mass flow rate (kg s^{-1})

n lifetime of the exchanger (year)

N_b number of baffles

N_p number of tube passes

N_{ss} number of sealing strip pairs

N_t total number of tubes

OC operating cost ($\$ year^{-1}$)

op annual operating period (h)

Pr Prandtl number

P_t tube pitch (m)

$P_{s,t}$ Pumping power on tube and shell sides (W)

Q heat duty (W)

R fouling resistance (m^2 kW^{-1})

Re Reynolds number

t tube thickness (m)

T temperature (°C)

TC annualized cost of the heat exchanger ($\$ year^{-1}$)

U_o overall heat transfer coefficient (W m^{-2} K)

v flow velocity (m s^{-1})

Greek symbols

ζ shell-side pressure drop correction factor

μ viscosity (Pa s)

δ density (kg m^{-3})

ΔP pressure drop

ΔT_{lm} log-mean temperature difference

Subscript

c cold fluid, centre of the exchanger

h hot fluid

i tube inlet

id ideal

M material

o tube outlet

P pressure

s shell-side

t tube-side

w tube wall

3.9 References

1. Schlunder EU. *Heat Exchanger Design Handbook.* Hemisphere: New York, 1983.
2. Hewitt GF. *Hemisphere Handbook of Heat Exchanger Design.* Hemisphere: New York, 1990.
3. Saunders EA. *Heat Exchanges: Selection, Design and Construction.* Longman Scientific and Technical: New York, 1988.
4. Shah RK., Sekulic DP. *Fundamentals of Heat Exchanger Design.* Wiley: New York, 2003.
5. Serna M, Jiminez A. An efficient method for the design of shell and tube heat exchangers. *Heat Transfer Engineering* 2004; **25**:5–16.

6. Gosselin L, Tye-Gingras M, Mathieu-Potvin F. Review of utilization of genetic algorithms in heat transfer problems. *International Journal of Heat and Mass Transfer* 2009; **52**:2169-2188.
7. Deb K. *Multi-objective optimization using evolutionary algorithms.* Wiley: New York, 2001.
8. Selbas R, Kizilkan O, Reppich M. A new dsign approach for shell and tube heat exchangers using genetic algorithms from economic point of view. *Chemical Engineering and Processing* 2006; **45**:268-275.
9. Wildi-Tremblay P, Gosselin L. Minimizing shell-and-tube heat exchanger cost. *International Journal of Energy Research* 2007, **31**:867–885.
10. Allen B, Gosselin L. Optimal geometry and flow arrangement for minimizing the cost of shell-and-tube condensers. *International Journal of Energy Research* 2008, **32**:958-969.
11. Babu BV, Munawar SA. Differential evolution strategies for optimal design of shell-and-tube heat exchanger. *Chemical Engineering Science* 2007, **14**:3720-3739.
12. Ozcelik, Y. Exergetic optimization of shell and tube heat exchangers using a genetic based algorithm. *Applied Thermal Engineering* 2007. **27**:1849-1856.
13. Caputo AC., Pelagagge PM., Salini P. Heat exchanger design based on economic optimization. *Applied Thermal Engineering* 2008, **28**:1151-1159.
14. Hajabdollahi H, Ahmadi P, Dincer I. Thermoeconomic optimization of a shell and tube condenser using both genetic algorithm and particle swarm. *International Journal of Refrigeration* 2011, **34**:1066-1076.
15. Haupt RL, Haupt SE. *Practical Genetic Algorithms.* Wiley: New Jersey, 2004.
16. Hilbert R, Janiga G, Baron R, Thevenin D. Multi-objective shape optimization of a heat exchanger using parallel genetic algorithms. *International Journal of Heat and Mass Transfer* 2006, **49**:2567-2577.
17. Ahmadi P, Hajabdollahi H, Dincer I. Cost and Entropy Generation Minimization of a Cross-Flow Plate Fin Heat Exchanger Using Multi-Objective Genetic Algorithm. *Journal of Heat Transfer* 2011, **133**:021801-1 021801-10.
18. Hajabdollahi H, Tahani M, Shojaee Fard MH. CFD modeling and multi-objective optimization of compact heat exchanger using CAN method. *Applied Thermal Engineering* 2011, **31**:2597-2604.

19. Belanger S, Gosselin L. Multi-objective genetic algorithm optimization of thermoelectric heat exchanger for waste heat recovery. International Journal of Energy Research 2011. DOI: 10.1002/er.1820
20. Sanaye S., Hajabdollahi H. Multi-objective optimization of shell and tube heat exchangers. *Applied Thermal Engineering* 2010, **30**: 1937-1945.
21. Smith, R. *Chemical Process Design and Integration.* Wiley: New York, 2005.
22. Towler G, Sinnott R. *Chemical engineering design: principles, practice and economics of plant and process design.* Elsevier: New York, 2007.
23. Turton R, Bailie RC, Whiting WB., Shaeiwitz JA. *Analysis, Synthesis, and Design of Chemical Processes*. Prentice Hall: New Jersey, 1998.
24. Perry R, Green D. *Perry's Chemical Engineers' Handbook* (7th Edition ed.). McGraw-Hill: New York, 1997.
25. Tubular Exchanger Manufacturers Association, Inc. *Standards of the Tubular Exchanger Manufacturers Association* (9^{th} Ed.). Tarrytown, New York, 2007.
26. Tan K, Khor E, Lee T. *Multiobjective Evolutionary Algorithms and Applications.* Springer: London, 2005.
27. Mukherjee R. Effectively design shell-and-tube exchangers. *Chemical Engineering Progress* 1998, **94**: 21-37.

Chapter 4: A new algorithm using front prediction and NSGA-II for solving two and three-objective optimization problems

Salim Fettaka, Jules Thibault and Yash Gupta
Department of Chemical and Biological Engineering
University of Ottawa

Abstract

In this paper, a new hybrid algorithm (FP-NSGA-II) is proposed by combining the fast and elitist non-dominated sorting genetic algorithm-II (NSGA-II) with a simple front prediction algorithm. Due to the significant computational time of evaluating objective functions in real life engineering problems, the aim of this hybrid approach is to better approximate the Pareto front of difficult constrained and unconstrained problems while keeping the computational cost similar to NSGA-II. FP-NSGA-II is similar to the original NSGA-II but generates better offsprings. This is achieved by using a prediction operator which utilizes the direction in the decision variable space between each solution in the first front and the nearest neighbour solution in the second front, in order to extrapolate future chromosomes. This enables the addition of solutions that are closer to the true Pareto front into the new generation. To assess the performance of the proposed approach, eight benchmark two-objective test problems and four three-objective test problems are used to compare FP-NSGA-II with NSGA-II. In addition, a three-objective heat exchanger network problem is examined to show the potential application of FP-NSGA-II in real-life problems. Results indicate that the FP-NSGA-II improves upon the performance of NSGA-II for a variety of benchmark test problems exhibiting different characteristics.

Keywords: Multiobjective optimization; Pareto domain; hybrid algorithm; NSGA-II

Publication Status: Optimization and Engineering, submitted.

4.1 Introduction

Many real-world engineering problems involve multiple, and often conflicting, objective functions subject to various constraints. In the absence of bias or preference, multiobjective optimization algorithms are used to approximate the Pareto front. The Pareto front refers to the set of non-dominated solutions which highlight trade-offs among the different objectives.

Evolutionary computation has been one of the most active area of research in the field of optimization and many evolutionary algorithms (EAs) were developed and successfully applied in a wide range of real-world complex computational problems with conflicting objectives [1-3]. EAs are population-based search techniques that mimic the principles of genetics and natural selection [1-3].

The origins of EAs can be traced back to the late 1950's [4, 5], and the first applications of EAs were developed for single objective optimization in the 1960's. Rechenberg and Schewefel proposed evolution strategy (ES) [6, 7] while independently Fogel proposed evolutionary programming (EP) [8]. This was later followed by genetic algorithms (GA) introduced by Holland [9]. However, it was not until 1984, that Schaffer developed the first multiobjective evolutionary algorithm (MOEA) for finding multiple trade-off solutions called the vector evaluated genetic algorithm (VEGA) [10].

Since then researchers around the world developed various MOEAs following the three above approaches to approximate evolutionary processes. In the 1990's, additional approaches emerged: genetic programming (GP) [11], and differential evolution (DE) [12].

Today the field of evolutionary computation includes evolutionary algorithms (EP, ESs, GAs, GP, DE), swarm intelligence algorithms [13-15] (particle swarm optimization (PSO), ant colony optimization (ACO), bacterial foraging optimization (BFO), bees algorithm), as well as learnable evolution model [16], harmony search [17], and artificial immune system [18].

Once the Pareto domain is obtained, usually some higher-level decision making considerations are used to choose a solution such as to satisfy the user preference and experience. The methods used in the selection of the preferred solution include compromise programming approach [19, 20], marginal rate of substitution approach [21], net flow method [22-24], rough set method [24, 25], hierarchical clustering techniques [26].

Although, many EAs have been published in the literature over the years such as NSGA-II [27], PAES [28] and SPEA2 [29] to only name a few, research has been limited mainly to two-objective problems. It is well known that a MOEA should achieve the following two goals [1]:

1. Convergence towards the true Pareto front: The known Pareto front (PF_{known}) should approximate as closely as possible the true Pareto front (PF_{true}).
2. Diversity of solutions: The known Pareto front (PF_{known}) should be uniformly distributed and spread over the entire feasible objective space to adequately capture the trade-offs.

The fast and elitist non-dominated sorting genetic algorithm-II (NSGA-II) is the current state of the art MOEA, and has been shown to work well for two-objective problems by attaining near-optimal diverse and uniformly distributed Pareto solutions [27]. To evolve the population towards the PF_{true} while maintaining a uniformly diverse set of individuals, a MOEA should exert a pressure $\vec{P}_n$ to promote the individuals in a direction normal to the PF_{known} and another pressure tangential to the PF_{known} $\vec{P}_u$ to improve the spread and diversity of solutions [3]. In NSGA-II, $\vec{P}_n$ and $\vec{P}_u$ are included in the non-dominated sorting and crowded-distance assignment features, respectively.

However, NSGA-II performance decreases for problems with three or more objective functions. When the dimensionality of the objective space increases, the percentage of non-dominated solutions within the initial population increases. As a result, the difficulty of finding non-dominated solutions close to PF_{true} and maintaining the diversity of solutions increases [1].

Purshouse and Fleming studied NSGA-II for problems with large numbers of objectives to compare its efficiency [30]. Their results indicate that NSGA-II performed well for low numbers of objectives whereas its performance decreased when the number of objectives increases. In addition, it was shown that using a large population size does not necessarily improve the performance of NSGA-II for problems having a large number of objectives.

One approach to handle this difficulty was suggested by Kukkonen and Deb [31] and consists of a pruning method based on the crowding estimation techniques to remove the most crowded non-dominated solutions and improve the efficiency of the distribution of non-dominated solutions when solving problems with many objectives. Later Koppen and Yoshida [32] proposed the idea of replacing crowding distance measurement in NSGA-II with new measurement schemes for a solution to be nearly-dominated by another solution, based on the

following criteria: number of better objectives, magnitude of all better objectives, and a combination of both.

Hartikainen et al. [33] proposed a Pareto front interpolation method (PAINT) that interpolates between a set of non-dominated solutions and can be used with interactive methods such as the NIMBUS method [34].

In this paper, a new hybrid algorithm, referred to as the front prediction based non-dominated sorting genetic algorithm (FP-NSGA-II), is proposed to solve two and three-objective optimization problems. The proposed method is similar to the original NSGA-II but uses a prediction algorithm to produce better offsprings. Following the fast non-dominated sorting procedure, the prediction operator computes the direction in the decision variable space between each solution in the first front and the nearest neighbour solution in the second front, which is then used to extrapolate future chromosomes. This front prediction enables the addition of solutions that are closer to the true Pareto front. The main purpose for such an approach is to reduce the overall number of fitness function evaluations and computational time while at the same time obtaining a good approximation both in terms of convergence and diversity of the Pareto front. To the best of our knowledge this is the first time that this hybrid approach is used.

To assess the robustness and performance of the proposed algorithm, a wide variety of benchmark test problems are used to compare FP-NSGA-II with NSGA-II. The test problems include eight benchmark two-objective test problems designated in the literature as ZDT1, ZDT2, ZDT3, ZDT4, ZDT6, CONTR, SRN, TNK [1, 35-37], and four three-objective test problems, namely DTLZ1, DTLZ2, DTLZ3, and DTLZ4 [38]. In addition, a multiobjective optimization of the heat exchange areas for a three heat-exchanger network was carried out as an additional test problem.

In the next section, the basic concepts of multiobjective optimization necessary to set the foundation of the proposed algorithm are reviewed. This is followed by a detailed description of FP-NSGA-II in Section 4.3. The performance metrics used to evaluate the algorithm and benchmark test problems are formulated in Sections 4.4 and 4.5, respectively. Subsequently, the experimental results are shown and discussed in Section 4.6, and finally the conclusions are drawn in Section 4.7.

4.2 Basic concepts

A multiobjective optimization problem (MOOP) consists of multiple objectives that are maximized, minimized or a combination of both. It is usually subjected to a number of constraints and can be defined in the following mathematical terms [1]:

$$\text{Minimize / Maximize} \quad \mathbf{f}(\mathbf{x}) = (f_1(\mathbf{x}), f_2(\mathbf{x}), \ldots, f_m(\mathbf{x}), \ldots, f_M(\mathbf{x}))^{\mathrm{T}} \tag{1}$$

$$\text{Subject to} \quad x_n^{(L)} \le x_n \le x_n^{(U)} \qquad n = 1,2,\ldots,N \tag{2}$$

$$g_u(\mathbf{x}) \le 0, \qquad u = 1,2,\ldots,U \tag{3}$$

$$h_v(\mathbf{x}) = 0, \qquad v = 1,2,\ldots,V \tag{4}$$

where $\mathbf{x}$ is a N-dimensional decision variable vector, $\mathbf{x} = (x_1, x_2, \ldots, x_N)^{\mathrm{T}}$, which is used to calculate the M-dimensional objective function vector $\mathbf{f}(\mathbf{x})$. The MOOP must usually satisfy U inequality constraints $\mathbf{g}(\mathbf{x}) = (g_1(\mathbf{x}), g_2(\mathbf{x}), \ldots, g_U(\mathbf{x}))^{\mathrm{T}}$ and V equality constraints $\mathbf{h}(\mathbf{x}) = (h_1(\mathbf{x}), h_2(\mathbf{x}), \ldots, h_V(\mathbf{x}))^{\mathrm{T}}$. The domain of decision variables is usually bounded such that each decision variable (x_n) lies within a lower ($x_n^{(L)}$) and an upper ($x_n^{(U)}$) bound.

The first step in multiobjective optimization is to reduce the domain of feasible solutions to the domain of Pareto-optimal solutions. The concept of Pareto optimality is described using the following definitions. For simplicity, these definitions are written only in terms of minimization problems. Similar definitions can be easily written for maximization problems.

Definition 1 (Concept of domination): A vector of objective functions $\mathbf{f}(\mathbf{x}^{(1)})$, associated to a vector of decision variables $\mathbf{x}^{(1)}$, is said to dominate another vector $\mathbf{f}(\mathbf{x}^{(2)})$ if and only if it is not worse than another solution in all its objectives and it is better with respect to at least one objective [1]: $\forall m \in \{1,\ldots,M\}: f_m(\mathbf{x}^{(1)}) \le f_m(\mathbf{x}^{(2)}) \wedge \exists m \in \{1,\ldots,M\}: f_m(\mathbf{x}^{(1)}) < f_m(\mathbf{x}^{(2)})$. This is denoted by $\mathbf{f}(\mathbf{x}^{(1)}) \prec \mathbf{f}(\mathbf{x}^{(2)})$.

Definition 2 (Non-dominated set): Among a set of solutions P, the non-dominated set of solutions P' are those that are non-dominated by any other member of the set P [1].

Definition 3 (Globally Pareto-optimal set): The non-dominated set of the entire feasible search space S is the globally Pareto-optimal set [1].

4.3 The new hybrid method: FP-NSGA-II

The fast and elitist non-dominated genetic sorting algorithm (NSGA-II) relies on the genetic crossover and mutation operators to produce offsprings from parent chromosomes [27]. FP-NSGA-II differs from the original NSGA-II by the incorporation of an additional predictive operator. Figure 4.1 presents an information flow diagram for the implementation of FP-NSGA-II. First, as in NSGA-II, the parent population P_t of chromosomes or vectors containing the decision variables of size N_{pop} is initialized with uniform random values within the specified range of the decision variables. The values of the objective functions for each chromosome are then evaluated. A pair-wise comparison of all solutions is then performed to determine the number of times each solution is dominated, thereby establishing the domination score. The entire population is then sorted based on the domination score and classified into different fronts according to the domination scores (F_i, i= 1,2, .., etc.) where F_1 corresponds to the subset of solutions with the lowest domination score number, F_2 corresponds to solutions having the next lowest domination score, and so on for the entire population. If more than one front exists, the prediction operator computes for each of the J solutions contained in F_1, J new solutions based on an extrapolation with the nearest solutions in F_2 in the objective space. The step size value, which is the difference between the vectors in the decision variable space associated respectively to a solution in F_1 and the nearest solution in F_2, is added to the decision variable vector associated to a solution in F_1 to form a new chromosome. The (N-J) remaining offsprings to complete the new population are generated using the usual tournament selection, recombination, and mutation operators to create the offspring population Q_t. The three populations P_t, Q_t, and J_t are combined to form population R_t of size $2N_{pop}$. Then, as in the regular NSGA-II, a global domination evaluation is performed and all the fronts F_i are identified. The new population is filled with the best fronts having the lowest domination score numbers without exceeding N_{pop}. When the last allowable front is considered, the crowding-sorting algorithm is performed using the crowding distance metric. This procedure can be iterated many times to provide the final result as shown in Figure 4.1. It should be mentioned that if the population converged to a single non-dominated front, then the algorithm will follow the NSGA-II procedure and generate offsprings using the crossover and mutation operators.

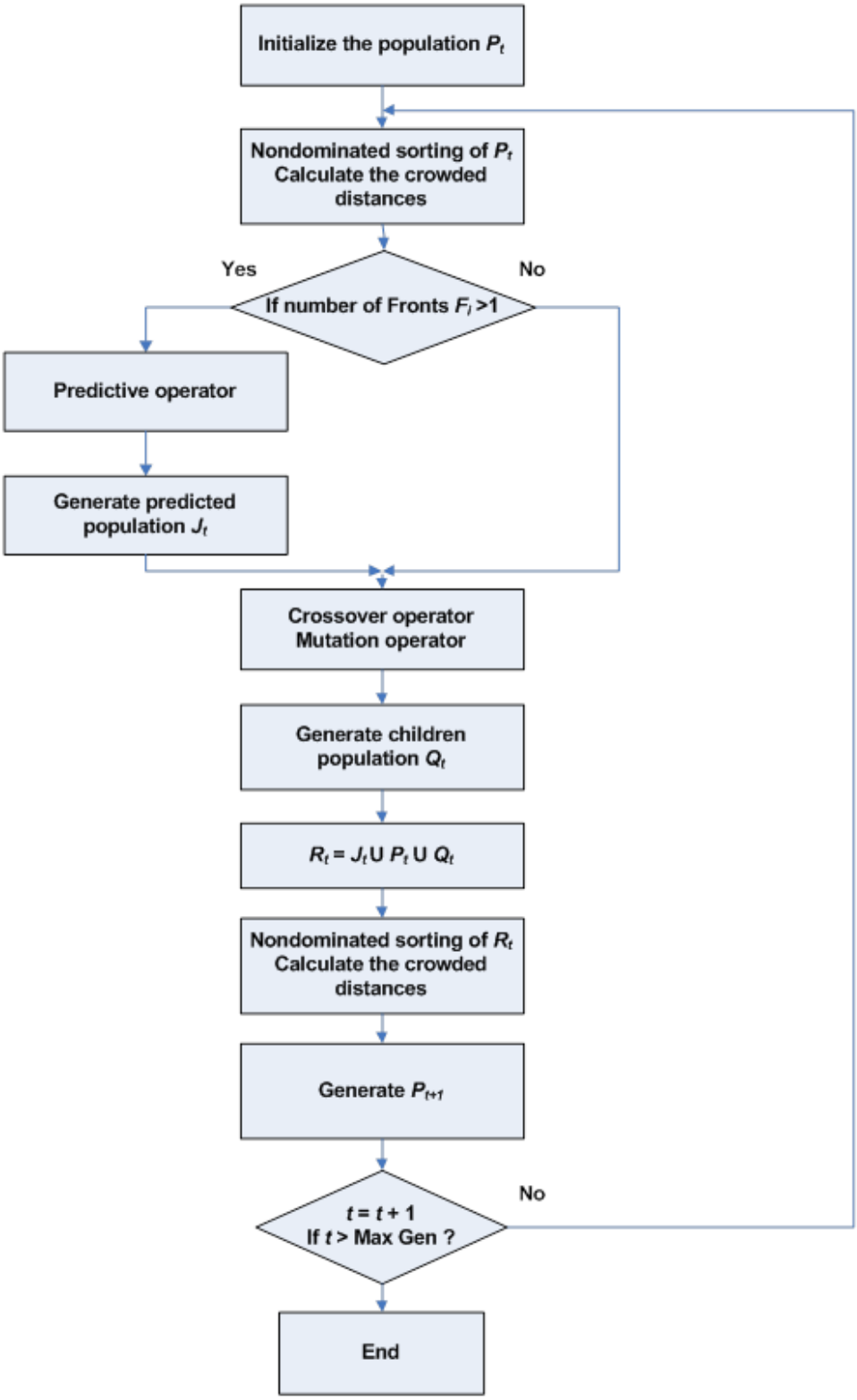

Figure 4.1 - FP-NSGA-II procedure.

The prediction operator routine can be summarized as follows:

1. First the Euclidean distance in the objective variable space is calculated between each solution in the first front $F_1 = \left\{ \mathbf{f}\left(\mathbf{x}^j_{Front1}\right) : j = 1, 2, ..., J \right\}$ where J is the number of solutions in F_1, and the solutions in the second front $F_2 = \left\{ \mathbf{f}\left(\mathbf{x}^k_{Front2}\right) : k = 1, 2, ..., K \right\}$ where K is the number of solutions in F_2. The formula of the Euclidean distance is given by:

$$d_j^k(\mathbf{x}) = \sqrt{\sum_{m=1}^{M} \left(f_m\left(\mathbf{x}^j_{Front1}\right) - f_m\left(\mathbf{x}^k_{Front2}\right) \right)^2} \qquad (5)$$

2. Then, the minimum distance between solution j in Front 1 and the closest solution k in Front 2 is determined.

$$d_j^{\min} = \min_{k=1}^{K} d_j^k \qquad (6)$$

and the index k^* for the minimum distance is also recorded.

$$k^* = \left\{ k : d_j^k = d_j^{\min} \right\} \qquad (7)$$

3. The step size in the decision space between the two chromosomes, associated to solutions j and k^*, is computed as follows:

$$step(\mathbf{x}) = \mathbf{x}^j_{Front1} - \mathbf{x}^{k^*}_{Front2} \qquad (8)$$

4. Thereafter, for each chromosome $\mathbf{x}^j_{Front1}$ associated with all solutions of the first front F_1, a predicted chromosome is generated using

$$\mathbf{x}^j_{Predicted} = \mathbf{x}^j_{Front1} + step(\mathbf{x}) \qquad (9)$$

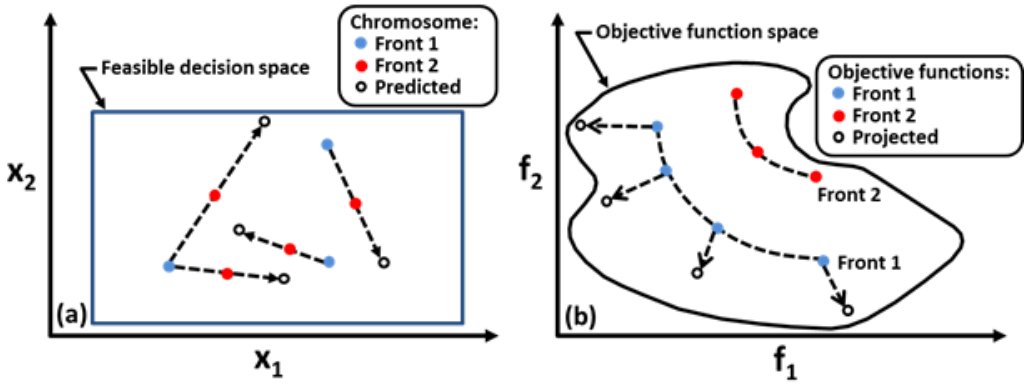

Figure 4.2 - (a) Feasible region in the decision space, with the predicted chromosomes; (b) feasible region in the objective space with the improvement pressures in FP-NSGA-II.

If the predicted chromosome is outside the bounds for a given decision variable (x_n), then it is truncated to lie within the lower ($x_n^{(L)}$) and upper ($x_n^{(U)}$) bounds. The procedure of NSGA-II is then continued with the resulting population of $2N_{pop}$ individuals.

4.4 Performance metrics

There exist numerous metrics to examine and compare the performance of the proposed algorithm. Four diversified performance metrics were used in this study:

1. Generational distance Υ - Metric Υ measures the ability of the optimization algorithm to circumscribe a Pareto front (PF_{known}) that is as close as possible to the true Pareto front (PF_{true}). It is therefore desired to minimize the sum of the Euclidean distance (d_i) of each solution between PF_{known} and PF_{true} solutions:

$$\Upsilon = \left(\frac{1}{n} \sum_{i=1}^{n} d_i^2 \right)^{1/2} \qquad (10)$$

   This metric can obviously only be used when the true Pareto domain is known. This is the case, as in this investigation, to compare optimization algorithms using known benchmark optimization problems.

2. Spread Δ - Metric Δ measures the evenness of the distribution of the solutions in the Pareto front. It is defined as:

$$\Delta = \frac{\sum_{m=1}^{M} d_m^e + d_l + \sum_{i=1}^{N} \left| d_i - \bar{d} \right|}{\sum_{m=1}^{M} d_m^e + N \cdot \bar{d}} \qquad (11)$$

   where d_m^e represent the Euclidean distances between the extreme solutions of the true Pareto front and the known Pareto front. d_i is the Euclidean distance between consecutive solutions and $\bar{d}$ is the mean value of the distances of all Euclidean distances d_i. It should be mentioned that the value of Δ for an ideal distribution is zero. However, the value increases as the distribution becomes non-uniform and clustered.

3. Number of non-dominated solutions - This metric is used to compare between the numbers of non-dominated solutions for each method obtained at the end of a simulation run when the maximum number of generations has been achieved. This number should ideally be equal to the total population number.
4. CPU time - This metric is used to compute the time required to converge to the final Pareto front.

4.5 Experiments

4.5.1 Function optimization

To assess the improvement of the new algorithm, FP-NSGA-II is initially compared with the real-coded NSGA-II on two-objective optimization well-known benchmark test problems ZDT1, ZDT2, ZDT3, ZDT4, ZDT6, CONTR, SRN, and TNK [1, 5-7]. Then, both algorithms are tested using three-objective optimization benchmark problems DTLZ1, DTLZ2, DTLZ3 and DTLZ4 [38].

In all cases, the decision variables have bound constraints. These problems were chosen to cover a wide range of problem complexity encountered in multiobjective optimization such as convex, non-convex, and disconnected Pareto fronts, linear and nonlinear objective functions and constraints.

The first five problems (ZDT1, ZDT2, ZDT3, ZDT4, ZDT6) were developed by Zitzler et al. [35] and the Pareto front is a two-dimensional front which can be continuous or discontinuous. These five problems have two objectives which must be minimized.

The first problem ZDT1 is a problem comprised of 30 decision variables and the Pareto front is continuous, uniform and convex. Likewise, ZDT2 is a problem comprised of 30 decision variables but leads to a non-convex Pareto front. The difficulty with this particular problem is to converge to the true Pareto front. ZDT3 is also a 30-dimensional problem which has 5 discontinuous non-convex fronts. On the other hand, ZDT4 is a problem with 10 decision variables giving rise to a total of 2^{19} local Pareto fronts. ZDT6 is also a 10 decision variable problem with a non-uniformly distributed and non-convex Pareto front, which challenges the ability of the algorithm to find a good distribution of non-dominated solutions when the density of the solutions is uneven. Table 4.1 shows the number of decision variables, their bounds, and the nature of the Pareto-optimal front for each problem.

Table 4.1 - Unconstrained two-objective test problems used in this study.

Problem	*n*	Variable bounds	Objective functions	Features
ZDT1	30	[0, 1]	$f_1(x) = x_1$ $f_2(x) = g(x)\left(1 - \sqrt{x_1 / g(x)}\right)$ $g(x) = 1 + 9\left(\sum_{i=2}^{n} x_i\right)/(n-1)$	Convex
ZDT2	30	[0, 1]	$f_1(x) = x_1$ $f_2(x) = g(x)\left(1 - (x_1 / g(x))^2\right)$ $g(x) = 1 + 9\left(\sum_{i=2}^{n} x_i\right)/(n-1)$	Non-convex
ZDT3	30	[0, 1]	$f_1(x) = x_1$ $f_2(x) = g(x)\left[1 - \sqrt{x_1 / g(x)} - \frac{x_1}{g(x)}\sin(10\pi x_1)\right]$ $g(x) = 1 + 9\left(\sum_{i=2}^{n} x_i\right)/(n-1)$	Convex Disconnected
ZDT4	10	$x_1 \in [0,1]$ $x_i \in [-5,5]$ $i \in 2,\ldots,n$	$f_1(x) = x_1$ $f_2(x) = g(x)\left[1 - \sqrt{x_1 / g(x)}\right]$ $g(x) = 1 + 10(n-1) + \sum_{i=2}^{n}\left[x_i^2 - 10\cos(4\pi x_i)\right]$	Non-convex
ZDT6	10	[0, 1]	$f_1(x) = 1 - \exp(-4x_1)\sin^6(6\pi x_1)$ $f_2(x) = g(x)\left[1 - (f_1(x) / g(x))^2\right]$ $g(x) = 1 + 9\left[\sum_{i=2}^{n} x_i / (n-1)\right]^{0.25}$	Non-convex; Non uniformly spaced

Three constrained optimization problems were also used: CONTR [1], SRN [37] and TNK [36]. These three problems have two decision variables, two objective variables and two inequality constraints. These test problems are summarized in Table 4.2. All the test problems with constraints are handled by using the tournament selection based on constraint-domination principle proposed by Deb et al. [1].

Table 4.2 - Constrained two-objective test problems used in this study.

Problem	n	Variable bounds	Objective functions	Constraints
CONSTR	2	$x_1 \in [0.1,1.0]$	$f_1(x) = x_1$	$g_1(x) = x_2 + 9x_1 \geq 6$
		$x_2 \in [0,5]$	$f_2(x) = (1 + x_2)/x_1$	$g_2(x) = -x_2 + 9x_1 \geq 1$
SRN	2	$x_i \in [-20,20]$	$f_1(x) = (x_1 - 2)^2 + (x_2 - 2)^2 + 2$	$g_1(x) = x_1^2 + x_2^2 \leq 225$
		$i \in 1,2$	$f_2(x) = 9x_1 - (x_2 - 1)^2$	$g_2(x) = x_1 - 3x_2 + 10 \leq 0$
TNK	2	$x_i \in [0,\pi]$	$f_1(x) = x_1$	$g_1(x) = -x_1^2 - x_2^2 + 1 + 0.1\cos(16\arctan(x_1/x_2)) \leq 0$
		$i \in 1,2$	$f_2(x) = x_2$	$g_2(x) = (x_1 - 0.5)^2 + (x_1 - 0.5)^2 \leq 0.5$

To demonstrate the algorithm ability to handle more than two objectives, four three-objective test problems DTLZ1-4 [30] were studied, and the objective functions are presented in Table 4.3. DTLZ1 has a linear global Pareto front and (2^5-1) local Pareto fronts. On the other hand, DTLZ2 has a non-convex spherical Pareto front. DTLZ3 has the same global Pareto front as DTLZ2 but its search space has (3^{10}-1) local Pareto fronts. Lastly DTLZ4 has a variable density of solutions that hinders MOEAs from finding uniform solutions.

Table 4.3 - Three-objective test problems used in this study.

Problem	n	$\lvert x_M \rvert$	Variable bounds	Objective functions	Constraints
DTLZ1	7	5	[0, 1]	$f_1(x) = \frac{1}{2} x_1 x_2 (1 + g(x_M))$ $f_2(x) = \frac{1}{2} x_1 (1 - x_2)(1 + g(x_M))$ $f_3(x) = \frac{1}{2}(1 - x_1)(1 + g(x_M))$	$g(x_M) = 100\left[\lvert x_M \rvert + \sum_{x_i \in x_M} (x_i - 0.5)^2 - \cos(20\pi(x_i - 0.5))\right]$
DTLZ2	12	10	[0, 1]	$f_1(x) = \cos(x_1\pi/2)\cos(x_2\pi/2)(1 + g(x_M))$ $f_2(x) = \cos(x_1\pi/2)\sin(x_2\pi/2)(1 + g(x_M))$ $f_3(x) = \sin(x_1\pi/2)(1 + g(x_M))$	$g(x_M) = \sum_{x_i \in x_M} (x_i - 0.5)^2$
DTLZ3	12	10	[0, 1]	$f_1(x) = \cos(x_1\pi/2)\cos(x_2\pi/2)(1 + g(x_M))$ $f_2(x) = \cos(x_1\pi/2)\sin(x_2\pi/2)(1 + g(x_M))$ $f_3(x) = \sin(x_1\pi/2)(1 + g(x_M))$	$g(x_M) = 100\left[\lvert x_M \rvert + \sum_{x_i \in x_M} (x_i - 0.5)^2 - \cos(20\pi(x_i - 0.5))\right]$
DTLZ4	12	10	[0, 1]	$f_1(x) = \cos(x_1^{100}\pi/2)\cos(x_2^{100}\pi/2)(1 + g(x_M))$ $f_2(x) = \cos(x_1^{100}\pi/2)\sin(x_2^{100}\pi/2)(1 + g(x_M))$ $f_3(x) = \sin(x_1^{100}\pi/2)(1 + g(x_M))$	$g(x_M) = \sum_{x_i \in x_M} (x_i - 0.5)^2$

In addition to the benchmark test problems, a simplified heat exchanger network problem is used as a practical engineering application of the proposed algorithm. This problem was modified from Avrial and Williams [39]. As shown in Figure 4.3, one cold stream flowing

through three heat exchangers in series must be heated from 40°C to 220°C using three hot streams with different inlet temperatures, being in this problem 150°C, 200°C, 250°C. It is desired to minimize the surface areas of all three heat exchangers.

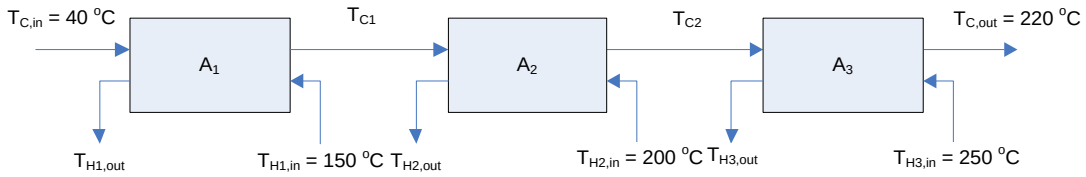

Figure 4.3 - Heat exchanger network design problem.

The decision variables are the exit temperature of the first and second heat exchangers (T_{C1} *and* T_{C2}) and the exit temperature of the hot streams of the three heat exchangers ($T_{H1,out}$, $T_{H2,out}$ and $T_{H3,out}$). This implies that the flow rates of the three hot streams will be adjusted to match these temperatures. Alternatively, the latter three decision variables could be the three hot stream flow rates. The lower and upper bounds of these five decision variables are

$$40 < T_{C1} < 140^{o}\text{C} \quad (12)$$
$$40 < T_{C2} < 190^{o}\text{C} \quad (13)$$
$$40 < T_{H1,out} < 150^{o}\text{C} \quad (14)$$
$$40 < T_{H2,out} < 200^{o}\text{C} \quad (15)$$
$$40 < T_{H3,out} < 250^{o}\text{C} \quad (16)$$

The three objective variables are calculated by Equations (17-19), assuming a geometric correction factor of one for the three heat exchangers.

$$A_1 = \frac{F_C C_p \left(T_{C1} - T_{C,in}\right) \ln\left[\left(T_{H1,in} - T_{C1}\right) / \left(T_{H1,out} - T_{C,in}\right)\right]}{U_1 \left[\left(T_{H1,in} - T_{C1}\right) - \left(T_{H1,out} - T_{C,in}\right)\right]} \quad (17)$$

$$A_2 = \frac{FC_p \left(T_{C2} - T_{C1}\right) \ln\left[\left(T_{H2,in} - T_{C2}\right) / \left(T_{H2,out} - T_{C1}\right)\right]}{U_2 \left[\left(T_{H2,in} - T_{C2}\right) - \left(T_{H2,out} - T_{C1}\right)\right]} \quad (18)$$

$$A_3 = \frac{FC_p \left(T_{C,out} - T_{C2}\right) \ln\left[\left(T_{H3,in} - T_{C,out}\right) / \left(T_{H3,out} - T_{C2}\right)\right]}{U_2 \left[\left(T_{H3,in} - T_{C,out}\right) - \left(T_{H3,out} - T_{C2}\right)\right]} \quad (19)$$

where $F_C C_p$ = 53 kW/K, U_1 = 380 W/m^{2}K, U_2 = 250 W/m^{2}K and U_3 = 125 W/m^{2}K. All parameters were assumed to be independent of temperature.

The following three constraints were implemented to ensure a 10^{o}C approach temperature in the three heat exchangers:

$$T_{H1,out} - T_{C,in} \geq 10°C \quad (20)$$

$$T_{H2,out} - T_{C1} \geq 10°C \quad (21)$$

$$TH_{3,out} - T_{C2} \geq 10^o C \quad (22)$$

4.5.2 Parameter settings of optimization algorithms

The parameters used for both optimization algorithms are summarized in Table 4.4. The simulated binary crossover (SBX) operator and polynomial mutation are used for real-coded chromosomes. The crossover probability p_c was set to 0.9 and the mutation probability p_m was equaled to $1/n$ where n is the number of decision variables. The distribution index η_c for crossover and η_m for mutation operators were set to 20. The population size for two and three-objective optimization was set to 100 and 200, respectively. The maximum number of generations was set to 250 generations and the population obtained at the end of the run was used to compute the performance metrics presented in the previous section. The optimization was performed on a personal computer with Intel Core i5 U540 CPU of 2 x 1.20 GHz and 4.00 GB of RAM.

Table 4.4 - Algorithm configurations for the generic evolutionary platform adopted in the experimental study

Chromosome	Real coding
Selection	Binary tournament selection
Crossover rate	0.9
Crossover method	Simulated Binary Crossover
Distribution index for crossover η_c	20
Mutation rate	$1/n$
Mutation method	Polynomial mutation
Distribution index for mutation η_m	20
Constraint handling strategy	Constrained tournament method
Maximum number of generations	250

4.6 Results and discussion

In order to compare the performance of FP-NSGA-II and NSGA-II, 30 simulation runs were performed for each test problem, and the results illustrated using box plots to compare the performances for both algorithms. In each box plot, the minimum value, lower quartile (Q1), median (Q2), upper quartile (Q3), and maximum value of each metric are depicted. In addition, a box plot shows separately the presence of estimated outliers.

Given the probability that a difference in the average of the performance metrics between the two algorithms can be due to a mere effect of chance, the analysis of variance (ANOVA) was used to determine the significance of the differences in their mean values. The significance level, $p > 0.01$, of the ANOVA test indicates the viability of the null hypothesis, which states that there is no significant difference between the performance metrics for the algorithms. Using ANOVA, multiple comparison tests are performed to determine the significance of the differences in the mean values.

4.6.1 Two-objective optimization

The box plot results of Υ, Δ, number of non-dominated solutions, and CPU time obtained on test problems ZDT1, ZDT2, ZDT3, ZDT4, ZDT6 are shown in Figures 4.4a-4.4e. Figure 4.4a demonstrates the ability of FP-NSGA-II in converging more closely to the true Pareto front while increasing the diversity in the Pareto front and the number of non-dominated solutions compared to the NSGA-II for the benchmark problem ZDT1. However, this comes at the expense of slightly higher mean value of CPU time to complete the 250 generations. As it will be seen later for FP-NSGA-II, the number of non-dominated solutions equal to the population size was reached prior to the maximum number of generations such the CPU time would be lower if the optimization procedure would be stopped when only non-dominated points are obtained.

Next, results of the performance metrics for the problem ZDT2 are shown in Figure 4.4b. This problem has a non-convex Pareto-optimal front. FP-NSGA-II significantly improved upon the values of the metrics Υ, Δ, and number of non-dominated solutions. On the other hand, there is no statistical difference for the mean CPU time between FP-NSGA-II and NSGA-II.

Figure 4.4c shows the results of the performance metrics for the ZDT3 problem. FP-NSGA-II performed better than NSGA-II with respect to convergence to the true Pareto front, and the number of non-dominated solutions. On the other hand, the distribution of solutions and

CPU time are better for NSGA-II. It seems that the disconnected Pareto-optimal front for ZDT3 caused convergence difficulty for NSGA-II whereas it performed extremely well for FP-NSGA-II at the expense of slightly increasing Δ and CPU time values.

The box plots of Υ, Δ, number of function evaluations, and CPU time obtained by FP-NSGA-II and NSGA-II for problem test ZDT4 are shown in Figure 4.4d. The problem ZDT4 has 2^{19} different local Pareto-optimal fronts, and one corresponds to the global Pareto front. Both algorithms faced difficulty in solving the problem and the mean value of performance metrics Υ and Δ are statistically similar. However, for the number of non-dominated solutions and CPU time, FP-NSGA-II had statistically significant better values.

Finally, Figure 4.4e shows that FP-NSGA-II achieves a higher number of non-dominated solutions and lower average CPU time for test problem ZDT6 compared to NSGA-II. However, the Δ mean value of NSGA-II is better.

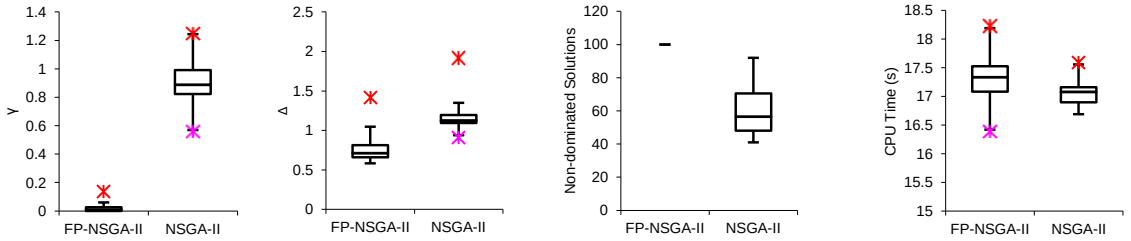

(a) ZDT1

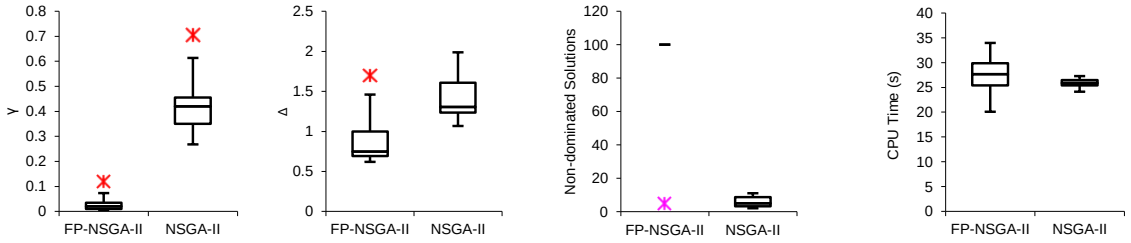

(b) ZDT2

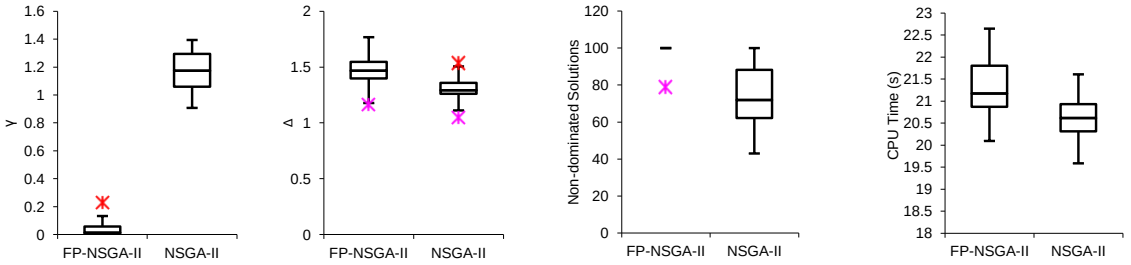

(c) ZDT3

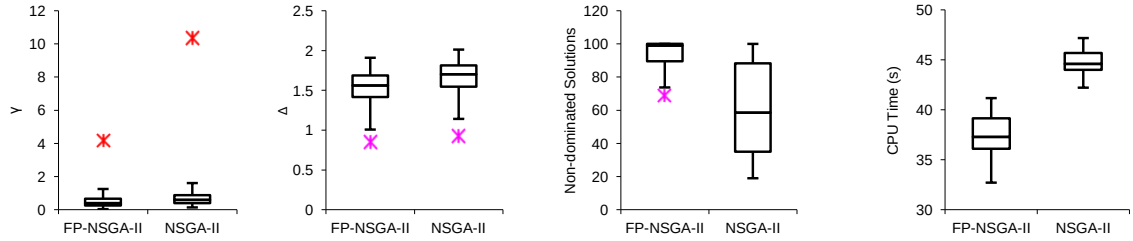

(d) ZDT4

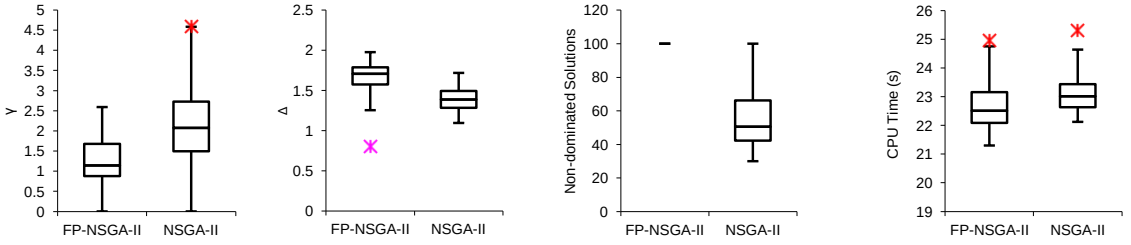

(e) ZDT6

Figure 4.4 - Box plots showing ϒ, Δ, number of non-dominated solutions and CPU time for ZDT1, ZDT2, ZDT3, ZDT4, and ZDT6 benchmark problems. Stars indicate outliers detected by the box plot algorithm.

The box plot results of ϒ, Δ, number of non-dominated solutions, and CPU time obtained for test problems CONSTR, SRN and TNK are shown in Figures 4.5a-4.5c. Figure 4.5a shows that for the performance metric results for the CONSTR problem, there are no statistical differences between FP-NSGA-II and NSGA-II with respect to ϒ, Δ, number of non-dominated solutions. However, FP-NSGA-II is able to obtain the final solution with a lower CPU time. The performance metric results for the SRN and TNK problems are shown in Figures 4.5b and 4.5c, respectively. There are no statistical differences for the performance metrics between FP-NSGA-II and NSGA-II for both problems. For these three benchmark problems, it appears that there is no advantage of incorporating the front prediction algorithm to the NSGA-II algorithm. On the other hand, incorporating the front prediction did not lead to a decrease in performance.

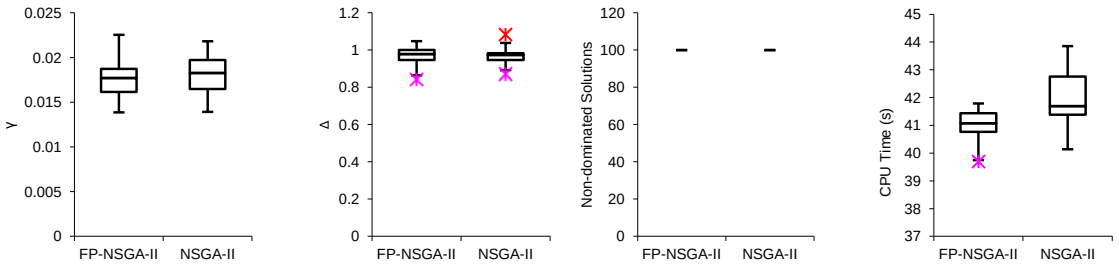

(a) CONSTR

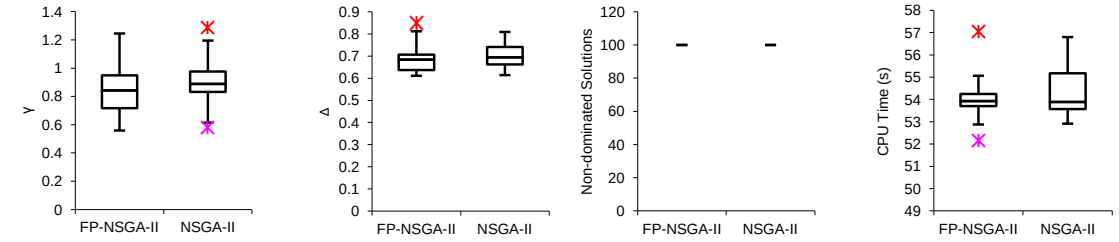

(b) SRN

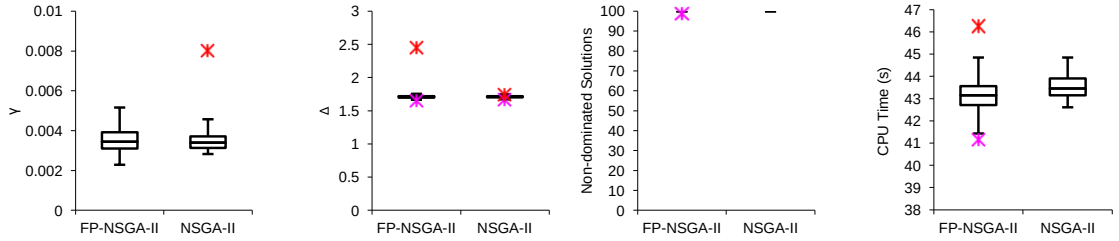

(c) TNK

Figure 4.5 - Box plots showing ϒ, Δ, number of non-dominated and CPU time for CONSTR, SRN, and TNK.

In order to obtain further insights into the workings of FP-NSGA-II, the variation of the metrics ϒ and Δ with the number of generations was studied, and it was observed that ϒ decreases as the number of generations increases due to convergence toward PF_{true}. As shown on Figure 4.6a, the drop is more significant for FP-NSGA-II in the early stage of evolution when solving the ZDT3 problem. At the same time, the values of Δ stay in the same range for both algorithms as shown in Figure 4.6b.

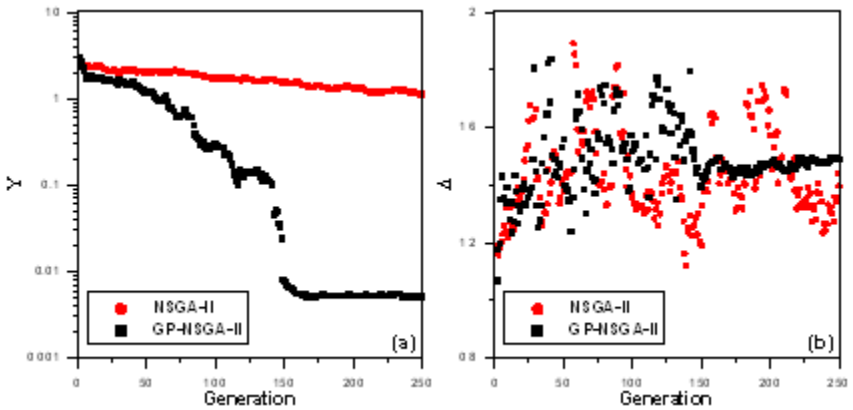

Figure 4.6 - ϒ and Δ as a function of the number of generations for ZDT3.

Overall, the FP-NSGA-II attained better performance metrics than NSGA-II for unconstrained problems whereas it had statistically similar performance for constrained problems. In order to investigate these algorithms further, the number of non-dominated solutions was added as a stopping criterion along with the maximum number of generations, and 30 additional simulation runs were performed for each test function. Both FP-NSGA-II and NSGA-II algorithms were stopped as soon as the population reached 100 non-dominated solutions or the number of generations exceeded 250.

Figures 4.7a-4.7e show the box plot results of ϒ, Δ, number generations, and CPU time obtained on test problems ZDT1, ZDT2, ZDT3, ZDT4, ZDT6 . It was observed that the FP-NSGA-II converged earlier to non-dominated solutions with a lower number of generations and overall had an improved value of ϒ and CPU time, while the value of Δ is better for NSGA-II. However, using the number of non-dominated solution as a stopping criterion resulted in a higher value of ϒ and a deteriorated convergence to PF_{true} for both algorithms when compared with the results obtained previously when simulation runs completed the 250 generations.

Figures 4.8a-4.8c show the box results obtained for the constrained problems CONSTR, TNK, and SRN. It can be seen from Figure 4.8a that there are no statistical differences between FP-NSGA-II and NSGA-II with respect to ϒ and Δ for the CONSTR problem. However, FP-NSGA-II was able to obtain 100 non-dominated solutions within a lower number of generations and a lower CPU time. Figure 4.8b shows the results for the SRN problem. There are no statistical differences for ϒ, Δ and CPU time between FP-NSGA-II and NSGA-II. However, the number of generations is lower for FP-NSGA-II. Finally, in the TNK problem, better results were obtained with FP-NSGA-II for the number of generations and CPU time, while the values of ϒ and Δ are statistically the same as shown in Figure 4.8c. Interestingly for constrained problems, using the number of non-dominated solutions as a stopping criterion results in convergence to the true Pareto front that it is similar to the results obtained with 250 generations, and there is little gain obtained by waiting for the algorithms to reach the maximum number of generations.

The improvements observed with FP-NSGA-II are due to the pressure exerted by the prediction operator in the early stages of simulation. This is coupled with the elitism, generic operators and crowding distance assignment of the NSGA-II to encourage the uniform distribution of the solutions in the Pareto front at a later stage, which resulted in a synergistic effect.

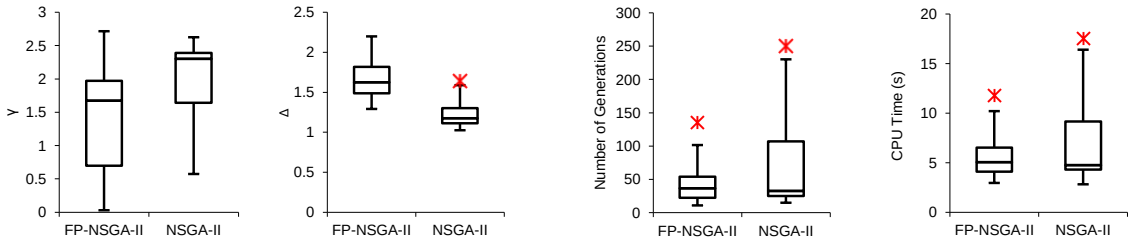

(a) ZDT1

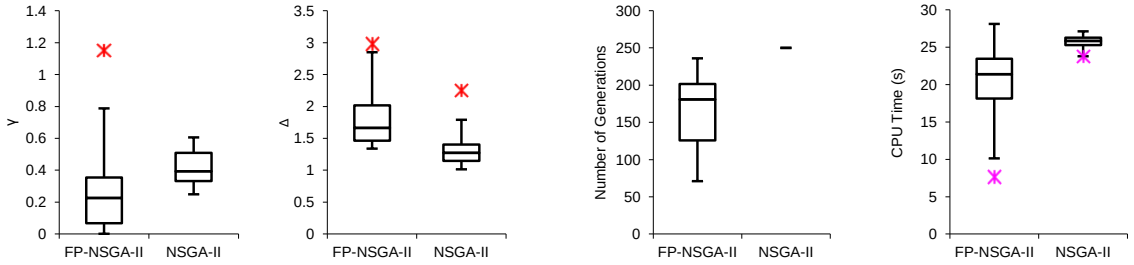

(b) ZDT2

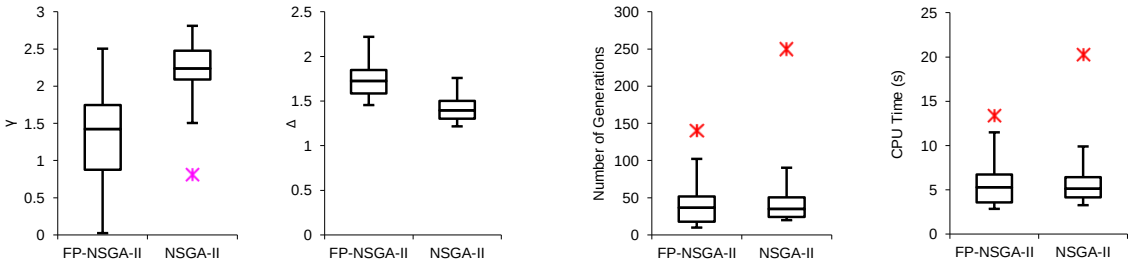

(c) ZDT3

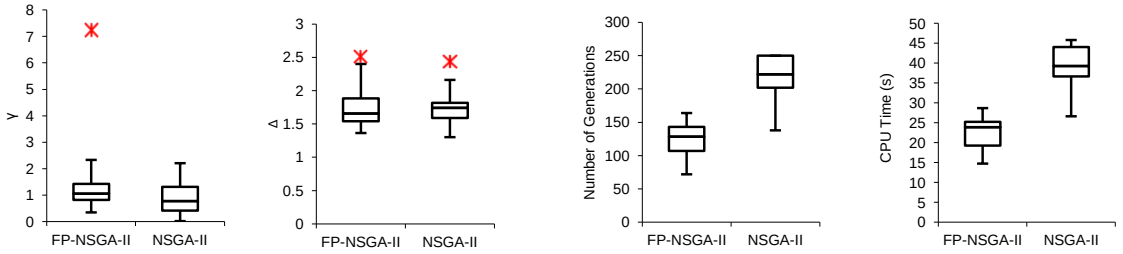

(d) ZDT4

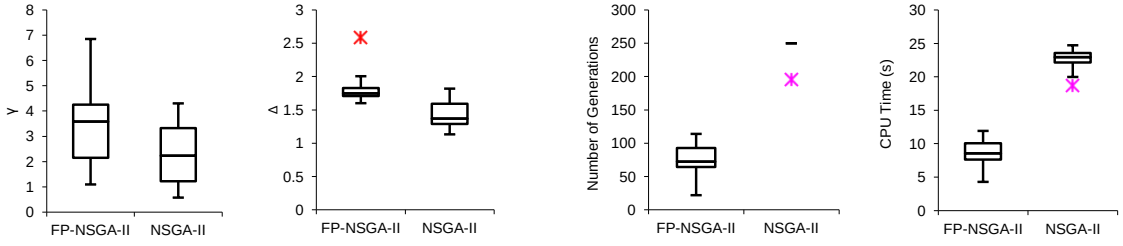

(e) ZDT6

Figure 4.7 - Box plots showing ϒ, Δ, number of generations and CPU time for ZDT1, ZDT2, ZDT3, ZDT4, and ZDT6 benchmark problems with the number of non-dominated solutions as stopping criterion. Stars indicate outliers detected by the box plot algorithm.

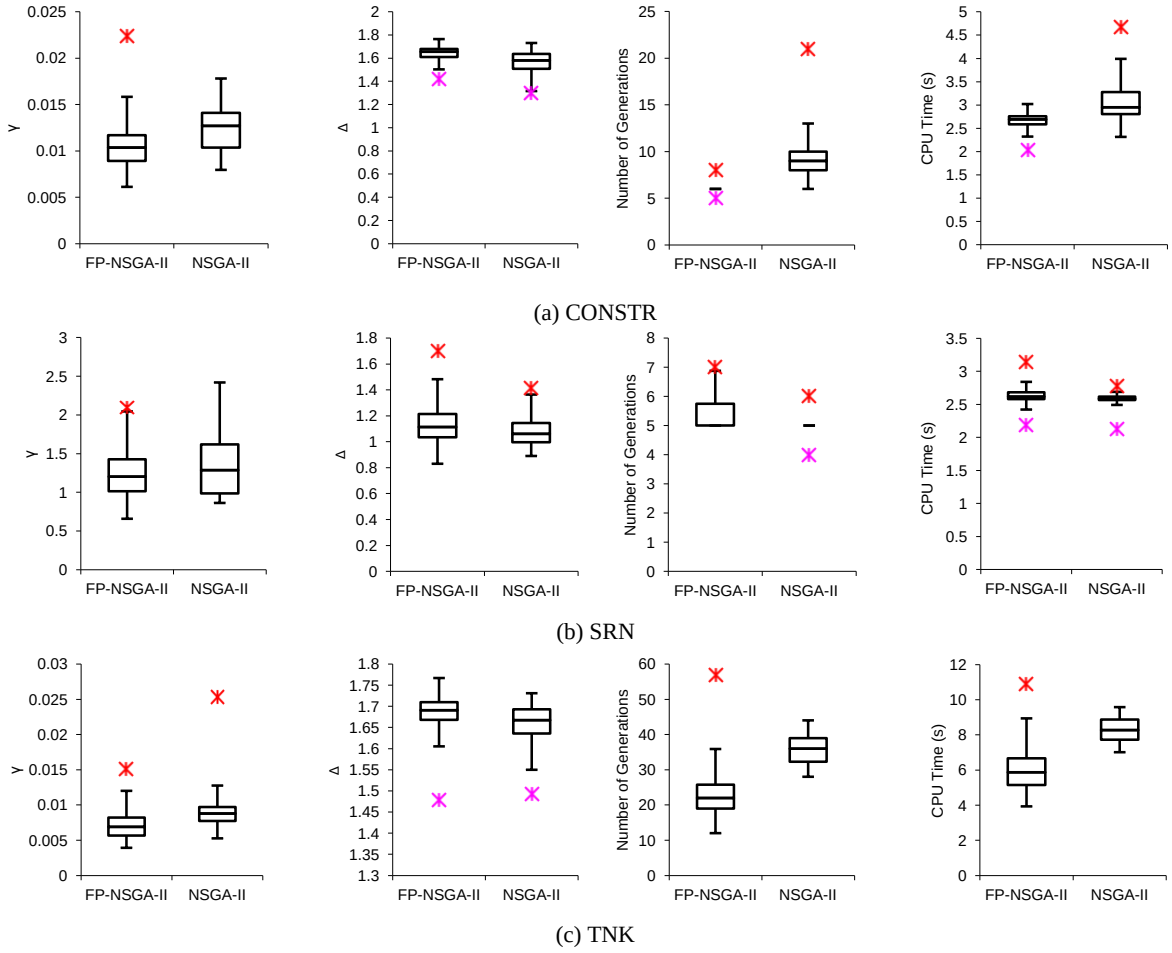

Figure 4.8 - Box plots showing ϒ, Δ, number of generations and CPU time for CONSTR, SRN, and TNK with the number of non-dominated solutions as stopping criterion. Stars indicate outliers detected by the box plot algorithm.

4.6.2 Three-objective optimization

Figures 4.9a-4.9d show the box plots of the performance metrics obtained by both algorithms after the maximum number of generations is reached for the DTLZ1-4 test problems. It can be noticed that FP-NSGA-II performed better than NSGA-II in DTLZ1 by achieving significantly better mean value of ϒ, Δ, and CPU time. In DTLZ2, FP-NSGA-II showed improvement for the CPU time while maintaining statistically similar performance to NSGA-II on the rest of the performance metrics. In the case of DTLZ3, it can be observed that FP-NSGA-II had better Δ value and CPU time. In addition, it did not get trapped in local Pareto fronts and

the percentage of non-dominated solutions at the end of the runs is higher when compared to NSGA-II. Lastly in DTLZ4, a better distribution of solutions was obtained with FP-NSGA-II, and the Pareto front was more evenly spread in the objective space as opposed to NSGA-II where solutions are localized along the f_1-f_2 and f_1-f_3 planes.

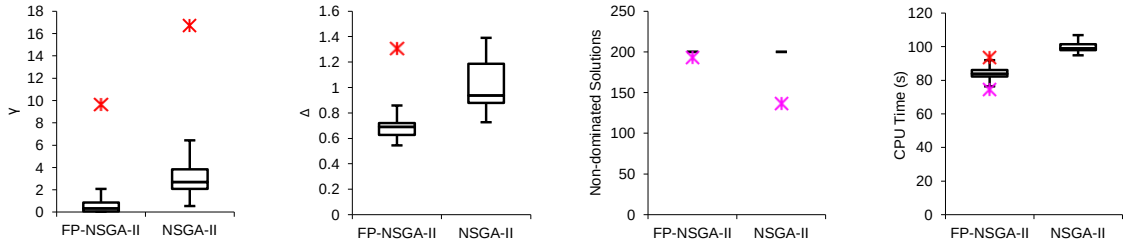

(a) DTLZ1

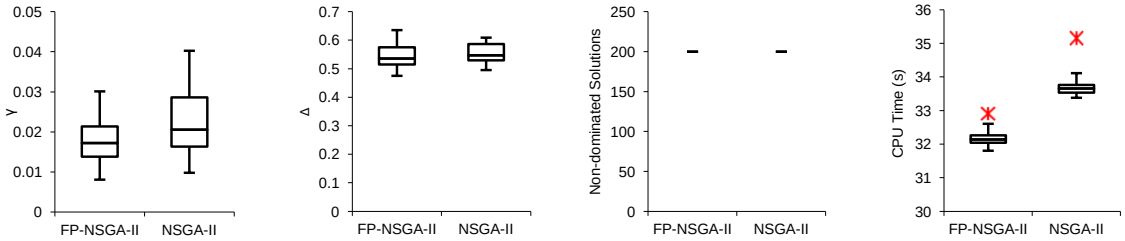

(b) DTLZ2

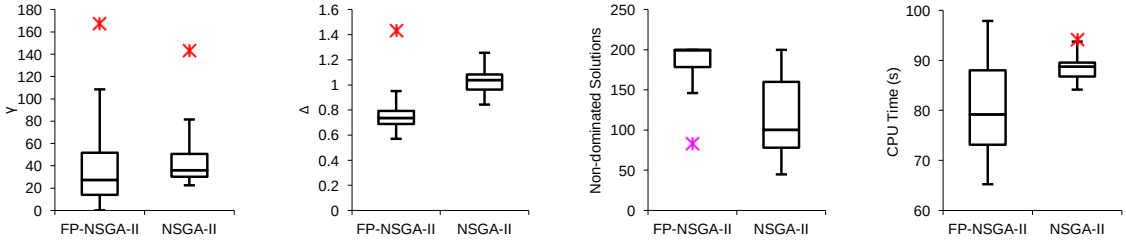

(c) DTLZ3

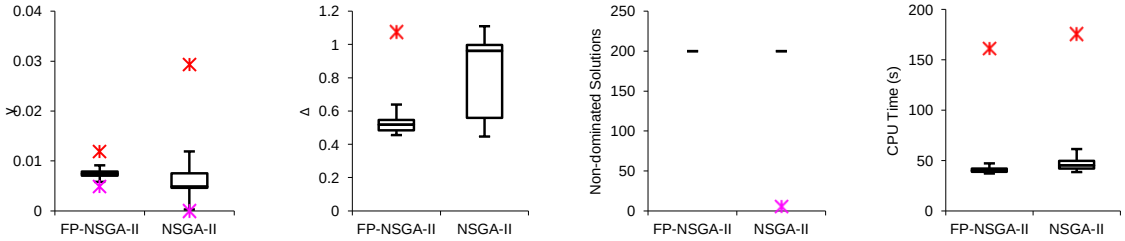

(d) DTLZ4

Figure 4.9 - Box plots showing Υ, Δ, number of non-dominated solutions and CPU time for DTLZ1, DTLZ2, DTLZ3, and DTLZ4. Stars indicate outliers detected by the box plot algorithm.

Lastly, the multiobjective optimization of a heat exchanger network was carried out to compare the proposed algorithm with the original NSGA-II. A reference solution set (the true Pareto front or a close approximation of true Pareto front) is required in order to compare the

results obtained by NSGA-II and FP-NSGA-II. To obtain this nearly perfect representation of the Pareto front, the original NSGA-II algorithm was first run for 1000 generations, i.e. 5 times more than the number of generations used to compare the two algorithms. The population size was 200. The Pareto front obtained is shown in Figure 4.10 where a compromise between the three heat exchange areas needs to be made.

For both methods, 30 simulation runs were performed. The performance metrics were calculated based on these 30 runs and plotted on Figure 4.11. Results show an improvement in the CPU time with FP-NSGA-II.

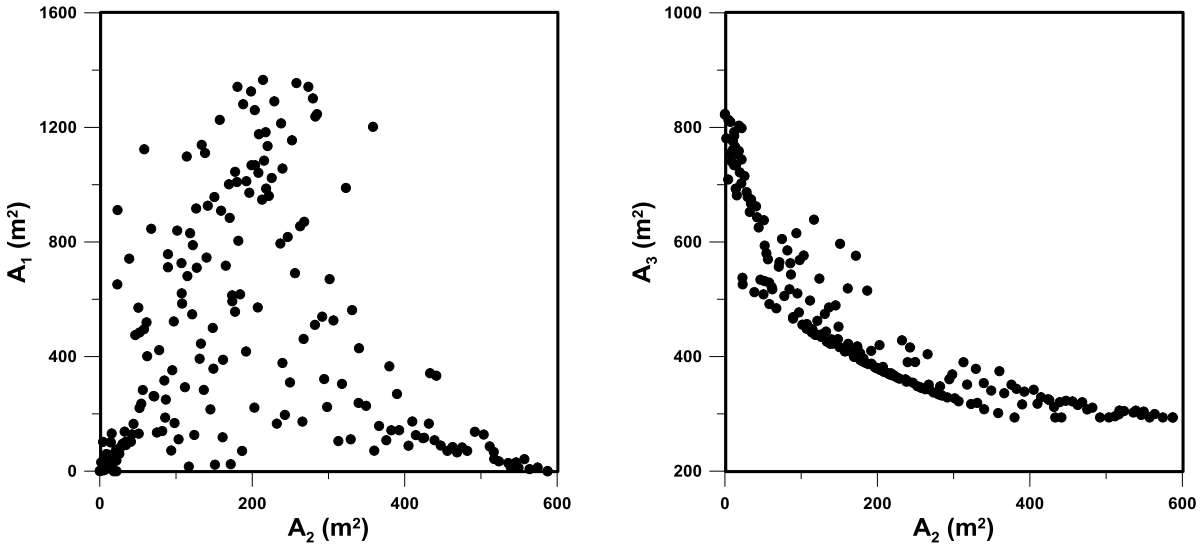

Figure 4.10 - Non-dominated solutions for minimizing the three heat exchanger surface areas with NSGA-II after 1000 generations.

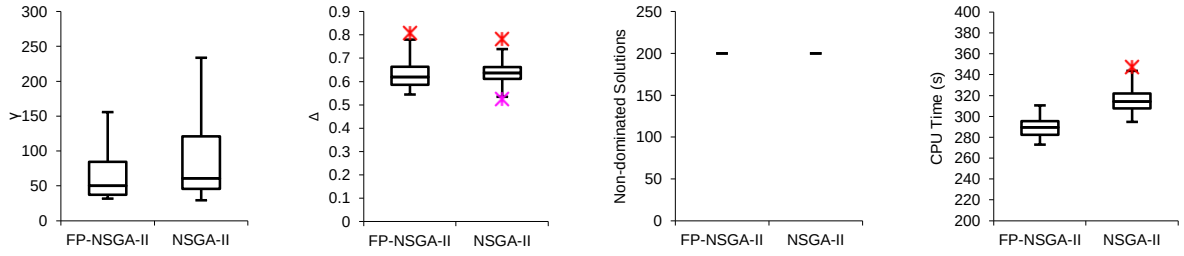

Figure 4.11 - Box plots showing ϒ, Δ, number of non-dominated solutions and CPU time for the heat exchanger network problem. Stars indicate outliers detected by the box plot algorithm.

4.7 Conclusion

In this paper, a new algorithm, FP-NSGA-II is proposed by combining a front prediction algorithm with the fast and elitist non-dominated sorting genetic algorithm-II (NSGA-II). The prediction operator is used to promote the convergence of individual solutions closer to the true Pareto front based on the direction between the first and second fronts of the current population. The performance of FP-NSGA-II was compared with NSGA-II on eight two objective benchmark test problems (ZDT1, ZDT2, ZDT3, ZDT4, ZDT6, CONSTR, SRN, TNK), and four three-objective benchmark problems (DTLZ1, DTLZ2, DTL3, DTLZ4). In addition, a comparison of performance is presented on a three-heat exchanger network problem. The results indicate that in most cases FP-NSGA-II improves the performance of NSGA-II, currently one of the most popular MOEA, for a variety of benchmark test problems exhibiting different characteristics. For future work, different constraint handling methods such as preserving feasibility of solutions and penalty functions could be investigated with FP-NSGA-II as well as using different fitness evaluation mechanisms to remove most crowded solutions when solving problems with many objectives.

4.8 Acknowledgements

The first author acknowledges support from the Natural Sciences and Engineering Research Council of Canada (NSERC) through the Alexander Graham Bell Canada Graduate Scholarships (CGSM).

4.9 References

1. Deb K. Multi-objective optimization using evolutionary algorithms. New York: Wiley; 2001.
2. Haupt RL, Haupt SE. Practical genetic algorithms. Hoboken: John Wiley & Sons; 2004.
3. Tan KC, Khor EF, Lee TH, Multiobjective evolutionary algorithms and applications. London: Springer; 2005.
4. Fraser A. Simulation of genetic systems by automatic digital computers. Australian Journal of Biological Sciences 1957; 10:484–491.

5. Box GE. Evolutionary operation: A method for increasing industrial productivity. Applied Statistics 1957;6, 81–101.
6. Rechenberg I. Evolutionsstrategie: Optimierung technischer Systeme nach Prinzipien der biologischen Evolution. Stuttgart: Frommann-Holzboog; 1973.
7. Schwefel HP. Numerische Optimierung von Computer-Modellen. Birkhäuser; 1977.
8. Fogel LJ, Owens AJ, Walsh MJ. Artificial Intelligence through Simulated Evolution. New York: John Wiley; 1966.
9. Holland JH. Adaptation in Natural and Artificial Systems. Ann Arbor: University of Michigan Press; 1975.
10. Schaffer D. Multiple objective optimization with vector evaluated genetic algorithms. In: Proceedings of the First International Conference on Genetic *Algorithms*, 1985, p. 93–100.
11. Koza JR. Genetic programming: On the programming of computers by means of natural evolution. Massachusetts: MIT Press; 1992.
12. Storn R, Price KV. Differential evolution: A simple and efficient adaptive scheme for global optimization over continuous spaces, ICSI, USA, tech. rep. TR-95-012, 1995. <http://icsi.berkeley.edu/~storn/litera.html>.
13. Kennedy J, Eberhart RC, Shi Y. Swarm Intelligence. San Francisco: Morgan Kaufmann; 2001.
14. Bonabeau E, Dorigo M, Theraulaz G. Swarm intelligence: From natural to artificial system. New York: Oxford University Press; 1999.
15. Engelbrecht AP. Fundamentals of Computational Swarm Intelligence. John Wiley & Sons; 2006.
16. Wojtusiak J, Michalski RS. The LEM3 Implementation of learnable evolution model and Its testing on complex function optimization problems. In: Proceedings of genetic and evolutionary computation conference (GECCO), Seattle, 2006, p. 1281 – 1288.
17. Lee KS, Geem ZW. A new metaheuristic algorithm for continuous engineering optimization: harmony search theory and practice. Computer methods in applied mechanics and engineering 2005;194:3902–3933.
18. Dasgupta D. Artificial immune systems and their applications. Berlin: Springer-Verlag; 1999.

19. Yu PL. A class of solutions for group decision problems. Management Science 1973;8:936-946.
20. Zeleny M. Compromise programming. In: Cochrane JL, Zeleny M, editors. Multiple Crieteria Decision Making, Columbia SC: University of South Carolina Press; 1973, p. 262-301.
21. Miettenen K. Nonlinear Multiobjective Optimization. Boston: Kluwer; 1999.
22. Brans JP, Mareschal B, Vincke P. PROMETHEE: A New Family of Outranking Methods in Multicriteria Decision Making. Operations Research 1984;84:477-498.
23. Derot B, Gareau J, Kiss LN, Martel JM. The Solver of Volvox Multicriteria Table. In: Climaoi J, editor. Multicriteria Analysis. Springer-Verlag; 1997, p. 113-126.
24. Thibault, J. Net flow and rough sets: Two methods for ranking the pareto domain. In: Rangaiah G, editor. Multi-Objective Optimization: Techniques and Applications in Chemical Engineering. World Scientific Publishing; 2008.
25. Pawlak Z. Rough set approach to knowledge-based decision support. European Journal of Operational Research 1997; 99:48-57.
26. Cheikh M, Jarboui B, Taicir L. A method for selecting Pareto optimal solutions in multiobjective optimization. Journal of Informatics and Mathematical Sciences 2010;2: 51-62.
27. Deb K, Argawal S, Pratap A, Meyarivan T. A fast and elitist multi-objective genetic algorithm: NSGA-II. IEEE Transactions on Evolutionary Computation 2002;6:182-197.
28. Knowles J, Corne D. The pareto archived evolution strategy: A new baseline algorithm for multiobjective optimization. In: Proceedings of the 1999 Congress on Evolutionary Computation, Piscataway, 1999, p. 9-105.
29. Zitzler E, Laumanns M, Thiele L. SPEA2: Improving the strength pareto evolutionary algorithm. Computer Engineering and Networks Laboratory (TIK). Zurich, Switzerland, tech. rep. 103, 2001.
30. Purshouse RC, Fleming PJ. Evolutionary multi-objective optimisation: An exploratory analysis. In: Proceedings of the 2003 Congress on Evolutionary Computation (CEC'2003), vol. 3. Canberra, Australia: IEEE Press, 2003, p. 2066–2073.

31. Kukkonen S, Deb K. A fast and effective method for pruning of non-dominated solutions in many-objective problems. In: Parallel problem solving from nature - PPSN IX, 9th international conference, ser. lecture notes in computer science, no. 4193. Reykjavik, Iceland: Springer-Verlag, 2006, p. 553-562.
32. Koppen M, Yoshida K. Substitute distance assignments in nsga-II for handling many-objective optimization problems. In: Evolutionary Multi-Criterion Optimization, 4th International Conference (EMO) 2007, Matshushima, Japan: Springer. Lecture Notes in Computer Science Vol. 4403, 2007, p. 727-741.
33. Hartikainen M, Miettinen K, Wiecek MW. PAINT: Pareto front interpolation for nonlinear multiobjective optimization. Computational optimization and applications 2011; DOI: 10.1007/s10589-011-9441-z.
34. Miettinen K, Mäkelä MM. On scalarizing functions in multiobjective optimization. OR spectrum 2002;24:193-213.
35. Zitzler E, Deb K, Thiele L. Comparison of multiobjective evolutionary algorithms: Empirical results. Evolutionary Computation Journal 2000;8:125-148.
36. Tanaka M. GA-based decision support system for multi-criteria optimization, In: Proc. Int. Conf. Systems, Man and Cybernetics, 1995, p. 1556-1561.
37. Chankong V, Haime YY. Multiobjective decision making theory and methodology. New York: North-Holland; 1983.
38. Deb K, Thiele L, Laumanns M, Ziztler E. Scalable test problems for evolutionary multi-objective optimization. Computer engineering and networks laboratory (TIK), Zurich, Switzerland, tech. rep. 112, 2001.
39. Avriel M, Williams AC. An extension of geometric programming with applications in engineering optimization. Journal of Engineering Mathematics 1971;5:187-194.

Chapter 5: Conclusions and recommendations

In this chapter, the results of the evolutionary algorithms employed to optimize chemical engineering systems are summarised. In addition, potential directions for future work are presented.

5.1 Conclusions

The objectives of this research were twofold. First, the application of multiobjective optimization in the design of complex chemical engineering systems was investigated. Second, the development of a novel algorithm was proposed to better approximate the Pareto front of difficult problems without compromising the computational time.

In Chapter 2, the dual population evolutionary algorithm (DPEA) was employed in order to maximize the selectivity, productivity and yield of an industrial styrene reactor. It was found that DPEA led to Pareto domains for which the spread of each objective covers a wider range of values of non-dominated solutions compared to those reported previously in the literature. In addition, the current industrial operating conditions appear to give a dominated solution. An alternative ranking method, NFM was also used to incorporate the preferences of the expert into the optimization strategy to rank all the Pareto-optimal solutions.

Then in Chapter 3, a multiobjective optimization of the heat transfer area and pumping power of a shell-and-tube heat exchanger was performed using the fast non-dominated sorting genetic algorithm (NSGA-II). The results indicated that one can achieve a lower optimal value of the heat transfer area and the pumping power as compared to the previously published values. Furthermore, it was found that discretization of the tube length, diameter and thickness had a very minor effect on the optimal cost design. The values of L_{bc}, d_o, and δ_{tb}. are the decision variables that are mainly responsible for the trade-off observed in the Pareto domain for both case studies, while for the first case study the tube layout and N_p were also found to play a role, and the tube length had a significant effect in the second case study. The remaining decision variables did not affect the trade-off significantly.

Lastly in Chapter 4, a new algorithm, FP-NSGA-II is proposed by combining a front prediction algorithm with NSGA-II. The prediction operator is used to promote the convergence of individual solutions closer to the true Pareto front based on the direction between the first and second fronts of the current population. The results indicated that in most cases FP-NSGA-II

improves the performance of NSGA-II, currently one of the most popular MOEA, for a variety of benchmark test problems exhibiting different characteristics.

The results highlight the clear benefits from employing multiobjective optimization algorithms in the chemical engineering design. It was shown that this approach allowed finding Pareto fronts with a wider range of optimal decision variables. The designer can choose one solution from all Pareto-optimal solutions based on his knowledge of the process as well as examining the cost of the design. The enviable advantages of the multiobjective optimization are the ability for the designer to readily visualize the trade-offs being made in choosing a given design, in addition to finding solutions that can be counter-intuitive at times if one relies on heuristics.

5.2 Recommendations

As more focus is placed on solving multi-dimensional problems with four and higher objectives, a natural area for future work is to study the impact higher-dimension optimization on the presented evolutionary algorithms. The proposed FP-NSGA-II allows for much more customization. An interesting area is to investigate different constraint handling methods such as preserving feasibility of solutions and penalty functions with FP-NSGA-II. Further research could be undertaken as well to implement different fitness evaluation mechanisms to remove most crowded solutions when solving problems with many objectives.